

Oxygen depletion in Lake Geneva

THÈSE N° 7569 (2017)

PRÉSENTÉE LE 5 MAI 2017

À LA FACULTÉ DE L'ENVIRONNEMENT NATUREL, ARCHITECTURAL ET CONSTRUIT
LABORATOIRE DE PHYSIQUE DES SYSTÈMES AQUATIQUES - CHAIRE MARGARETHA KAMPRAD
PROGRAMME DOCTORAL EN GÉNIE CIVIL ET ENVIRONNEMENT

ÉCOLE POLYTECHNIQUE FÉDÉRALE DE LAUSANNE

POUR L'OBTENTION DU GRADE DE DOCTEUR ÈS SCIENCES

PAR

Robert Vincent SCHWEFEL

acceptée sur proposition du jury:

Prof. U. von Gunten, président du jury
Prof. A. J. Wüest, Dr D. Bouffard, directeurs de thèse
Prof. D. McGinnis, rapporteur
Dr L. Umlauf, rapporteur
Prof. T. Battin, rapporteur



ÉCOLE POLYTECHNIQUE
FÉDÉRALE DE LAUSANNE

Suisse
2017

Abstract

Low oxygen concentrations remain a global concern for the ecological health of lakes. High nutrient inputs and climate-induced changes in stratification and mixing are anthropogenic threats which largely impact aquatic oxygen budgets and overall ecosystem health. In this thesis, the relevant processes for hypolimnetic oxygen depletion were investigated on different temporal and spatial scales in the deep perialpine Lake Geneva and the corresponding total oxygen budget was estimated. The short-term variability of sediment oxygen uptake (SOU) and its dependency on the bottom boundary layer currents were investigated using microprofile measurements. Sediment core analyses for reduced substances profiles allowed distinguishing between SOU caused by both oxic respiration and the flux of reduced substances out of the sediment. Long-term monitoring data were used to estimate the relative importance of SOU for the total oxygen depletion in the lake. Finally, one-dimensional numerical models were used to reproduce lake temperature and oxygen concentrations and to assess the impact of changing environments on the oxygen budget of the deep-water.

The results of the microprofile measurements led to a new parameterization of turbulent diffusion close to the sediment and enabled a similarity scaling of diffusivity as well as oxygen close to the sediment. However, the comparison of microprofile measurements at different lake depths showed that SOU decreased consistently with depth from $\sim 1 \text{ g m}^{-2} \text{ d}^{-1}$ at 40 m to $\sim 0.2 \text{ g m}^{-2} \text{ d}^{-1}$ at 133 m independently from the small-scale variability due to hydrodynamic forcing. Similar vertical structures of SOU and total oxygen depletion have been found in other Swiss lakes. The decrease of SOU with depth was attributed to the greater amount of easily degradable organic matter available in the upper layers. The comparison between SOU and the reduced substances flux revealed that oxic respiration is by far the dominant pathway of organic matter mineralization.

While the long-term monitoring data did not show a decreasing trend in either the areal hypolimnetic mineralization rate ($1.34 \text{ g m}^{-2} \text{ d}^{-1}$) or the extent of hypoxia, a strong relationship between deep mixing in winter hypoxic conditions was found. Hence, deep-water oxygen concentrations were predominantly controlled by resupply during the unstratified period in winter. To assess the long-term changes of winter mixing in Lake Geneva, the one-dimensional model SIMSTRAT was used to reproduce lake temperature and stratification between 1981 and

2012 and was run afterwards under atmospheric conditions representative for the years 2045–2076 and 2070–2101, according to the IPPC scenario A1B. The simulations predicted (i) a decrease in winter mixing depth from an average of ~172 m to only ~127 m at the end of this century, and (ii) complete homogenization of temperature and oxygen in winter will decrease by ~50%. Hence, changes in mixing may have stronger impact than eutrophication on the deep-water oxygen. A simple oxygen model coupled to SIMSTRAT predicted an increase in hypoxic conditions in the deep part of Lake Geneva by ~25%.

Additionally, a detailed oxygen model was developed based on the observational findings of this dissertation which takes the spatial variability of oxygen depletion and its dependency on lake turbulence into account. This model can be generalized to understand and predict climate-induced changes of future oxygen concentrations in other deep lakes.

Keywords

Lake Geneva, oxygen depletion, hypoxia, sediment oxygen uptake, microprofile measurements, numerical modelling

Zusammenfassung

Niedrige Sauerstoffkonzentrationen stellen ein weltweites Problem für den ökologischen Zustand von Seen dar. Anthropogene Änderungen wie Nährstoffeinträge oder klimabedingte Änderung des Schichtungs- und Mischungsverhaltens beeinflussen ihren Sauerstoffgehalt signifikant. In dieser Dissertation werden für die Sauerstoffzehrung verantwortliche Prozesse in verschiedenen räumlichen und zeitlichen Auflösungen anhand eines tiefen, perialpinen Sees (Genfersee) untersucht sowie ihr Einfluss auf das Gesamtsauerstoffbudget abgeschätzt. Die kurzfristige Variation der Sedimentsauerstoffzehrung (*sediment oxygen uptake*, SOU) und ihre Abhängigkeit von Stömungen in Sedimentnähe wurde mittels Mikroprofilmessungen untersucht.

Sedimentkernanalysen ermöglichten eine Unterscheidung zwischen SOU durch oxische Respiration und reduzierte Substanzen aus den tieferen Sedimentschichten. Langzeitmessreihen wurden verwendet, um den Beitrag der SOU an der gesamten Sauerstoffzehrung des Sees abzuschätzen. Zusätzlich wurden numerische Modelle benutzt um Seetemperaturen und –sauerstoff zu reproduzieren und den Einfluss einer sich verändernden Umwelt auf den Sauerstoffgehalt des Tiefenwassers abzuschätzen.

Die Resultate der Mikroprofilmessungen führten zu einer Parametrisierung der turbulenten Diffusion nahe des Sediments und ermöglichten die Formulierung eines Ähnlichkeitsgesetzes für turbulente Diffusivität und Sauerstoff. Mikroprofilmessungen in verschiedenen Tiefen des Sees zeigten, dass die SOU von $\sim 1 \text{ g m}^{-2} \text{ d}^{-1}$ (40 m) auf $\sim 0.2 \text{ g m}^{-2} \text{ d}^{-1}$ (133 m) abnahm, unabhängig von der kurzzeitigen Variabilität durch sich ändernde hydrodynamische Randbedingungen. Diese Abnahme wurde auf die höhere Verfügbarkeit an leicht mineralisierbaren organischen Substanzen im oberen Bereich des Sees zurückgeführt, ähnliche Abnahmen der Zehrungsrate wurden auch in anderen Seen beobachtet. Vergleiche der SOU mit dem im Sedimentkernporenwasser gemessenen Fluss reduzierter Substanzen zeigten, dass oxische Respiration der dominierende Mineralisierungsprozess ist.

Langzeitmessreihen zeigten weder eine Abnahme der Mineralisierungsrate ($1.34 \text{ g m}^{-2} \text{ d}^{-1}$) noch in der Ausdehnung von Sauerstoffminimumzonen. Stattdessen fand sich ein starker Zusammenhang zwischen Konvektion im Winter und hypoxischen Zuständen. Dies verdeutlicht, dass der Sauerstoff im Tiefenwasser zu einem großen Teil durch den Eintrag im Winter kontrolliert wird. Das eindimensionale Modell SIMSTRAT wurde benutzt, um Änderungen des

Mischungsverhaltens zu untersuchen. Es reproduzierte Temperaturen und Schichtung des Sees für die Jahre 1981-2012 und wurde anschließend mit Randbedingungen gemäß IPCC-Klimaszenarien für 2045–2076 und 2070–2101 eingesetzt. Die Simulationen prognostizierten eine Abnahme der Mischungstiefe von heute ~172 m auf ~127 m Ende des Jahrhunderts. Winter mit vollständiger Mischung des Tiefenwassers werden um etwa 50% abnehmen. Klimabedingte Änderungen des Mischungsverhaltens haben folglich größere Auswirkungen auf den Sauerstoffgehalt des Tiefenwassers als Eutrophierung. Ein an SIMSTRAT gekoppeltes Sauerstoffmodell sagte um 25 % zunehmende hypoxische Verhältnisse voraus.

Auf Grundlage der Messresultate dieser Dissertation wurde ein komplexeres Sauerstoffmodell entwickelt, das die vertikale Variabilität der Sauerstoffzehrung sowie ihre Abhängigkeit von der Turbulenz berücksichtigt. Dieses Modell kann auch auf andere Seen angewandt werden um die Änderungen ihres Sauerstoffgehaltes zu verstehen und vorherzusagen.

Schlagwörter

Genfersee, Sauerstoffzehrung, Hypoxie, Sedimentsauerstoffzehrung, Mikroprofilmessungen, numerische Modellierung

Acknowledgments

This thesis would not have been possible without the support of many people. I am very grateful to my supervisor Alfred Johny Wüest who made this project possible and supported and encouraged me continuously over the last four years.

My co-supervisor Damien Bouffard I would like to thank for many fruitful discussions, the great support during the fieldwork and the proofreading (sorry that I always forget to label the axes in my figures...).

I would also like to thank the rest of my thesis committee, Urs von Gunten, Tom Battin, Dan McGinnis and Lars Umlauf for their interest in my work.

Many thanks to Lee Bryant, who helped me a lot with the handling of microsenors and with the interpretation of the fieldwork results. Thanks to Beat Müller and Tom Steinsberger for the collaboration and the great field campaigns, to Miki Hondzo for the fabulous work during his stay in Lausanne. Thanks to Peter Holtermann and Lars Umlauf for the great collaboration on the numerical modelling of Lake Geneva. Thanks to all the technicians, especially Sébastien Lavanchy, Patrick Kathriner and Michael Schurter and all the other people who helped during the fieldwork

A big thanks to the whole APHYS-group (Johny, Damien, Love, Vincent, Natacha, Theo, Oscar, Hannah, Tania) for the great time and the support. When I started, we were only three and it is very nice to have so many great colleagues now (not only for stealing pencils).

Finally, I have to thank my family, my friends and my parents. Without them, I would not be where I am now.

Hope, I did not forget anybody ...

Table of Content

Abstract	3
Zusammenfassung	3
Acknowledgments	5
Table of Content	7
1. Introduction	9
1.1 Oxygen depletion and hypoxia in lakes	9
1.2 Lake Geneva	15
1.3 Objectives and approach	19
2. Scaling oxygen microprofiles at the sediment interface of deep stratified waters	29
2.1 Introduction	31
2.2 Materials and Methods	33
2.3 Results and Discussion	35
2.4 Conclusions	45
Supporting information for chapter 2	51
3. Using small-scale measurements to estimate hypolimnetic oxygen depletion in a deep lake	57
3.1 Introduction	59
3.2 Methods	60
3.3 Results	68
3.4 Discussion	71
3.5 Conclusions	78
Supporting information for chapter 3	85
4. Effects of climate change on deep-water oxygen and winter mixing in a deep lake (Lake Geneva) – Comparing observational findings and modeling	89
4.1 Introduction	91
4.2 Methods	94
4.3 Results	102

4.4 Discussion	112
4.5 Conclusions	116
Supporting information for chapter 4	123
5. Modelling oxygen depletion in lakes	135
5.1 Introduction.....	137
5.2 Oxygen depletion in lakes	138
5.3 Modelling oxygen in Lake Geneva.....	145
6. Summary and Outlook.....	155
6.1 Summary	156
6.2 Outlook	158
Curriculum Vitae	169

Chapter 1:

Introduction

1.1 Oxygen depletion and hypoxia in lakes

1.1.1 Oxygen in lakes

Oxygen is a crucial element for all forms of higher life. In lakes and oceans, the concentration of dissolved oxygen is one of the most important parameters for the ecological health of the aquatic system and consequently the oxygen budget of lakes has been a fundamental topic in limnology since its early beginnings (*Forel 1895, Thienemann 1928, Hutchinson 1957*). Nowadays, low oxygen concentration (*hypoxia*) is a problem for many lakes on a global scale (*Nürnberg 2002, Friedrich et al. 2014*) and large regions of the ocean (*Diaz et al. 2001*).

Hypoxia are often the result of man-made eutrophication processes. High nutrient inputs increase the primary production in the upper layer (*epilimnion*) and lead, in turn, to increased organic matter mineralization in the deep layers (*hypolimnion*). While this phenomenon might increase the oxygen concentrations in the epilimnion, where oxygen is produced by photosynthesis, the increased mineralization of organic matter leads to oxygen deficits below.

In addition to the availability of nutrients for primary production, the oxygen content in lakes is also controlled by several physical processes. Sediment oxygen uptake, for example, depends on the hydrodynamic forcing in the bottom boundary layer (BBL). The resupply of oxygen in the hypolimnion is caused by turbulent transport which is controlled by energy input and lake stratification. Especially the latter experienced significant changes in the last decades: Increasing lake surface temperatures were observed globally and are predicted for the future (*Schneider and Hook 2010, Schmid et al. 2014, O'Reilly et al. 2015*). The resulting increase in stratification is an additional challenge for sustaining ecologically acceptable oxygen concentrations in lakes.

Increased stratification due to globally higher lake temperatures and stronger temperature gradients hinder the reoxygenation of hypolimnia because of a lengthened stratification period (*Jankowski et al. 2006, Foley et al. 2012, North et al. 2014*) or a reduction of deep convective winter mixing (*Matzinger et al. 2007, Sahoo et al. 2013, Schwefel et al. 2016*).

Low oxygen concentrations might have severe impacts on the ecology of lakes and oceans. In Switzerland, a threshold of 4 mg L⁻¹ is targeted by the federal law based on minimally tolerable oxygen concentrations for fish egg survival (*Müller et al. 2012, Barbier and Quetin 2016*).

Anoxic conditions finally lead to the end of all forms of higher life. Especially the benthic ecosystem is sensitive to hypoxic conditions since oxygen depletion is most pronounced close to

the sediment. Indirectly, this affects other non-benthic fauna as well, e.g. because of difficulties in reproduction: fish might avoid hypoxic areas for hatching or the eggs will not hatch due to anoxic conditions in the upper sediments (Zhang *et al.* 2010).

1.1.2 Oxygen depletion processes and oxygen budget

Several processes are important for the oxygen budget of lakes: (i) oxygen production in the epilimnion by photosynthesis, (ii) oxygen depletion in epi- and hypolimnion, (iii) gas exchange with the atmosphere, (iv) turbulent diffusion from layers of higher to lower concentrations, and (v) river inflows. While production and exchange with the atmosphere take place in the epilimnion, the depletion processes occur over the whole depth of the lake. Most relevant for the occurrence of hypoxia in the hypolimnion are the depletion during the stratified period and the resupply of oxygen during unstratified seasons. Resupply happens typically once per year during winter for warm-monomictic lakes of temperate climate zones or twice per year in spring and autumn for dimictic lakes.

In shallow lakes with one or two seasonal deep mixing per year, hypoxia are largely controlled by oxygen depletion processes at the sediment. In warm-monomictic lakes like Lake Geneva, not only the depletion during summer but also the amount of supplied oxygen during winter and spring is important for the amount and severity of hypoxic conditions. The deep layer is only reoxygenized during winter, when deep convective mixing homogenizes the water column and allows the oxygen to reach the deep layers. During summer, the stable stratification reduces turbulent diffusion. Changes in the winter mixing behavior will have an important impact on the oxygen budget (Straile *et al.* 2003, Matzinger *et al.* 2007, Sahoo *et al.* 2013). The dependence of oxygen content of deep lakes on winter mixing and in turn on winter temperatures is discussed in chapter 4.

Since oxygen depletion is an important process for the lake's ecosystem, a wealth of empirical models were developed to predict oxygen depletion rates as a function of other variables such as phosphorus content, lake temperature and lake morphology (Rast and Lee 1978, Cornett and Rigler 1979, Monod *et al.* 1992). Although these models were empirically tested (Cornett and Rigler 1980, Rippey and McSorley 2009), open questions remain concerning the relationship between nutrient input and oxygen. In many lakes, biomass production decreased often less strongly than nutrient inputs, and oxygen depletion rates did not show significant decreasing trends. Consequently, lake recovery programs did often not show the expected results in terms of

reestablishing non-hypoxic environments (Müller *et al.* 2012b, Scavia *et al.* 2014). Depletion of oxygen occurs in various ways within the lake hypolimnion. While oxic respiration, the main depletion process, takes place over the whole lake, its effect is normally offset by oxygen production or gas exchange with the atmosphere in the epilimnion. Severe oxygen depletion is therefore only observed in the hypolimnion. Oxygen is consumed by animals, plants and especially by bacteria throughout the whole water column, but most strongly at the sediment surface, where bacterial concentrations are significantly higher than in the open water. Below a shallow oxic zone, in which oxic respiration takes place, oxygen is completely used up and anaerobic processes mineralize organic carbon. These processes lead to the production of reduced substances, such as CH_4 , NH_4^+ , Fe^{2+} , or Mn^{2+} , which diffuse out into the oxic zone or the overlying water. Here, they are oxidized again and thereby consume oxygen (Jørgensen and Boudreau 2001, Matzinger *et al.* 2010). The lower the oxygen concentration above the sediment-water interface (SWI), the higher the importance of reduced substances for the sediment oxygen uptake (SOU) and the total oxygen depletion. In small lakes their contribution to the total oxygen depletion can be up to 80% due to the small hypolimnion volume which leads to (i) a high sediment-to-volume ratio (α) and (ii) a rapid depletion of the hypolimnetic oxygen during stratification which favors anoxic mineralization (Müller *et al.* 2010).

Because of the decreasing α , the influence of sediment processes on oxygen depletion decreases with increasing lake depth (Livingstone and Imboden 1996). While the oxygen depletion in small lakes is almost entirely determined by SOU (Müller *et al.* 2012), it contributes only to 51-53% of the total oxygen depletion in Lake Erie (Bouffard *et al.* 2013), 40-50% in the San Vicente Reservoir (California) (Beutel *et al.* 2007) and only 30% in Lake Geneva (see chapter 3). The relative contribution of SOU to the oxygen depletion compared to the mineralization in the water column is discussed in chapters 3 and 5.

Albeit less important than the mineralization in the water column in deep lakes, SOU has been found to be extremely variable (Lorke *et al.* 2003, Bryant *et al.* 2010) and depends on several external factors. A proper understanding of SOU processes is crucial for a precise calculation of oxygen budgets of lakes. The flux of oxygen into the sediment (F_{O_2}) under lake-typical low-turbulence conditions is largely controlled by diffusional transport through the ~1 mm thick diffusive boundary layer (DBL) between the sediment and the overlying water:

$$F_{O_2} = D \frac{C_{BBL} - C_{SWI}}{\delta_{DBL}}$$

with the BBL concentration C_{BBL} , the SWI concentration C_{SWI} , the DBL thickness δ_{DBL} and the molecular diffusivity D . While D shows only minor variations in the hypolimnion, variations of the concentration difference $C_{BBL} - C_{SWI}$ and δ_{DBL} impact the SOU significantly. A higher concentration difference due to high oxygen levels in the overlying water leads to increasing SOU. This effect is responsible for the high oxygen depletion rates in artificially aerated lakes (Müller *et al.* 2012, Bierlein *et al.*, *subm.*). Similarly, δ_{DBL} is not constant, but varies with turbulence conditions in the BBL. Higher turbulence in the BBL compresses the DBL and results in smaller δ_{DBL} and in turn increased SOU (Lorke *et al.* 2003, Bryant *et al.* 2010a, Bryant *et al.* 2010b). δ_{DBL} can be parametrized in different ways as a function of the Schmidt number (Sc) and the friction velocity u_* . While δ_{DBL} consistently shows a decreasing trend with friction velocity ($\delta_{DBL} \propto \frac{1}{u_*}$) in several studies (Steinberger and Hondzo 1999, Lorke *et al.* 2003, Wang *et al.* 2016), the dependency on the Schmidt number is not as clear: Lorke *et al.* (2003) propose a scaling with $Sc^{-1/2}$ but laboratory measurements by Steinberger and Hondzo 1999 suggest a proportionality with $Sc^{-1/3}$. However, in lake hypolimnia Sc remains relatively constant and the variation of u_* is of much higher relevance. Variations of SOU due to varying δ_{DBL} can be of almost one order of magnitude (Bryant *et al.* 2010a). Hence a proper description of the SOU is of high importance to understand the oxygen depletion of lakes. A scaling law for oxygen concentrations was proposed by Hondzo *et al.* (2005) based on laboratory measurements. A modified law based on field measurements in Lake Geneva is presented in chapter 4.

1.1.3 Measuring sediment oxygen uptake

Three different methods have been used in the past to measure SOU: (1) benthic chambers, (2) eddy-correlation and (3) oxygen microprofiling (Glud 2008). All three techniques provide comparable results (Berg *et al.* 2009) but have specific advantages and disadvantages. Benthic chambers measure the oxygen depletion in a closed environment separated from the natural hydrodynamic boundary conditions (Tengberg *et al.* 1995, Glud 2008). While it is a valuable method to compare SOU of different environments, e.g. sediments from different lakes, it is not suitable to determine the dependency of SOU on hydrodynamic forcing.

Eddy correlation has routinely been used in atmospheric science for several decades (*Swinbank* 1951), but it is a relatively new technology for aquatic sciences (*Berg et al.* 2003, *McGinnis et al.* 2008, *Lorrai et al.* 2010, *McGinnis et al.* 2014). Problems for eddy correlation applications in lakes are generally low turbulences and non-steady-state conditions (*Brand et al.* 2008).

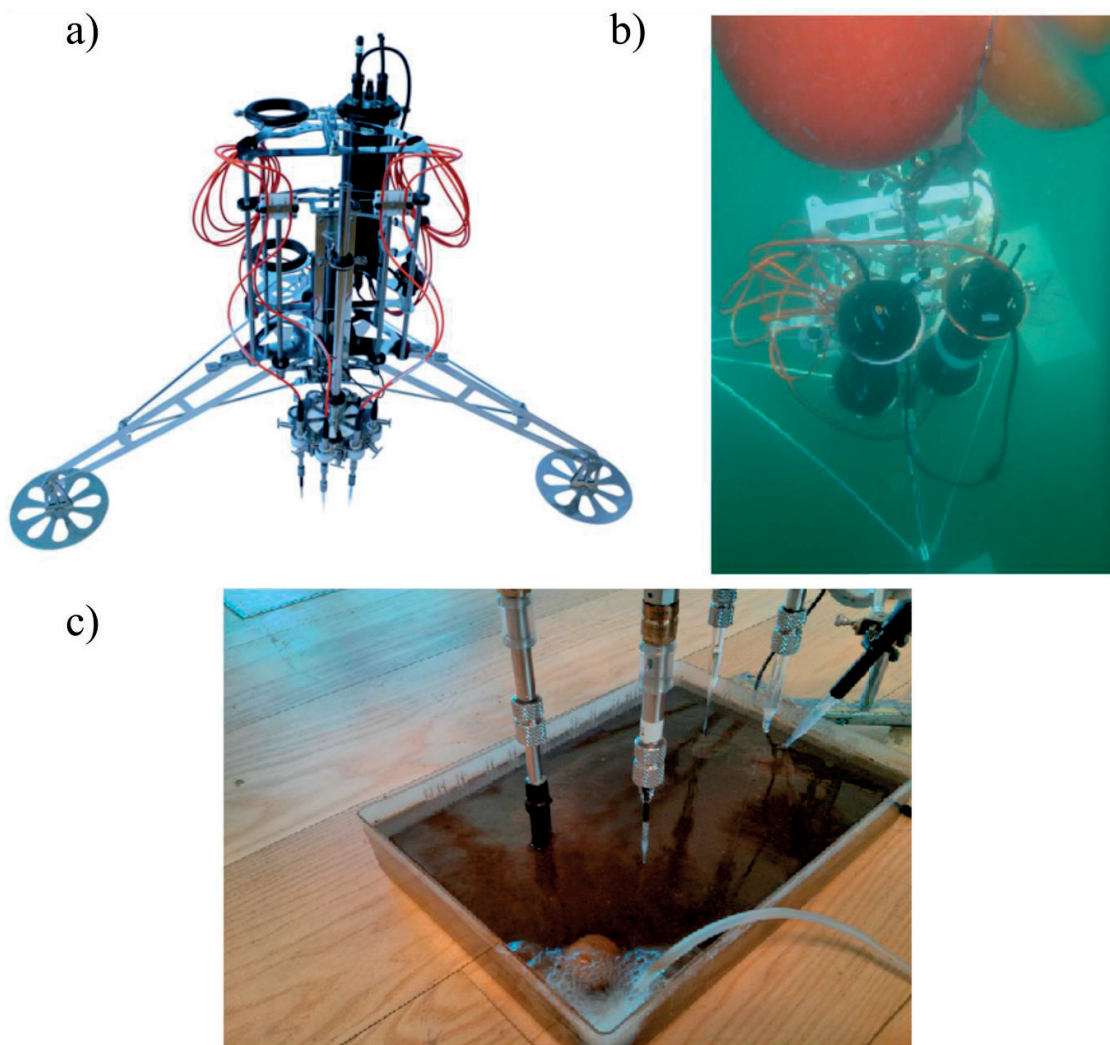


Figure 1.1: a) The Microprofiler MP8 which was used for the fieldwork of this thesis. b) Sinking microprofiler during field measurements in Lake Geneva. c) Microprofilers during a laboratory test.

Microprofile measurements (*Jørgensen and Revsbech 1985*; Figure 1.1) allow measuring oxygen concentration at both sides of the SWI. Accordingly, oxygen fluxes can be measured below and above the SWI using different approaches (*Bryant et al. 2010b*). Measurements are performed under natural conditions and microprofiles were used in lakes in several studies (*Lorke et al. 2003*, *Bryant et al. 2010a*, *Horppila et al. 2015*).

In general, all of these three methods measure the sum of two different oxygen depletion processes: direct oxic respiration and indirect oxygen consumption by reduced substances diffusing out of the deep anoxic layers of the sediment. A separation of these two contributors is possible through parallel measurements of SOU and the concentration of the reduced substances. While oxygen concentrations are measureable *in-situ*, ion-selective electrodes are only available for *in-situ* measurements of certain reduced substances (*Kühl and Revsbech 2001*). Therefore, reduced substances are generally measured *ex-situ* from sediment core porewater. A new method of porewater analysis uses MicroRhizon samplers to extract subsamples from the side of sediment cores (*Seeberg-Elverfeldt et al. 2005*) for subsequent analysis via capillary electrophoresis (*Torres et al. 2013*, *Steinsberger et al.*, in prep.). Using extremely small sampling volumes of only 20 µL, this technique allows measuring charged ions in sub-cm resolution. However, this ion-sensitive measurement technique is not applicable for the neutral CH₄ molecule, one of the most important reduced substances in lake sediments. It has to be measured using gas chromatography in lower spatial resolution due to larger sample sizes.

1.2 Lake Geneva

1.2.1 General overview

Lake Geneva (Figure 1.2) is a deep perialpine lake between France and Switzerland. With a surface area of 580 km² and a volume of 89 km³, resulting in a mean depth of 151 m, it is the largest freshwater reservoir in Western Europe and is very important for drinking water supply, tourism and local fishery.

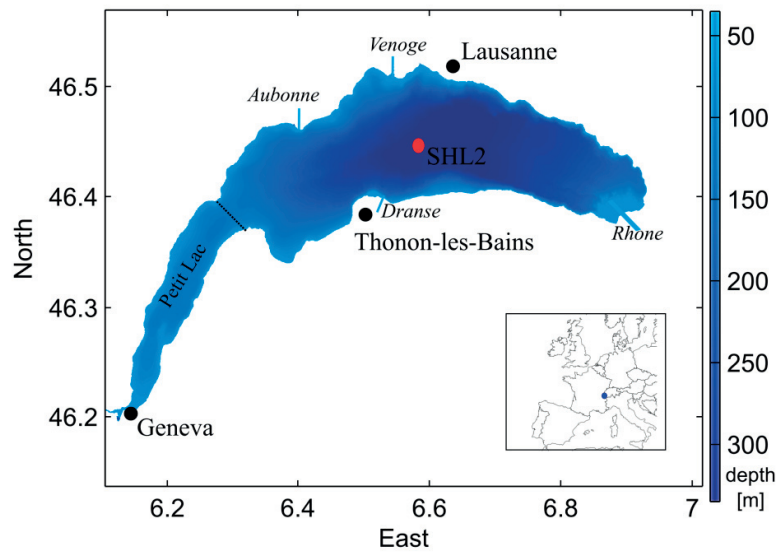


Figure 1.2: Map of Lake Geneva with major cities and major inflows. Red dot: Measurement point SHL2. Dotted line: Border between Grand Lac and Petit Lac.

The lake consists of two basins, the smaller and more shallow *Petit Lac* (maximum depth: 70 m) in the west and the larger *Grand Lac* (maximum depth: 310 m) which contains 96% of the total volume. The main inflow is the Rhône with a mean flow of $184 \text{ m}^3 \text{ s}^{-1}$, other inflows are the Dranse, Aubonne, Venoge and several other small inflows. The only outflow is the Rhône which is regulated at the *Barrage du Seujet* in Geneva. The mean residence time is 11.6 years.

Lake Geneva is a warm monomictic lake with a continuously deepening thermocline during summer and autumn. A weak stratification typically remains even in winter, complete homogenization due to deep convective mixing only occurs during particularly cold winters (on average, every ~ 5 years). This mixing behavior directly affects the oxygen content and thus the biological conditions in the deep hypolimnion. Between 1983 and 2000, the mean annual surface temperature increased by 1°C with seasonally higher increases in summer (up to 2°C) compared to winter (Gillet and Quétin 2006). Molinero *et al.* (2007) showed that the increase in water temperature was correlated to local temperature and humidity as well as to large scale climate patterns such as the North Atlantic Oscillation. The length of the stratification period consequently increased (Anneville *et al.* 2013) and the frequency of deep-water mixing in winter will therefore decrease (see chapter 4).

The surrounding topography of the Jura in the north-west and the Alps in the south and south-east largely determine the wind field over the lake. Predominant winds are the *Vent* from south-east and the *Bise* from north-west (Lemmin and D'Adamo 1997). Wind speeds are generally low and rarely exceed 5 m s^{-1} . However, they have significant influence on the generation of internal waves and in turn on the currents in the hypolimnion (Lemmin *et al.* 2005, Umlauf and Lemmin 2005). The size of the lake is five times larger than the internal Rossby-radius. Hence, internal waves are expected to be affected by earth rotation. Dominant internal waves are Kelvin waves with a period of 70 to 100 h and Poincaré waves with a shorter period of approximately 14 h (Bouffard and Lemmin 2013).

1.2.2 Eutrophication and hypoxia

Once considered as a classical example of an oligotrophic mountain lake (Forel 1895, Thienemann 1928), Lake Geneva suffered from severe eutrophication due to increased nutrient inputs in the second half of the 20th century (Lachavanne 1980). First measurements of oxygen concentrations of the surface water of Lake Geneva were already performed in 1846 (Deville 1848). However, systematic measurements of oxygen concentration did not start before 1957, only few data are available to estimate the oxygen budget of the pre-eutrophication era before the 1960s, especially for the deeper layers. All early studies showed significantly higher oxygen concentrations in the hypolimnion compared to values obtained from the systematic measurements after 1957 (Forel 1895, Delebecque 1898, Vivier 1944, Hubault 1947; Figure 1.3). Besides direct oxygen measurements, sediment cores of Lake Geneva were analyzed to determine hypoxic events in the past but showed no indications of anoxia in the deep hypolimnion before the 1960s (Jenny *et al.* 2014).

After first warnings about unusual algae blooms by fishermen, the results of the first systematic monitoring campaign 1957-1961 revealed several indications of eutrophication, i.e. increase in phosphorus concentrations, decrease in Secchi Disk depth, and hypoxic conditions in the deep layers (Loizeau and Dominik 2005).

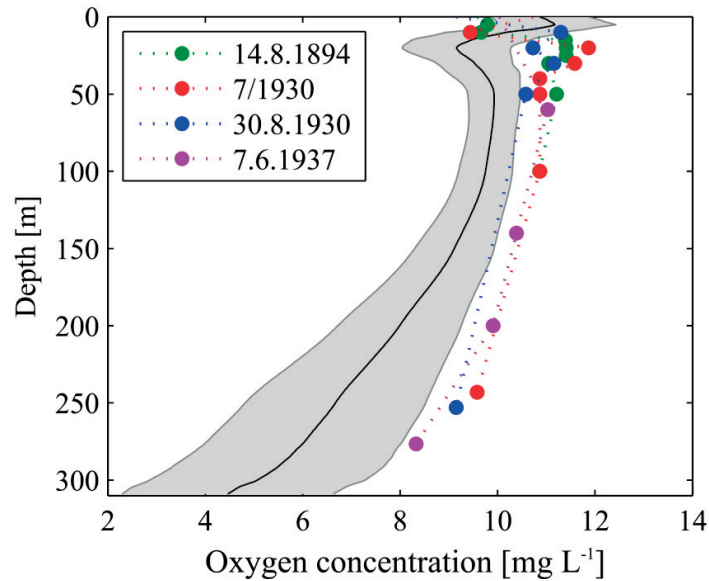


Figure 1.3: Mean oxygen concentrations during summer 1957-2012 (black line with standard deviation in grey) compared to historical oxygen measurements (green: *Delebecque* 1898; red and light blue: *Vivier* 1944; violet: *Hubault* 1947). The historical profiles show consistently higher concentrations in the deep layers and no metalimnetic minimum.

Monod (1956) reported an increased supersaturation of oxygen in the surface waters already in the 1950s. While the saturation did not exceed 120% before 1950 (between 95% and 116% in summer 1895, 112% in June 1937), he found a saturation of 130% in June and July 1954. He attributed this supersaturation to an increase in primary production due to anthropogenic eutrophication. In the following decades, the saturation exceeded 120% almost every summer with considerable higher values in many years (e.g. >200% in 1986 and ~180% in 2003 and 2007). With the foundation of the *Commission Internationale pour la Protection des Eaux du Léman* and the results of the first systematical measurements starting in May 1957, the consequences of man-made eutrophication processes in Lake Geneva became clearer: From 1960 to 1976, the phosphorus concentration increased from ~10 to ~90 mg m⁻³. In parallel, the nitrogen concentration increased by a factor of two. The main reasons for this increase were the use of phosphorus in detergents (*Loizeau and Dominik* 2005), which were released into the lake by wastewater inputs. As a result of the nutrient increase, the phytoplankton community changed and the volume of phytoplankton increased from ~3 mL m⁻³ before 1965 to > 5 mL m⁻³ in the 1970s. In parallel, the Secchi Disk depth as a proxy of phytoplankton concentration decreased drastically while no change was observed in the first measurements performed in 1875 to the

1960s (Loizeau and Dominik 2005). Starting in the 1970s, improved wastewater treatment and changes in the agricultural practice have led to a significant reduction of phosphorus concentrations to a present concentration of $\sim 20 \text{ mg m}^{-3}$ (Barbier and Quetin 2016). However, neither the total biomass nor primary production or oxygen depletion showed a significant diminishing trend: The total biomass showed high annual fluctuations and tended to decrease slightly until ~ 1990 but increased afterwards again (Anneville and Pelletier 2000). The primary production fluctuated without significant trend and was not correlated to the total biomass, but weakly correlated to nanoplankton biomass (Anneville and Pelletier 2000). Recent measurements show still no trend and fluctuated around a mean of $5 \text{ mg h}^{-1} \text{ m}^{-3}$ in the uppermost 20 m (Perga et al. 2016). Oxygen depletion remained high with a mean value of $1.34 \text{ g m}^{-2} \text{ d}^{-1}$ (depth $> 15 \text{ m}$; see chapter 3). The oxygen profiles showed consistently lower values compared to the measurements before the eutrophication period. Below the thermocline, a metalimnetic minimum, which is typical for eutrophic lakes, and was not observed before 1957, is still visible even after 30 years of phosphorus reduction (Figure 1.3). Fishery studies show that the lake charr (*Salvelinus umbla*) population is still not self-sustaining and the fishery relies on stocking (Caudron et al. 2014). Besides changes in fishing techniques, an important reason for this is the lack of oxygen in the sediment surface (Rubin 1992).

1.3 Objectives and approach

The objectives of this dissertation are (i) to investigate the oxygen depletion processes in Lake Geneva, (ii) to reproduce the oxygen concentrations in the lake by numerical modelling and (iii) to assess the sensitivity of the oxygen budget to external forcing. Field measurements including small-scale ADCP and microprofile measurements were taken and analyzed together with long-term monitoring data to understand and quantify the variability of oxygen depletion on different spatial and temporal scales. The results were used to find a realistic parameterization of oxygen depletion processes for one-dimensional oxygen models. Together with realistic parameterizations of gas exchange (Cole and Caraco 1998) and oxygen production (Fang and Stefan 2009), an oxygen model was set up to reproduce the oxygen budget of Lake Geneva and to test the sensitivity to changing boundary conditions such as increasing atmospheric temperature or varying primary production or depletion. The thesis is structured as follows:

Chapter 2 uses the results of two microprofile measurement campaigns in combination with small-scale ADCP measurements to find a functional relationship between SOU and BBL dynamics. A scaling law for eddy viscosity above the SWI was proposed. Based on this new parameterization of eddy viscosity, a general scaling law for oxygen concentrations in and above the DBL was developed. The results improve the understanding of small-scale variability of SOU and enable to parameterize DBL thickness and SOU as a function of BBL dynamics.

Chapter 3 focusses on the field measurements on Lake Geneva on a larger scale. The results of microprofile and sediment core measurements are used to investigate the spatial variability of SOU and the relative contribution of different processes (water column mineralization, oxic respiration at the sediment, reduced substances) to the total oxygen depletion in the lake. In combination with historical data, the conceptual model for oxygen depletion introduced by *Livingstone and Imboden* (1996) was extended to take the variability of oxygen depletion processes with depth into account.

Chapter 4 describes the mixing behavior of Lake Geneva. Based on more than 40 years of historical data of lake temperature, oxygen and mixing depth, the dependency of oxygen concentrations in the deep hypolimnion on deep convective mixing was investigated and the one-dimensional model SIMSTRAT (*Goudsmit et al.* 2002) was calibrated based on these field data. In a second step, the model was run under differing boundary conditions based on IPCC climate predictions (*IPCC* 2013, *CH2011* 2011). The results show that hypoxic conditions in the deep hypolimnion are strongly related to weak mixing in winter. Increased air temperatures caused by climate change might hence lead to a significant decrease in the hypolimnetic oxygen concentrations.

Chapter 5 brings the findings of chapter 2-4 into a broader perspective by comparing oxygen depletion rates of Lake Geneva with other Swiss lakes (Lake Biel, Lake Constance and Lake Neuchâtel). Besides the comparison of the oxygen depletion rates, the findings of chapter 2 and 3 are used to set-up and calibrate a one-dimensional oxygen depletion model which was coupled to the hydrodynamic model SIMSTRAT. With this model, the impact of varying atmospheric temperatures and oxygen depletion rates on the oxygen budget of Lake Geneva was analyzed.

In a final **chapter 6**, a conclusion of the previous chapters of this dissertation is given and possible future research questions are addressed.

References

- Anneville, O., and J. P. Pelletier. 2000. Recovery of Lake Geneva from eutrophication: quantitative response of phytoplankton. *Arch. Hydrobiol.* **148**: 607–624. doi:10.1127/archiv-hydrobiol/148/2000/607
- Anneville, O., M. Beniston, N. Gallina, C. Gillet, S. Jacquet, and M. Perroud. 2013. L’empreinte du Changement climatique sur le Léman. *Arch. Sci.* **66**: 157–172.
- Barbier, C., and P. 2016. Rapport Commission International pour la Protection des eaux du Léman, Campagne 2015: Évolution physico-chimique des eaux du Léman (Éléments majeurs) et données météorologiques. Commission International pour la Protection des Eaux du Léman (CIPEL).
- Berg, P., H. Røy, F. Janssen, V. Meyer, B. B. Jørgensen, M. Huettel, and D. de Beer. 2003. Oxygen uptake by aquatic sediments measured with a novel non-invasive eddy-correlation technique. *Mar Ecol Prog Ser* **261**: 75–83. doi:10.3354/meps261075
- Beutel, M., I. Hannoun, J. Pasek, and K. B. Kavanagh. 2007. Evaluation of Hypolimnetic oxygen demand in a large eutrophic raw water reservoir, San Vicente Reservoir, Calif. *J. Environ. Eng.* **133**: 130–138. doi:10.1061/(ASCE)0733-9372(2007)133:2(130)
- Bierlein, K., M. Rezvani, S. Socolofsky, L. D. Bryant, A. Wüest, and J. C. Little. 2017. Increased sediment oxygen flux in oxygenated lakes: the impact of hypolimnetic oxygenation. Submitted to *Water Resour. Res.*
- Bouffard, D., J. D. Ackerman, and L. Boegman. 2013. Factors affecting the development and dynamics of hypoxia in a large shallow stratified lake: Hourly to seasonal patterns. *Water Resour. Res.* **49**: 2380–2394. doi:10.1002/wrcr.20241
- Bouffard, D., and U. Lemmin. 2013. Kelvin waves in Lake Geneva. *J. Great Lakes Res.* **39**: 637–645. doi:10.1016/j.jglr.2013.09.005
- Brand, A., D. F. McGinnis, B. Wehrli, and A. Wüest. 2008. Intermittent oxygen flux from the interior into the bottom boundary of lakes as observed by eddy correlation. *Limnol. Oceanogr.* **53**: 1997. doi:10.4319/lo.2008.53.5.1997
- Bryant, L. D., C. Lorrai, D. McGinnis, A. Brand, A. Wüest, and J. C. Little. 2010a. Variable sediment oxygen uptake in response to dynamic forcing. *Limnol. Oceanogr.* **55**: 950–964. doi:10.4319/lo.2009.55.2.0950

- Bryant, L. D., D. F. McGinnis, C. Lorrai, A. Brand, J. C. Little, and A. Wüest. 2010b. Evaluating oxygen fluxes using microprofiles from both sides of the sediment-water interface. *Limnol. Oceanogr. Meth.* **8**: 610–627. doi:10.4319/lom.2010.8.0610
- Caudron, A., E. Lasne, C. Gillet, J. Guillard, and A. Champigneulle. 2014. Thirty years of reoligotrophication do not contribute to restore self-sustaining fisheries of Arctic charr, *Salvelinus alpinus*, in Lake Geneva. *Fish. Res.* **154**: 165–171. doi:10.1016/j.fishres.2014.01.023
- CH2011. 2011. Swiss Climate Change Scenarios CH2011. C2SM, Zurich.
- Cole, J. J., and N. F. Caraco. 1998. Atmospheric exchange of carbon dioxide in a low-wind oligotrophic lake measured by the addition of SF₆. *Limnol. Oceanogr.* **43**: 647–656. doi:10.4319/lo.1998.43.4.0647
- Cornett, R. J., and F. H. Rigler. 1979. Hypolimnetic oxygen deficits: Their prediction and interpretation. *Science* **205**: 580–581. doi:10.1126/science.205.4406.580
- Cornett, R. J., and F. H. Rigler. 1980. The areal hypolimnetic oxygen deficit: An empirical test of the model. *Limnol. Oceanogr.* **25**: 672–679. doi:10.2307/2835755
- Delebecque, A. 1898. *Les lacs français*, Typographie Chamerot et Renouard.
- Deville, H. S. C. 1848. Recherches analytiques sur la composition des eaux potables. *Ann. Chim. Phys.* **23**: 32–47.
- Fang, X., and H. G. Stefan. 2009. Simulations of climate effects on water temperature, dissolved oxygen, and ice and snow covers in lakes of the contiguous United States under past and future climate scenarios. *Limnol. Oceanogr.* **54**: 2359–2370. doi:10.4319/lo.2009.54.6_part_2.2359
- Foley, B., I. D. Jones, S. C. Maberly, and B. Rippey. 2012. Long-term changes in oxygen depletion in a small temperate lake: effects of climate change and eutrophication. *Freshwater Biol.* **57**: 278–289. doi:10.1111/j.1365-2427.2011.02662.x
- Forel, F. 1895. *Le Léman: Monographie Limnologique. Tome II. Mécanique, Hydraulique, Thermique, Optique, Acoustique, Chimie*, Lausanne, F. Rouge.
- Gillet, C., and P. Quétin. 2006. Effect of temperature changes on the reproductive cycle of roach in Lake Geneva from 1983 to 2001. *J. Fish Biol.* **69**: 518–534. doi:10.1111/j.1095-8649.2006.01123.x
- Glud, R. N. 2008. Oxygen dynamics of marine sediments. *Mar. Biol. Res.* **4**: 243–289. doi:10.1080/17451000801888726

- Goudsmit, G. H., H. Burchard, F. Peeters, and A. Wüest. 2002. Application of k - ϵ turbulence models to enclosed basins: The role of internal seiches. *J. Geophys. Res.* **107**: 3230. doi:10.1029/2001JC000954
- Hondzo, M., T. Feyaerts, R. Donovan, and B. L. O'Connor. 2005. Universal scaling of dissolved oxygen distribution at the sediment-water interface: A power law. *Limnol. Oceanogr.* **50**: 1667–1676.
- Horppila, J., P. Kõngäs, J. Niemistö, and S. Hietanen. 2015. Oxygen flux and penetration depth in the sediments of aerated and non-aerated lake basins. *Internat. Rev. Hydrobiol.* **100**: 106–115. doi:10.1002/iroh.201401781
- Hubault, E. 1947. Etudes thermiques, chimiques et biologiques des eaux des lacs de l'est de la France (Vosges, Jura, Alpes de Savoie), Berger-Levrault.
- Hutchinson, G. E. 1957. A treatise of limnology. Vol. 1 Geography, Physics and Chemistry, Wiley, New York, New York, USA.
- IPCC. 2013. Climate Change 2013: The Physical Science Basis. Contribution of Working Group I to the Fifth Assessment Report of the Intergovernmental Panel on Climate Change. Cambridge University Press.
- Jenny, J.-P., F. Arnaud, B. Alric, J.-M. Dorioz, P. Sabatier, M. Meybeck, and M.-E. Perga. 2014. Inherited hypoxia: A new challenge for reoligotrophicated lakes under global warming. *Global Biogeochem. Cy.* **28**: 1413–1423. doi:10.1002/2014GB004932
- Jørgensen, B. B., and N. P. Revsbech. 1985. Diffusive boundary layers and the oxygen uptake of sediments and detritus. *Limnol. Oceanogr.* **30**: 111–122. doi:10.2307/2836220
- Jørgensen, B. B., and B. Boudreau. 2001. Diagenesis and sediment-water exchange, p. 211–244. *In The Benthic Boundary Layer*. Oxford University Press.
- Kühl, M., and N. P. Revsbech. 2001. Biogeochemical microsenors for boundary layer studies, p. 180–210. *In The Benthic Boundary Layer*. Oxford University Press.
- Lachavanne, D. P. J.-B. 1980. Les manifestations de l'eutrophisation des eaux dans un grand lac profond: le Léman (Suisse). *Schweiz. Z. Hydrologie* **42**: 127–154. doi:10.1007/BF02502431
- Lemmin, U., and N. D'Adamo. 1997. Summertime winds and direct cyclonic circulation: observations from Lake Geneva. *Ann. Geophys.* **14**: 1207–1220. doi:10.1007/s00585-996-1207-z
- Lemmin, U., C. H. Mortimer, and E. Bäuerle. 2005. Internal seiche dynamics in Lake Geneva. *Limnol. Oceanogr.* **50**: 207–216. doi:10.4319/lo.2005.50.1.0207

- Livingstone, D. M., and D. M. Imboden. 1996. The prediction of hypolimnetic oxygen profiles: a plea for a deductive approach. *Can. J. Fish. Aquat. Sci.* **53**: 924–932. doi:10.1139/f95-230
- Loizeau, J.-L., and J. Dominik. 2005. The history of eutrophication and restoration of Lake Geneva. *Terre et Environnement* **50**: 43–56.
- Lorke, A., B. Müller, M. Maerki, and A. Wüest. 2003. Breathing sediments: The control of diffusive transport across the sediment:water interface by periodic boundary-layer turbulence. *Limnol. Oceanogr.* **48**: 2077–2085. doi:10.2307/3597808
- Lorrai, C., D. F. McGinnis, P. Berg, A. Brand, and A. Wüest. 2010. Application of oxygen eddy correlation in aquatic systems. *J. Atmos. Oceanic Technol.* **27**: 1533–1546. doi:10.1175/2010JTECHO723.1
- Matzinger, A., M. Schmid, E. Veljanoska-Sarafiloska, and others. 2007. Eutrophication of ancient Lake Ohrid: Global warming amplifies detrimental effects of increased nutrient inputs. *Limnol. Oceanogr.* **52**: 338–353. doi:10.4319/lo.2007.52.1.0338
- Matzinger, A., B. Müller, P. Niederhauser, M. Schmid, and A. Wüest. 2010. Hypolimnetic oxygen consumption by sediment-based reduced substances in former eutrophic lakes. *Limnol. Oceanogr.* **55**: 2073–2084. doi:10.4319/lo.2010.55.5.2073
- McGinnis, D. F., P. Berg, A. Brand, C. Lorrai, T. J. Edmonds, and A. Wüest. 2008. Measurements of eddy correlation oxygen fluxes in shallow freshwaters: Towards routine applications and analysis. *Geophys. Res. Lett.* **35**: L04403. doi:10.1029/2007GL032747
- McGinnis, D. F., S. Sommer, A. Lorke, R. N. Glud, and P. Linke. 2014. Quantifying tidally driven benthic oxygen exchange across permeable sediments: An aquatic eddy correlation study. *J. Geophys. Res. Oceans* **119**: 6918–6932. doi:10.1002/2014JC010303
- Molinero, J. C., O. Anneville, S. Souissi, L. Lainé, and D. Gerdeaux. 2007. Decadal changes in water temperature and ecological time series in Lake Geneva, Europe—relationship to subtropical Atlantic climate variability. *Climate Research* **34**: 15–23. doi:10.3354/cr034015
- Molot, L. A., P. J. Dillon, B. J. Clark, and B. P. Neary. 1992. Predicting end-of-summer oxygen profiles in stratified lakes. *Can. J. Fish. Aquat. Sci.* **49**: 2363–2372. doi:10.1139/f92-260
- Monod, R. 1956. Contribution à l'étude des variations de la composition chimique de l'eau du lac Léman: phénomènes de pollution et d'autoépuration à l'embouchure du Flon à Vidy. PhD thesis. Université Lausanne.
- Müller, B., L. D. Bryant, A. Matzinger, and A. Wüest. 2012a. Hypolimnetic oxygen depletion in eutrophic lakes. *Environ. Sci. Technol.* **46**: 9964–9971. doi:10.1021/es301422r

- Müller, B., L. Och, and A. Wüest. 2012b. Entwicklung des Phosphorhaushalts und der Sauerstoffzehrung im Sempacher- und Baldeggersee. Eawag report.
- North, R. P., R. L. North, D. M. Livingstone, O. Köster, and R. Kipfer. 2014. Long-term changes in hypoxia and soluble reactive phosphorus in the hypolimnion of a large temperate lake: Consequences of a climate regime shift. *Glob. Change Biol.* **20**: 811–823. doi:10.1111/gcb.12371
- Nürnberg, G. K. 2002. Quantification of oxygen depletion in lakes and reservoirs with the hypoxic factor. *Lake Reserv. Manage.* **18**: 299–306. doi:10.1080/07438140209353936
- O'Reilly, C. M., S. Sharma, D. K. Gray, and others. 2015. Rapid and highly variable warming of lake surface waters around the globe. *Geophys. Res. Lett.* **42**: 2015GL066235. doi:10.1002/2015GL066235
- Perga, M., Leberre, B., and P. Perney. 2016. Rapport Commission International pour la Protection des eaux du Léman, Campagne 2015: Biomasse chlorophyllienne et production primaire dans le Léman. Commission International pour la Protection des Eaux du Léman (CIPEL).
- Rast, W., and G. F. Lee. 1978. Summary Analysis Of The North American (US Portion) OCED Eutrophication Project: Nutrient Loading - Lake Response Relationships And Trophic State Indices. U.S. Environmental Protection Agency Corvallis, Oregon.
- Rippey, B., and C. McSorley. 2009. Oxygen depletion in lake hypolimnia. *Limnol. Oceanogr.* **54**: 905–916. doi:10.4319/lo.2009.54.3.0905
- Rubin, J.-F. 1992. Biologie de l'omble chevalier (*Salvelinus alpinus*) dans le Léman (Suisse). *Bulletin de la Société Vaudoise des Sciences Naturelles* **82**: 1–10.
- Sahoo, G. B., S. G. Schladow, J. E. Reuter, R. Coats, M. Dettinger, J. Riverson, B. Wolfe, and M. Costa-Cabral. 2012. The response of Lake Tahoe to climate change. *Climatic Change* **116**: 71–95. doi:10.1007/s10584-012-0600-8
- Scavia, D., J. David Allan, K. K. Arend, and others. 2014. Assessing and addressing the re-eutrophication of Lake Erie: Central basin hypoxia. *J. Great Lakes Res.* **40**: 226–246. doi:10.1016/j.jglr.2014.02.004
- Schmid, M., S. Hunziker, and A. Wüest. 2014. Lake surface temperatures in a changing climate: A global sensitivity analysis. *Climatic Change* **124**: 301–315. doi:10.1007/s10584-014-1087-2
- Schwefel, R., A. Gaudard, A. Wüest and D. Bouffard. 2016. Effects of climate change on deepwater oxygen and winter mixing in a deep lake (Lake Geneva): Comparing

- observational findings and modeling. *Water Resour. Res.* **52**(12). doi: 10.1002/2016WR019194.
- Seeberg-Elverfeldt, J., M. Schlüter, T. Feseker, and M. Kölling. 2005. Rhizon sampling of porewaters near the sediment-water interface of aquatic systems. *Limnol. Oceanogr. Methods* **3**: 361–371. doi:10.4319/lom.2005.3.361
- Steinberger, N., and M. Hondzo. 1999. Diffusional mass transfer at sediment-water interface. *J. Environ. Eng.* **125**: 192–200. doi:10.1061/(ASCE)0733-9372(1999)125:2(192)
- Steinsberger, T., M. Schmid, A. Wüest, R. Schwefel, B. Wehrli, B. Müller. 2017. Organic carbon mass accumulation rate regulates the flux of reduced substances from the sediments of deep lakes. In preparation.
- Straile, D., K. Jöhnk, and H. Rossknecht. 2003. Complex effects of winter warming on the physicochemical characteristics of a deep lake. *Limnol. Oceanogr.* **48**: 1432–1438. doi:10.4319/lo.2003.48.4.1432
- Swinbank, W. C. 1951. The measurement of vertical transfer of heat and water vapor by eddies in the lower atmosphere. *J. Meteorol.* **8**: 135–145. doi:10.1175/1520-0469(1951)008<0135:TMOVTO>2.0.CO;2
- Tengberg, A., F. De Bovee, P. Hall, and others. 1995. Benthic chamber and profiling landers in oceanography — A review of design, technical solutions and functioning. *Prog. Oceanogr.* **35**: 253–294. doi:10.1016/0079-6611(95)00009-6
- Thienemann, A. 1928. Der Sauerstoff im eutrophen und oligotrophen See: ein Beitrag zur Seetypenlehre, E. Schweizerbart.
- Torres, N. T., P. C. Hauser, G. Furrer, H. Brandl, and B. Müller. 2013. Sediment porewater extraction and analysis combining filter tube samplers and capillary electrophoresis. *Environ. Sci. Process. Impacts* **15**: 715–720. doi:10.1039/c3em00068k
- Umlauf, L., and U. Lemmin. 2005. Interbasin exchange and mixing in the hypolimnion of a large lake: The role of long internal waves. *Limnol. Oceanogr.* **50**: 1601–1611. doi:10.4319/lo.2005.50.5.1601
- Vivier, P. 1944. Température et oxygène dissous dans le Léman français. *Travaux du laboratoire d'hydrobiologie de l'Université de Grenoble* **20**: 25–35.
- Wang, J., L. Zhao, R. Fan, and H. Wei. 2016. Scaling relationships for diffusive boundary layer thickness and diffusive flux based on in situ measurements in coastal seas. *Progress in Oceanography* **144**: 1–14. doi:10.1016/j.pocean.2016.03.001

Zhang, J., D. Gilbert, A. Gooday, and others. 2010. Natural and human-induced hypoxia and consequences for coastal areas: synthesis and future development. *Biogeosciences* 7: 1443–1467. doi:10.5194/bg-7-1443-2010

Chapter 2:

Scaling oxygen microprofiles at the sediment interface of deep stratified waters

Robert Schwefel¹, Miki Hondzo², Alfred Wüest^{1,3}, Damien Bouffard^{1,3}

¹ Physics of Aquatic Systems Laboratory, Margaretha Kamprad Chair, Ecole Polytechnique Fédérale de Lausanne, Institute of Environmental Engineering, CH-1015 Lausanne, Switzerland.

² Department of Civil, Environmental, and Geo-Engineering, St. Anthony Falls Laboratory, University of Minnesota, Minneapolis, USA.

³ Eawag, Swiss Federal Institute of Aquatic Science and Technology, Surface Waters – Research and Management, Kastanienbaum, Switzerland.

Geophysical Research Letters **44**

Robert Schwefel performed the fieldwork, the analysis of the results and the writing of the manuscript. Miki Hondzo contributed to the analysis of the results and the writing and revision of the manuscript. Damien Bouffard contributed to the fieldwork, the analysis of the results and the manuscript revision. Alfred Wüest contributed to the analysis of the results and the manuscript revision.

Abstract

Dissolved oxygen microprofiles at the sediment-water interface of Lake Geneva were measured concurrently with velocities 0.25 to 2 m above the sediment. The measurements and scaling analyses indicate dissolved oxygen fluctuations and turbulent fluxes in exceedance of molecular diffusion in the proximity of the sediment-water interface. The measurements allowed the parametrization of the turbulent diffusion as a function of the dimensionless height above the sediment and the turbulence above the sediment-water interface. Turbulent diffusion depended strongly on the friction velocity and differed from formulations reported in the literature that are based on concepts of turbulent and developed wall-bounded flows. The dissolved oxygen microprofiles and proposed parameterization of turbulent diffusion enable a foundation for the similarity scaling of oxygen microprofiles in proximity to the sediment. The proposed scaling allows the estimation of diffusive boundary layer thickness, oxygen flux, and oxygen microprofile distribution in the near-sediment boundary layer.

2.1. Introduction

Decreasing dissolved oxygen (DO) content of the world's oceans and lakes has gained significant attention in the research community (*Diaz and Rosenberg 2008, Keeling et al., 2010, Bouffard et al. 2013, Donnadieu et al. 2016*). The reduction in DO has been attributed to climate change and increased anthropogenic nutrient inputs (*Föllmi et al. 2012, Monteiro et al. 2012, Friedrich et al. 2014*). Deoxygenation in deep waters along the bottom boundary layer (BBL) is especially prone to the synergistic effects of climate change, including: increasing average water temperature, strength of water column stratification, and accelerated nutrient cycling (*Yoh et al. 1983, Gudas et al. 2010, Donnadieu et al. 2016*). Turbulence above the sediment-water interface (SWI) amplifies DO dynamics, changing the sediment oxygen uptake (SOU) which depends on the supply of the DO fluxes from the BBL to the sediments (*McGinnis et al. 2008, Scalo et al. 2013, Steele et al. 2016*). SOU is important for the DO budgets in stratified waters, as much of the organic matter decomposition occurs close below the SWI.

Current models for DO depletion typically assume a constant SOU which is independent of BBL oxygen concentration and dynamics. While this simple approach often provides useful results, it relies on lake-dependent calibration. The inclusion of BBL dynamics in DO depletion models will lead to more realistic parameterizations.

Our objective was to find a similarity scaling for near-sediment DO microprofiles and SOU based on high-resolution (< 0.1 mm) DO measurements. Following Fick's first law, DO flux was estimated from the DO gradient and molecular diffusivity (*Jørgensen and Revsbech 1985, Jørgensen and Des Marais 1990, Steinberger and Hondzo 1999*] in the thin region above the SWI, where molecular diffusion is the dominant transport process. This thin region is called diffusive boundary layer (DBL) with thickness δ_{DBL} . Various field studies have revealed a high dependency of DBL dynamics on BBL currents, which influence δ_{DBL} and the corresponding DO transport to the sediments (*Lorke et al. 2003, Bryant et al. 2010a, Bryant et al. 2010b, Horppila et al. 2015*].

We measured DO concentration microprofiles at the SWI of Lake Geneva at ~ 100 and ~ 130 m depth with $100 \mu\text{m}$ resolution. Concurrently, velocities were measured close to the SWI from 0.25 to 2.0 m above the bottom in close proximity to the microprofiler. The analysis of the results enabled a similarity scaling of the eddy diffusivity and DO microprofiles above the SWI. The

proposed scaling provides (i) the parameterization of turbulent diffusion, (ii) the thickness of the DBL (), (iii) the DO flux, and (iv) the DO vertical distribution above the SWI.

2.2 Materials and methods

2.2.1 Study site

The measurement sites were located in the northern part of Lake Geneva, a deep perialpine lake between France and Switzerland (6.523 oE, 46.496 oN and 6.519 oE, 46.487 oN, Figure 1). We report the results of two measurement campaigns with similar instrumentation setups. The first measurement was conducted in July 2014, at a depth of 109 m, the second in July 2015, at a depth of 133 m (Table 1). At both sites, the bottom slope is ~5% and the bed contains silty sediments and relatively thin oxic zones in the top few millimeters of the sediment surface.

2.2.2 Oxygen microstructure measurements

Concentrations of DO were quantified using a MP4/8 Microprofiler (Unisense A/S) equipped with Clark-type DO microsensors (Figure 2.1d). The sensor tip size was ~100 μm with a DO detection limit of 0.01 mg L^{-1} . The spatial resolution of the measurements is of the same size as the sensor tip. An optode (Aanderaa), sampling every 15 s, was positioned outside of the DBL to provide background DO time series during the operations of the MP4/8 Microprofiler. We performed a two-point calibration of the DO microsensors in the field by using the *in situ* data from the optode as the upper reference point and the anoxic sediment as the lower reference point.

During an initial stage of detection, the microsensor was lowered continuously until the DO signal was reduced to 60% of the bulk concentration (C_B) outside the DBL. The reduction of the DO concentration indicated the proximity of the SWI. Afterward, the sensors were raised by ~7 mm where the high-resolution DO microprofile measurements were initiated in steps of 100 μm (precision of motor: 50 μm). The stepper motor stopped for 12 s at each level to ensure steady-state conditions. Afterwards, six DO measurements were performed at 1.0 Hz sampling rate at the specified depth. The exact position of the SWI was determined from the change in gradient of the measured DO concentration. In addition, analysis of the DO concentration variance provided supporting evidence for the correct position of the SWI.

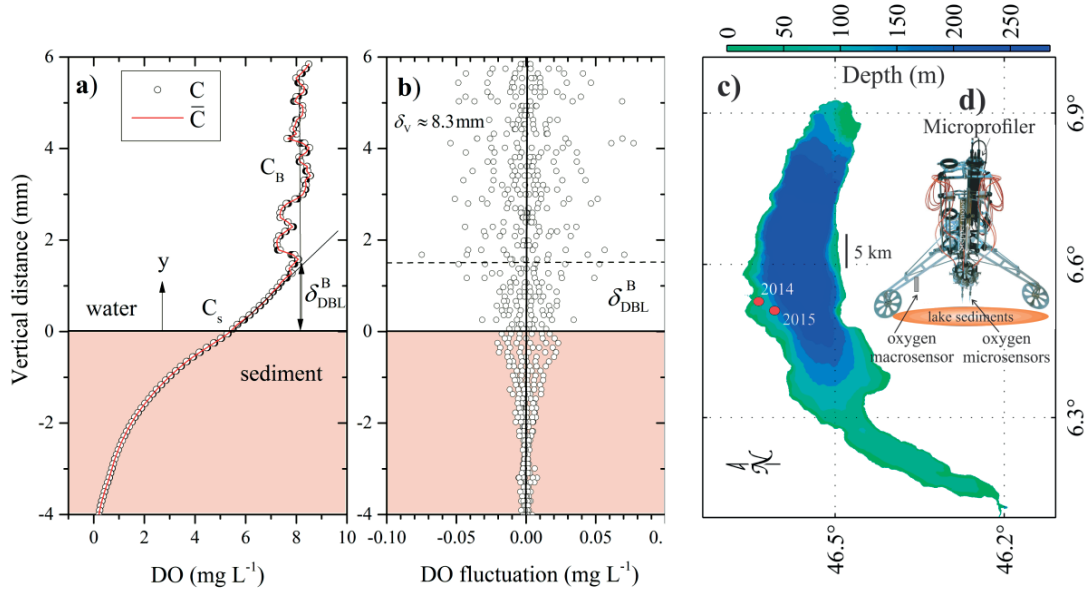


Figure 2.1: Example of a measured dissolved oxygen (DO) concentration microstructure profile at the sediment-water interface (SWI) of Lake Geneva. a) The vertical profiles of time-averaged DO concentrations (\bar{C}) with a schematic of DO gradient at the SWI (sloped solid line) and bulk DO concentration (C_B , vertical solid line). The intersection of the two solid black lines defines the upper height of the diffusive boundary layer (DBL) thickness (δ_{DBL}^B). b) The vertical distribution of corresponding instantaneous DO fluctuations ($C' = C - \bar{C}$) with the extent of the viscous sublayer (δ_v) above the sediment. c) Map of the two Lake Geneva sampling sites in 2014 and 2015 and the depth contours. d) Photograph of MP4/8 Microprofiler with DO sensors.

2.2.3 Current measurements

An upward-looking 2 MHz acoustic-Doppler current profiler (ADCP; Nortek Aquadopp) was deployed nearby on the lakebed. Currents were measured in 36 bins of 5 cm size each. The blanking distance, including the height of the instrument frame, was 21.5 cm. This setup enabled a three-dimensional measurement of the current over the vertical distance from ~ 0.25 m to ~ 2.0 m above the SWI. Data were acquired in burst mode with 1024 samples at 1.0 Hz sampling frequency every 20 min. During the post-processing, the strength of the acoustic signal was verified, and the recorded velocities were time-averaged. The distance between the ADCP and the MP4/8 Microprofiler was ~ 35 m (2015; 12 profiles) and ~ 100 m (2014; 2 profiles). Hence, the distance was large enough to exclude interference between the instruments. Systematic

deviation in the DO fluctuations with current velocity, which could indicate disturbance from the instruments, was not observed. Recent multibeam bathymetry measurements (the method is presented in Kremer et al., 2015) did not show significant local changes in the bathymetry close to the measurement locations.

2.2.4 Dissolved oxygen microprofile and fluxes at the sediment-water interface

A conventional method for relating estimates of the water-side DO flux, J_{wD} , to local DO gradients at the SWI is provided by Fick's first law

$$J_{wD} = -D \left. \frac{dC}{dy} \right|_{y=0} \quad (2.1)$$

where D is the molecular diffusion coefficient for DO, C is the DO concentration, y is the vertical distance (Figure 2.1a), and $\left. \frac{dC}{dy} \right|_{y=0}$ is the local DO gradient at the SWI. Similarly, in the water column, further away from the SWI, the turbulent DO flux, J_{wE} , is estimated by

$$J_{wE} = -E \left. \frac{d\bar{C}}{dy} \right|_y \quad (2.2)$$

where E is the turbulent diffusion coefficient for DO transport at distance y , and \bar{C} is the time-averaged DO concentration. The total DO flux, J_w , is the sum of molecular and turbulent diffusion processes which are defined analogous to Fick's first law as

$$J_w = -(D + E) \frac{d\bar{C}}{dy} = -E_t \frac{d\bar{C}}{dy} \quad (2.3)$$

where $E_t = D + E$ is the total diffusion coefficient.

In the absence of significant DO sinks in the DBL, J_{wD} and J_w are equal. Above the DBL, the ratio of the concentration gradients defines E_t/D (Higashino et al. 2008)

$$\frac{E_t}{D} = \frac{\left. \frac{d\bar{C}}{dy} \right|_{y=0}}{\left. \frac{d\bar{C}}{dy} \right|_y} \quad (2.4)$$

where $f = \frac{\bar{C} - \bar{C}_S}{\bar{C}_B - \bar{C}_S}$ is the DO concentration similarity group with \bar{C}_S as the time-averaged concentration at the SWI, and \bar{C}_B as the time-averaged bulk concentration in the BBL (Steinberger and Hondzo 1999).

In turbulent wall-bounded flows, the non-dimensional vertical distance reads $y^+ = \frac{y u_*}{\nu}$, where u_* is the friction velocity (Figure S2.1), and ν is the kinematic viscosity. Defining a non-dimensional DO concentration by

$$C^+ = \frac{(\bar{C} - \bar{C}_S) u_*}{J_w} \quad (2.5)$$

we can integrate equation (2.3) and obtain at height y^+

$$C^+ = - \int_0^{y^+} \frac{dy^{+'}}{\frac{1}{S_c} + \frac{E}{\nu}} \quad (2.6)$$

where $S_c = \nu/D$ is the Schmidt number [Dade, 1993; Hondzo et al., 2005]. To derive a scaling expression for C^+ against y^+ , a functional dependence of E_t/ν versus y^+ is required. We conducted field measurements to quantify DO microprofiles, currents (u , u_*), and subsequently develop the functional relationship between E_t/ν and the vertical distance above the SWI.

2.3. Results and discussion

2.3.1 Current measurements

Figure S2.1 represents longitudinal time-averaged vertical velocity profiles, starting with the first bin ~ 0.25 m above the SWI. Each symbol depicts a time-averaged velocity over one burst of 1024 s. The average thickness of the BBL, the height at which $\bar{u} = 0.99 \bar{u}_{\max}$, with \bar{u}_{\max} being the maximum velocity over the measured profile, was ~ 1.7 m. The overall depth-averaged

longitudinal velocity was 0.017 m s^{-1} with the maximum of 0.030 m s^{-1} . In the proximity of the SWI, the longitudinal velocities followed most of the time the turbulent log-law velocity profile, typical for a smooth bed, with $\frac{\bar{u}}{u_*} = \frac{1}{\kappa} \ln\left(\frac{yu_*}{\nu}\right) + B$ (Figure S2.1) where κ is the von Kármán constant, and B is an additive constant. The slope of the longitudinal velocity against $\ln(y^+)$ with the coefficient of determination $> 95\%$ were used to estimate u_* for the depicted velocity profiles (Table 2.1). For very low flows, velocity profiles did not follow the log-law (Lorke *et al.* 2002), which occurred particularly often during the first measurement campaign. Those measurements were omitted in this study. Using the averaged longitudinal velocity and BBL thickness, the Reynolds number was approximately 20000 indicating turbulent conditions. Lorke *et al.* [2002] showed that logarithmic velocity profiles were not observed for velocities below one cm s^{-1} , which was never the case in the profiles used in this study. The viscous sublayer thickness at the SWI, $\delta_v \approx 11 \frac{\nu}{u_*}$ (Wüest and Lorke 2003) ranged from 4 mm to 23 mm (Table 2.1). Due to the 21.5 cm blanking distance of the ADCP, the current measurements do not include the region of the viscous sublayer. With a friction velocity of $u_* \approx 3 \text{ mm s}^{-1}$, however, it takes only about five minutes for currents at a distance of $\sim 1 \text{ m}$ above the SWI to adjust to local sediment roughness. Since the ADCP measurements were averaged over one burst (1024 s; averaging over two bursts or only 600 s did not change the results significantly), u_* calculated from measured velocity gradients is a good estimate of turbulence close to the SWI. δ_v was significantly larger than the grain size of the sediment (typically $\sim 0.05 \text{ mm}$), which justified the smooth bed assumption for the SWI.

The time-averaged longitudinal velocity was approximately logarithmic from a minimum vertical distance of $y^+ = 140$ to the maximum distance of $y^+ = 4000$. The minimum vertical distance of the log-layer to the SWI was consistent with the condition of $y^+ > 30$, typical for turbulent wall-bounded flows (George 2007). The deviation from logarithmic behavior at maximum vertical distance was observed at an average distance of about $y^+ = 1800$. The flow was not fully developed; rather, it experienced acceleration and deceleration phases as typical for geophysical BBL flows (Lorke *et al.* 2003, Scalo *et al.* 2013). Low bottom velocities governed by the Poincaré waves with a period of $\sim 10 \text{ hrs}$ were detected. The existence of logarithmic velocity profiles, which are triggered by internal Poincaré and Kelvin waves in Lake Geneva, is in

accordance with the field measurements of *Bouffard and Lemmin* (2013). The analyses of spectral densities of longitudinally fluctuating velocities in the logarithmic region depicted the “5/3” inertial subrange over periods from 5 to 100 s and indicated turbulent flow in the proximity of the sediment.

2.3.2 Oxygen microprofiles

Fourteen DO microprofiles were collected for different flows above the SWI under log-law conditions. For each profile, the SWI was located from the change in the DO gradient due to the different diffusion coefficients in the water and sediment (*Røy et al.* 2004). The position of the SWI was set to $y = 0$. Figure 2.1a depicts a typical measured DO microprofile. Other examples are shown in Figure S2.2. In the water column above the SWI ($y > 3$ mm), time-averaged DO concentration profiles (\bar{C}) were almost constant. Although, well below the upper height of the viscous sublayer ($\delta_v \approx 8.3$ mm) the instantaneous DO concentrations (C) showed fluctuations. These fluctuations ($C' = C - \bar{C}$) with an absolute magnitude of up to 0.08 mg L^{-1} and a standard deviation of 0.01 to 0.03 mg L^{-1} above the SWI indicated appreciable high-frequency fluctuations in the DBL (Figure 2.1b). In the very proximity of the SWI ($y < 2$ mm) \bar{C} decreased towards the sediments due to the DO consumption in the sediments. In this region, the time-averaged DO profile approaches a straight line and intersects the bulk time-averaged DO concentration (\bar{C}_B) at the vertical distance δ_{DBL}^B from the SWI. The δ_{DBL}^B provides a basis for the customary estimation of water-side DO flux (1), which can be approximated by $J_{WD} \approx -\frac{D}{\delta_{DBL}^B}(\bar{C}_B - \bar{C}_S)$ at the SWI.

The fundamental premise of the flux estimation is that the DO concentration gradient at the SWI (equation 2.1) is accurately estimated by $\left. \frac{dC}{dy} \right|_{y=0} \approx \frac{(\bar{C}_B - \bar{C}_S)}{\delta_{DBL}^B}$ whereas molecular diffusion is the dominant transport mechanism of DO. However, fluctuations of DO were consistently detected within δ_{DBL}^B in all field data (Figure 2.1b). A distinct fluctuation maximum at the SWI, reported by *Røy et al.* (2004) in laboratory experiments, was not observed. Instead, C' remained high above δ_{DBL}^B and decreased within the DBL. The source of these fluctuations might be turbulent transport in proximity to the DBL or lateral variability of DO concentration above the DBL

which is transported downwards toward the SWI. The increase in turbulent diffusion (see section 2.3.3) very close to the DBL is, however, an indication of turbulent transport processes. Nonlinear concentration gradients close to the SWI were also reported in several other studies (Nishihara and Ackerman 2007, Hondzo et al. 2005, O'Connor and Hondzo 2008). Below, the SWI ($y < -1$ mm), the DO fluctuations were reduced to the precision of the DO sensors (~ 0.01 mg L⁻¹).

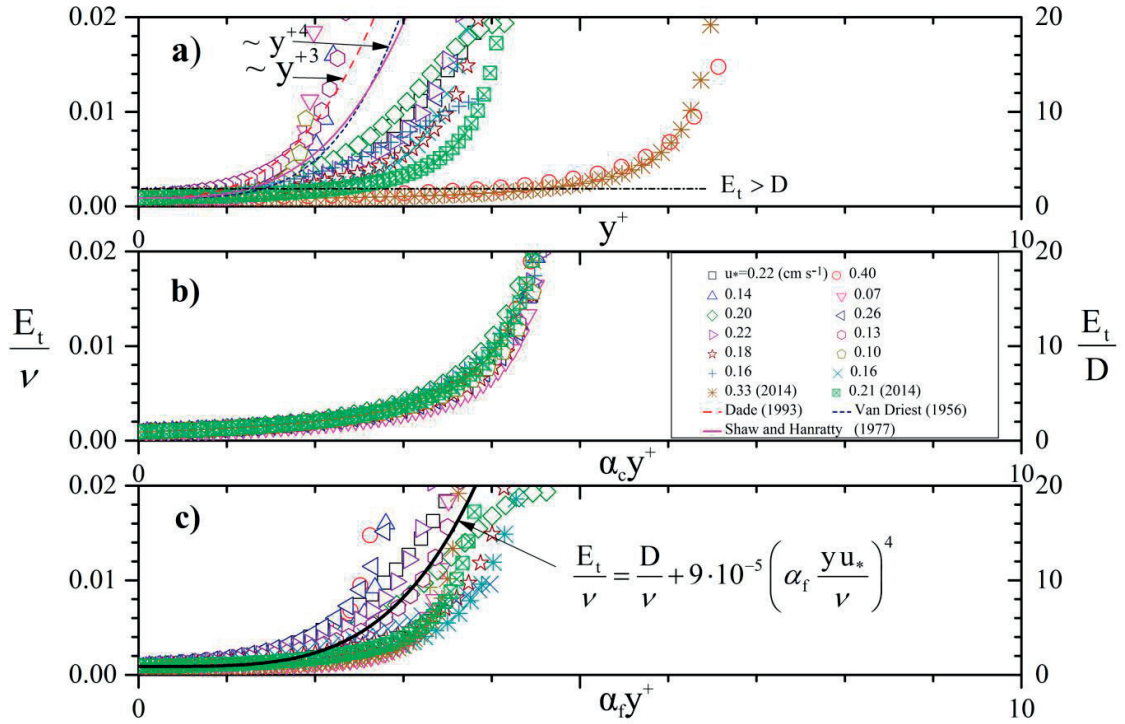


Figure 2.2: Dimensionless total diffusion (molecular and eddy) coefficient ($\frac{E_t}{\nu}$) variability against the dimensionless vertical distance above the SWI. a) The traditional scaling of $\frac{E_t}{\nu}$ against the wall units $y^+ = \frac{y u_*}{\nu}$. The data is compared to three parameterizations used in the literature. b) $\frac{E_t}{\nu}$ against the stretched wall units, $\alpha_c y^+$, where α_c is a constant (order ~ 1), different for each profile of $\frac{E_t}{\nu}$. c) $\frac{E_t}{\nu}$ against the predicted wall units, $\alpha_f y^+$, where $\alpha_f = 16 \cdot \exp(-21 \text{Re}_{\eta_B})$. $\text{Re}_{\eta_B} = \frac{u_* \eta_B}{\nu}$ is the Reynolds number defined by the Batchelor length scale ($\eta_B = (\frac{\nu D^2}{\epsilon})^{1/4}$, where D is the molecular DO diffusion coefficient, and ϵ is the energy dissipation rate).

Table 2.1. Summary of measured and estimated field variables. u_* is the shear velocity estimated using the 14 Aquadopp current profiles, ε is the rate of energy dissipation, δ_v is the viscous sublayer thickness, η_B is the Batchelor length scale, δ_{DBL}^B is the DBL thickness based on the bulk DO concentration and the DO gradient at the SWI, $\delta_{DBL}^{E_t}$ is the DBL thickness estimated based on the exceedance of E_t over 110% of the molecular diffusivity D . J_w is the water-side DO flux to the sediments, and J_s is the sediment-side DO uptake. The kinematic viscosity of lake water at the average temperature of 6 °C was $\nu = 1.48 \text{ mm}^2 \text{ s}^{-1}$, and the molecular diffusivity of DO was $D = 1.32 \times 10^{-3} \text{ mm}^2 \text{ s}^{-1}$.

u_*	ε	δ_v	η_B	δ_{DBL}^B	$\delta_{DBL}^{E_t}$	J_w	J_{mod}	J_s
(mm s^{-1})	($\text{mm}^2 \text{ s}^{-3}$)	(mm)	(mm)	(mm)	(mm)	($\text{g m}^{-2} \text{ day}^{-1}$)	($\text{g m}^{-2} \text{ day}^{-1}$)	($\text{g m}^{-2} \text{ day}^{-1}$)
2.2	4.30×10^{-2}	7.5	0.09	1.9	1.0	0.22	0.27	0.21
4.0	2.49×10^{-1}	4.1	0.06	1.9	1.1	0.26	0.32	0.25
1.4	1.07×10^{-2}	11.8	0.12	2.7	1.3	0.13	0.17	0.14
0.7	1.12×10^{-3}	23.6	0.22	4.1	3.3	0.16	0.17	0.16
2.0	3.76×10^{-2}	8.3	0.09	1.7	0.8	0.22	0.20	0.26
2.6	6.83×10^{-2}	6.4	0.08	1.5	0.8	0.18	0.16	0.26
2.2	4.30×10^{-2}	7.5	0.09	1.4	0.9	0.26	0.23	0.29
1.3	1.27×10^{-2}	12.7	0.12	2.1	1.0	0.23	0.25	0.24
1.8	2.33×10^{-2}	9.2	0.10	1.7	1.3	0.29	0.24	0.31
1.0	5.43×10^{-3}	16.5	0.15	2.9	2.2	0.14	0.11	0.18
1.6	1.62×10^{-2}	10.3	0.11	2.4	1.1	0.15	0.18	0.16
1.6	1.75×10^{-2}	10.3	0.11	1.5	1.7	0.27	0.20	0.29
3.3	1.44×10^{-1}	5.0	0.07	1.2	1.1	0.24	0.38	0.20
2.1	3.81×10^{-2}	7.9	0.09	2.1	1.6	0.26	0.32	0.22

2.3.3 Power-Law Scaling

The DO concentration microprofiles and equation (2.4) provided the basis for estimating diffusion coefficients at the SWI (Figure 2.2a). The profiles were fit with a 3rd degree polynomial ($R^2 > 0.85$ and with three exceptions $R^2 > 0.98$) and its derivative at height y and

height 0 were used to determine $\frac{E_t}{D} = \frac{\frac{df}{dy}|_{y=0}}{\frac{df}{dy}|_y}$. Values of E_t were determined precisely in

the DBL and in the lower transition zone above the DBL but not reliably further above since the change in DO concentration due to natural fluctuations became too high. The customary

approach to scaling is to seek a functional relationship $\frac{E_t}{\nu}$ versus y^+ (*Van Driest* 1956, *Shaw and Hanratty* 1977, *Dade* 1993). Figure 2.2a displays considerable variability of $\frac{E_t}{\nu}$ against y^+

and lack of similarity of profiles for different flows. The vertical scale on the right y-axis shows the equivalent $\frac{E_t}{D}$ variability and indicates that the turbulent diffusion exceeds the molecular

already at $y^+ < 3$ in the majority of profiles (Figure 2.2a, horizontal dotted line). The reported parameterizations of $\frac{E_t}{\nu}$ were found under laboratory conditions for developed turbulent flows,

which do not necessarily hold under field conditions in stratified waters. Near the SWI of

developed flows, $\frac{E_t}{\nu}$ scales as y^{+4} [*Van Driest*, 1956] or $\frac{E_t}{\nu} \sim y^{+3}$ (*Dade* 1993). To account

for the modulating effects of developing flows, a parameterization of $\frac{E_t}{\nu}$ versus “stretched”

wall units, $\alpha_c y^+$ was investigated (Figure 2.2b). The constant α_c was selected for each profile of

$\frac{E_t}{\nu}$ so that $\frac{E_t}{\nu}$ scales universally with $\alpha_c y^+$. α_c was of the order of 1, and had a strong

functional dependence on the Reynolds number ($Re_{\eta_B} = \frac{u_* \eta_B}{\nu}$), which is based on u_* and the

Batchelor microscale ($\eta_B = \left(\frac{\nu D^2}{\varepsilon} \right)^{1/4}$). The energy dissipation, ε , was determined by using the

log-law estimation, $\varepsilon \sim \frac{u_*^3}{\kappa y}$, averaged over the logarithmic region of the corresponding velocity profiles [O'Connor et al., 2009] (Table 1). The choice of another expression for ε , e. g. closer to the sediment depth [Lorke et al., 2003; Inoue et al., 2008] would not change the proportionality of α_c to u_*^3 . A fit of α_c as a function of Reynolds number resulted in $\alpha_f = 16 \cdot \exp(-21 \cdot \text{Re}_{\eta_B})$, which explained 85% of the variability of α_c (Figure S2.3). The new parameterization $\frac{E_t}{\nu}$ versus $\alpha_f y^+$ is depicted in Figure 2.2c. The scaling relationship $\frac{E_t}{\nu} \sim (\alpha_f y^+)^4 \sim (16 \cdot \exp(-21 \cdot \text{Re}_{\eta_B}) \cdot y^+)^4$ (Figure 2.2c) suggests that the total diffusivity has abrupt variations within the DBL and is much less pronounced in the developed flows far outside the DBL. The sharp increase in the dispersive transport of DO (including total diffusive transport and additional advective transport which scales with u_*) causes apparent variability in DO microprofiles, which is depicted by the varying slopes in the transition region from DBL to C_B (Figure 2.1a). We have observed similar transition patterns in several vertical microstructure DO profiles of Lake Geneva and other lakes [Bryant et al., 2010a, 2010b].

δ_{DBL} was estimated from the measured DO microprofiles following the above described conventional approach of Jørgensen and Revsbech (1985), based on the local time-averaged DO gradient at the SWI and the bulk DO concentration in the water column (Table 2.1, δ_{DBL}^B). The thickness δ_{DBL}^B ranged from 1.2 to 4.1 mm. In addition, we defined $\delta_{\text{DBL}}^{E_t}$ as the layer at which E_t exceeds D by 10%, indicating the region in which molecular diffusion is dominant. The estimates of $\delta_{\text{DBL}}^{E_t}$ are provided in Table 2.1. The thickness ranged from 0.8 mm to 3.3 mm. The average of δ_{DBL}^B was 50% larger than the corresponding $\delta_{\text{DBL}}^{E_t}$. Figure 2.3 displays the functional dependence of $\delta_{\text{DBL}}^{E_t}$ and δ_{DBL}^B versus the Batchelor scale η_B . We observe a linear increase of $\delta_{\text{DBL}}^{E_t}$ against the Batchelor scale, with the coefficient of determination 76%, as described by

$$\frac{\delta_{\text{DBL}}^{E_t}}{\eta_B} = 13 \quad (2.7)$$

Equation (2.7) allows to estimate the DBL thickness solely based on current measurements. A similar functional dependence of $\delta_{\text{DBL}}^{\text{B}}$ on η_{B} was suggested by Lorke et al. [2003]. The vertical extent of “y” was considered in the region with the log-law velocity distribution. The proposed functional relationship of E_{t}/ν versus y^+ was substituted into equation (2.6), the integral was split into the region with dominance of molecular diffusion and the region with dominance of turbulent diffusion, and upon integration, the following scaling expression for the distribution of DO with distance from the SWI was obtained:

$$\bar{C}^+ = y^+ S_{\text{c}} \quad \delta_{\text{DBL}}^+ > y^+ > 0 \quad (2.8a)$$

$$\bar{C}^+ = \delta_{\text{DBL}}^+ S_{\text{c}} + B \left(\frac{1}{\delta_{\text{DBL}}^{+3}} - \frac{1}{y^{+3}} \right) \quad y^+ \geq \delta_{\text{DBL}}^+ \quad (2.8b)$$

where $B = 0.05 \exp(84Re_{\eta_{\text{B}}})$, and $\delta_{\text{DBL}}^+ = \frac{\delta_{\text{DBL}}^{\text{E}_t} u_*}{\nu}$ with $\delta_{\text{DBL}}^{\text{E}_t}$ defined as the thickness, at which E_{t} exceeds D by 10%. In Figure 2.4a the measured DO profiles are compared to the proposed scaling (equation 2.8). Within δ_{DBL}^+ , the data is universally scaled by equation (2.8a) and indicates that the slope of $(\bar{C} - \bar{C}_{\text{s}})$ versus y provides the estimate of water-side DO flux (J_{w}). An estimate of sediment-side DO uptake (J_{s}) was determined by the *in situ* microstructure sediment data (Figure 2.1a) and the algorithm proposed by Berg et al. [1998]. The very porous first millimeter of the sediment was parameterized with a porosity of $\phi = 0.98$, and set to $\phi = 0.90$ below in the sediment (e.g. Bryant et al. 2010b). The diffusivity in the sediment (D_{S}) was calculated as $D_{\text{S}} = \phi D$ (Bryant et al. 2010b). Bioirrigation and oxygen production was assumed to be negligible in the sediment. The two independent estimates of J_{w} and J_{s} were similar confirming our estimate of J_{w} and indicating quasi steady-state flux conditions under which J_{w} was balanced by the corresponding J_{s} within the sediment (Table 2.1). An average time scale over which DO was transported across $\delta_{\text{DBL}}^{\text{E}_t}$ by molecular diffusion was $\frac{(\delta_{\text{DBL}}^{\text{E}_t})^2}{D} \sim 20$ min, and close to the total duration of sampling DO and currents in the field. Outside the DBL ($y^+ > \delta_{\text{DBL}}^+$), the proposed scaling (equation 2.8b) described data well (Figure 2.4a). One example of the proposed scaling and comparison with the data is depicted by the dotted black line.

Researchers often face the challenging questions of how to estimate J_w and DBL based on limited DO data. The proposed DO scaling (equation 2.8b) has two free parameters (J_w , δ_{DBL}^+) for given u_* and enables an estimate of the parameters by the limited DO data outside the δ_{DBL}^+ .

Furthermore, using equation (2.7) to estimate δ_{DBL}^+ and equation (2.8b) to calculate C^+ based

solely on current data, $J_{mod} = \frac{(\bar{C} - C_s)u_*}{C^+}$ can then be determined only from the DO

concentration in the mixed layer above the BBL and C_s . Using the measured values of C_s the modeled DO fluxes were very close to those derived from the measured microprofiles (Table 2.1). For an accurate description of the DO concentration at the SWI, the biological conditions at the sediment surface have to be considered. Monod's kinetic model can be implemented to describe microbial growth and associated oxygen uptake in the sediment to calculate C_s (Nakamura and Stefan 1994; Higashino *et al.*, 2008). However, even if the variation in C_s is neglected and a time-averaged concentration at the sediment surface is assumed instead, the observed fluxes are still close to the measured ones (Figure 2.4b) since the variability in the DO profiles is larger above the SWI than in the sediment (Scalo *et al.* 2013). Based on current data only, the proposed scaling is appropriate to the modeling of DO microprofiles and provides a description of the physical control of SOU. The directly measured rates of sediment oxygen uptake and those estimated from equations (2.7) and (2.8) are depicted in Figure 2.4b.

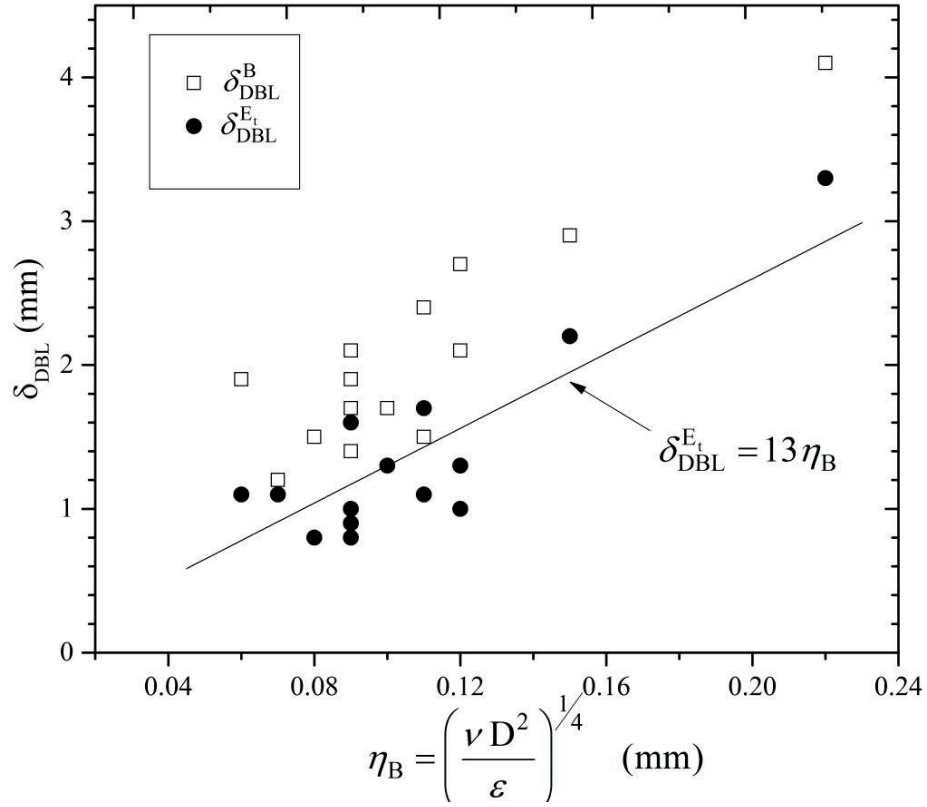


Figure 2.3: Dependence of DBL thickness on Batchelor scale at which DO fluctuations are smoothed by molecular diffusion. δ_{DBL}^B is the DBL thickness based on the bulk DO concentration and local time-averaged micro-oxygen concentration gradient at the SWI, $\delta_{DBL}^{E_t}$ the DBL thickness over which molecular diffusion dominates at the SWI.

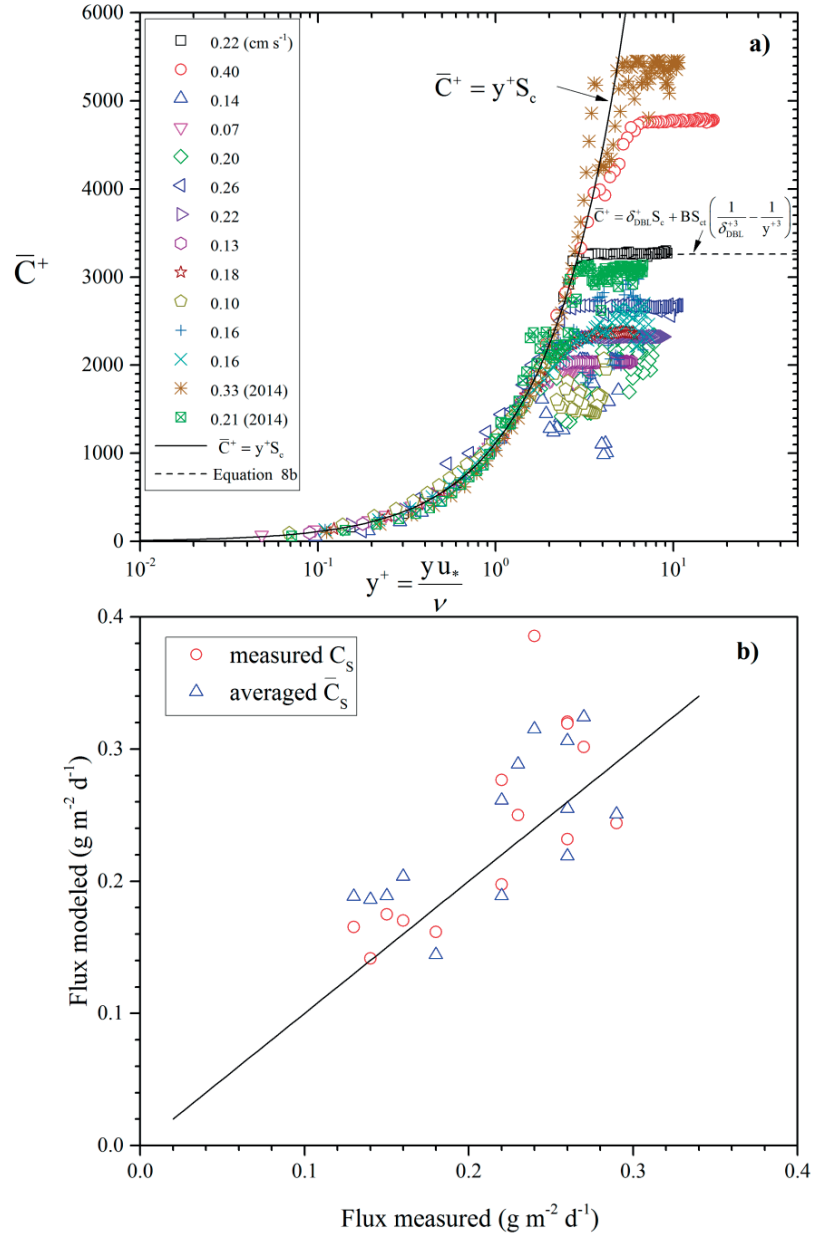


Figure 2.4: a) Measured and predicted near-sediment profiles of the dimensionless DO concentration ($C^+ = \frac{(\bar{C} - C_s)u_*}{J_w}$). The proposed scaling relationships are depicted within the DBL ($\bar{C}^+ = y^+ S_c$; $\delta_{DBL}^+ > y^+ > 0$) and in the water column above the DBL ($\bar{C}^+ = \delta_{DBL}^+ S_c + B \left(\frac{1}{\delta_{DBL}^{+3}} - \frac{1}{y^{+3}} \right)$; $y^+ \geq \delta_{DBL}^+$). S_c is the Schmidt number, S_{ct} is the turbulent Schmidt number, $\delta_{DBL}^+ = \frac{\delta u_*}{\nu}$ is the dimensionless DBL thickness, and $B = 0.05 \cdot \exp(84 \text{Re}_{\eta_B})$. $\text{Re}_{\eta_B} = \frac{u_* \eta_B}{\nu}$ is the Reynolds number defined by the Batchelor scale.

b) Flux of oxygen into the sediment calculated by equation (2.8) using δ_{DBL}^+ calculated by equation (2.7) as function of the measured fluxes J_w . The circles show the results using the measured oxygen concentration at the sediment as C_s , and the triangles use the time-averaged \bar{C}_s .

2.4. Conclusions

Simultaneous DO microprofile and ADCP measurements were performed in the BBL in the hypolimnion of Lake Geneva. The velocity profiles revealed, despite low (2 to 3 cm s⁻¹) currents, a turbulent flow with log-layer characteristics and traditionally-estimated DBL thickness of 1.2 to 4.1 mm. However, the sub-millimeter scale DO profile measurements demonstrated concentration fluctuations even within the DBL, where the conventional approach advocates molecular diffusion as dominant mechanism of DO flux to the sediments. Estimations of eddy diffusivity in proximity to the SWI showed that commonly used scaling functions derived under developed flow conditions do not apply for stratified natural waters and that eddy diffusion plays an important role for the DO transport close to the SWI. Accurate flux estimation based on measured DO concentration profiles depends on adequate measurement spatial resolution. Similar findings were reported for the estimates of heat flux through the double-diffusively convective layers in Lake Kivu. Estimating the fluxes in the molecular center of the interfaces (Sommer *et al.* 2013) provided 5-times larger values than a linear fit across the entire interfaces (Schmid *et al.* 2010), which are “contaminated” by turbulent fluctuations. Therefore, the risk of underestimating molecular fluxes applies to any turbulent-molecular transition region.

A new functional relationship between E_t / ν and the dimensionless height above the sediment was established based on the field data. E_t was not only proportional to y^{+n} . Instead, a factor depending on the turbulence above the SWI was necessary to obtain a scaling parametrization for eddy diffusivity. Based on this study, it is not possible to determine if this is a general phenomenon for low-turbulence conditions or caused by the dominant forcing by basin-scale internal waves typical for Lake Geneva. Using the relationship between E_t and u_* , a universal scaling law for C^+ can be derived. δ_{DBL} was shown to be dependent on the turbulence conditions in the BBL above the SWI. Based on this dependency and the universal scaling law (equation 2.8), sediment oxygen uptake can be determined solely from hydrodynamic conditions close to the sediment and DO concentrations at the sediment surface. This result will facilitate DO depletion estimates and will improve the practical parametrization of DO fluxes to the sediment in numerical modelling, where the impact of BBL hydrodynamics on sediment oxygen uptake is still largely neglected.

Acknowledgments

This work has been developed during the sabbatical leave of M. Hondzo to EPFL and we acknowledge the financial contribution by the ENAC Visiting Professor Program. We are thankful to the excellent collaboration with Lee Bryant (University of Bath), Beat Müller and Thomas Steinsberger (both Eawag) and Sebastian Lavanchy (EPFL). The first author was supported by the Swiss National Science Foundation grants 200021-146652 and 200020-165517. Field data can be accessed by the corresponding author.

References

- Berg, P., N. Risgaard-Petersen, and S. Rysgaard. 1998. Interpretation of measured concentration profiles in sediment pore water. *Limnol. Oceanogr.* **43**: 1500–1510. doi:10.4319/lo.1998.43.7.1500
- Berg, P., H. Røy, F. Janssen, V. Meyer, B. B. Jørgensen, M. Huettel, and D. de Beer. 2003. Oxygen uptake by aquatic sediments measured with a novel non-invasive eddy-correlation technique. *Mar Ecol Prog Ser* **261**: 75–83. doi:10.3354/meps261075
- Bouffard, D., J. D. Ackerman, and L. Boegman. 2013. Factors affecting the development and dynamics of hypoxia in a large shallow stratified lake: Hourly to seasonal patterns. *Water Resour. Res.* **49**: 2380–2394. doi:10.1002/wrcr.20241
- Bouffard, D., and U. Lemmin. 2013. Kelvin waves in Lake Geneva. *J. Great Lakes Res.* **39**: 637–645. doi:10.1016/j.jglr.2013.09.005
- Bryant, L. D., C. Lorrai, D. McGinnis, A. Brand, A. Wüest, and J. C. Little. 2010. Variable sediment oxygen uptake in response to dynamic forcing. *Limnol. Oceanogr.* **55**: 950–964. doi:10.4319/lo.2009.55.2.0950
- Bryant, L. D., D. F. McGinnis, C. Lorrai, A. Brand, J. C. Little, and A. Wüest. 2010. Evaluating oxygen fluxes using microprofiles from both sides of the sediment-water interface. *Limnol. Oceanogr. Meth.* **8**: 610–627. doi:10.4319/lom.2010.8.0610
- Dade, W. B. 1993. Near-bed turbulence and hydrodynamic control of diffusional mass transfer at the sea floor. *Limnol. Oceanogr.* **38**: 52–69. doi:10.4319/lo.1993.38.1.0052
- Diaz, R. J., and R. Rosenberg. 2008. Spreading dead zones and consequences for marine ecosystems. *Science* **321**: 926–929. doi:10.1126/science.1156401

- Donnadieu, Y., E. Puc  at, M. Moiroud, F. Guillocheau, and J.-F. Deconinck. 2016. A better-ventilated ocean triggered by Late Cretaceous changes in continental configuration. *Nature Communications* **7**. doi:10.1038/ncomms10316
- Friedrich, J., F. Janssen, D. Aleynik, and others. 2014. Investigating hypoxia in aquatic environments: diverse approaches to addressing a complex phenomenon. *Biogeosciences* **11**: 1215–1259. doi:10.5194/bg-11-1215-2014
- F  llmi, K. B. 2012. Early Cretaceous life, climate and anoxia. *Cretaceous Res.* **35**: 230–257. doi:10.1016/j.cretres.2011.12.005
- George, W. K. 2007. Is there a universal log law for turbulent wall-bounded flows? *Philos. T. R. Soc. A* **365**: 789–806. doi:10.1098/rsta.2006.1941
- Gudasz, C., D. Bastviken, K. Steger, K. Premke, S. Sobek, and L. J. Tranvik. 2010. Temperature-controlled organic carbon mineralization in lake sediments. *Nature* **466**: 478–481. doi:10.1038/nature09186
- Higashino, M., B. L. O’Connor, M. Hondzo, and H. G. Stefan. 2008. Oxygen transfer from flowing water to microbes in an organic sediment bed. *Hydrobiologia* **614**: 219–231.
- Hondzo, M., T. Feyaerts, R. Donovan, and B. L. O’Connor. 2005. Universal scaling of dissolved oxygen distribution at the sediment-water interface: A power law. *Limnol. Oceanogr.* **50**: 1667–1676.
- Horppila, J., P. K  ng  s, J. Niemist  , and S. Hietanen. 2015. Oxygen flux and penetration depth in the sediments of aerated and non-aerated lake basins. *Internat. Rev. Hydrobiol.* **100**: 106–115. doi:10.1002/iroh.201401781
- Inoue, T., Y. Nakamura, and M. Sayama. 2008. A new method for measuring flow structure in the benthic boundary layer using an acoustic Doppler velocimeter. *J. Atmos. Oceanic Technol.* **25**: 822–830. doi:10.1175/2007JTECHO531.1
- J  rgensen, B. B., and N. P. Revsbech. 1985. Diffusive Boundary Layers and the Oxygen Uptake of Sediments and Detritus. *Limnol. Oceanogr.* **30**: 111–122. doi:10.2307/2836220
- J  rgensen, B. B., and D. J. Des Marais. 1990. The Diffusive Boundary Layer of Sediments: Oxygen Microgradients Over a Microbial Mat. *Limnol. Oceanogr.* **35**: 1343–1355. doi:10.2307/2837444
- Keeling, R. F., A. K  rtzinger, and N. Gruber. 2010. Ocean deoxygenation in a warming world. *Annu. Rev. Mar. Sci.* **2**: 199–229. doi:10.1146/annurev.marine.010908.163855

- Kremer, K., M. Hilbe, G. Simpson, L. Decrouy, W. Wildi, and S. Girardclos. 2015. Reconstructing 4000 years of mass movement and tsunami history in a deep peri-Alpine lake (Lake Geneva, France-Switzerland). *Sedimentology* 62: 1305–1327. doi:10.1111/sed.12190
- Lorke, A., L. Umlauf, T. Jonas, and A. Wüest. 2002. Dynamics of turbulence in low-speed oscillating bottom-boundary layers of stratified basins. *Environ. Fluid Mech.* 2: 291–313. doi:10.1023/A:1020450729821
- Lorke, A., B. Müller, M. Maerki, and A. Wüest. 2003. Breathing sediments: The control of diffusive transport across the sediment:water interface by periodic boundary-layer turbulence. *Limnol. Oceanogr.* 48: 2077–2085. doi:10.2307/3597808
- Monteiro, F. M., R. D. Pancost, A. Ridgwell, and Y. Donnadieu. 2012. Nutrients as the dominant control on the spread of anoxia and euxinia across the Cenomanian-Turonian oceanic anoxic event (OAE2): Model-data comparison. *Paleoceanography* 27 PA4209. doi:10.1029/2012PA002351
- McGinnis, D. F., P. Berg, A. Brand, C. Lorrai, T. J. Edmonds, and A. Wüest. 2008. Measurements of eddy correlation oxygen fluxes in shallow freshwaters: Towards routine applications and analysis. *Geophys. Res. Lett.* 35: L04403. doi:10.1029/2007GL032747
- Nakamura, Y., and H. Stefan. 1994. Effect of flow velocity on sediment oxygen demand: Theory. *J. Environ. Eng.* 120: 996–1016. doi:10.1061/(ASCE)0733-9372(1994)120:5(996)
- Nishihara, G. N., and J. D. Ackerman. 2007. On the determination of mass transfer in a concentration boundary layer. *Limnol. Oceanogr. Methods* 5: 88–96. doi:10.4319/lom.2007.5.88
- O'Connor, B. L., and M. Hondzo. 2008. Dissolved oxygen transfer to sediments by sweep and eject motions in aquatic environments. *Limnol. Oceanogr.* 53: 566–578. doi:10.4319/lo.2008.53.2.0566
- O'Connor, B. L., M. Hondzo, and J. W. Harvey. 2009. Incorporating both physical and kinetic limitations in quantifying dissolved oxygen flux to aquatic sediments. *J. Environ. Eng.* 135: 1304–1314. doi:10.1061/(ASCE)EE.1943-7870.0000093
- Røy, H., M. Huettel, and B. B. Jørgensen. 2004. Transmission of oxygen concentration fluctuations through the diffusive boundary layer overlying aquatic sediments. *Limnol. Oceanogr.* 49: 686–692. doi:10.4319/lo.2004.49.3.0686

- Scalo, C., L. Boegman, and U. Piomelli. 2013. Large-eddy simulation and low-order modeling of sediment-oxygen uptake in a transitional oscillatory flow. *Journal of Geophysical Research: Oceans* **118**: 1926–1939. doi:10.1002/jgrc.20113
- Schmid, M., M. Busbridge, and A. Wüest. 2010. Double-diffusive convection in Lake Kivu. *Limnol. Oceanogr.* **55**: 225–238. doi:10.4319/lo.2010.55.1.0225
- Shaw, D. A., and T. J. Hanratty. 1977. Turbulent mass transfer rates to a wall for large Schmidt numbers. *AIChE J.* **23**: 28–37. doi:10.1002/aic.690230106
- Sommer, T., J. R. Carpenter, M. Schmid, R. G. Lueck, M. Schurter, and A. Wüest. 2013. Interface structure and flux laws in a natural double-diffusive layering. *J. Geophys. Res. Oceans* **118**: 6092–6106. doi:10.1002/2013JC009166
- Steinberger, N., and M. Hondzo. 1999. Diffusional mass transfer at sediment-water interface. *J. Environ. Eng.* **125**: 192–200. doi:10.1061/(ASCE)0733-9372(1999)125:2(192)
- Steele, E. C. C., W. A. M. Nimmo-Smith, and A. Vlasenko. 2016. Direct measurement of hairpin-like vortices in the bottom boundary layer of the coastal ocean. *Geophys. Res. Lett.* **43**: 1175–1183. doi:10.1002/2015GL067148
- van Driest, E. R. 1956. On turbulent flow near a wall. *J. Aero-Nautical Sci.* **23**: 1007–1019. doi:10.2514/8.3713
- Wang, J., L. Zhao, R. Fan, and H. Wei. 2016. Scaling relationships for diffusive boundary layer thickness and diffusive flux based on in situ measurements in coastal seas. *Progress in Oceanography* **144**: 1–14. doi:10.1016/j.pocean.2016.03.001
- Wüest, A., and A. Lorke. 2003. Small-scale hydrodynamics in lakes. *Ann. Rev. Fluid Mech.* **35**: 373–412. doi:10.1146/annurev.fluid.35.101101.161220
- Yoh, M., H. Terai, and Y. Saijo. 1983. Accumulation of nitrous oxide in the oxygen deficient layer of freshwater lakes. *Nature* **301**: 327–329. doi:10.1038/301327a0

Supporting information for chapter 2:

Scaling oxygen microprofiles at the sediment interface of deep stratified waters

Robert Schwefel¹, Miki Hondzo², Alfred Wüest^{1,3}, Damien Bouffard¹

¹ Physics of Aquatic Systems Laboratory, Margaretha Kamprad Chair, Ecole Polytechnique Fédérale de Lausanne, Institute of Environmental Engineering, CH-1015 Lausanne, Switzerland.

² Department of Civil, Environmental, and Geo-Engineering, St. Anthony Falls Laboratory, University of Minnesota, Minneapolis, USA.

³ Eawag, Swiss Federal Institute of Aquatic Science and Technology, Surface Waters – Research and Management, Kastanienbaum, Switzerland.

Submitted to *Geophysical Research Letters*.

Introduction

Text S1 gives a detailed derivation of the scaling law for oxygen microprofiles based on Fick's law and the proposed relationships between turbulent diffusivity and dimensionless height.

Figure S2.1 shows four of the measured microprofiles, Figure S2.2 shows the non-dimensional velocity as function of the dimensionless height above the sediment, and Figure S2.3 illustrates the functional relationship between the correction factor α_f used for the scaling of eddy viscosity and the Reynolds number.

Text S2.1. Derivation of Equations 2.6 and 2.8

The total dissolved oxygen flux is defined as (Equation 3):

$$J_w = -(D + E) \frac{d\bar{C}}{dy}, \quad (S2.1)$$

where D is the molecular diffusion coefficient, E the eddy diffusivity, and $\frac{d\bar{C}}{dy}$ is the gradient of time-averaged oxygen concentration over the height above the sediment y . Integrating equation S2.1 from $y = 0$ to $y = y'$ yields:

$$\frac{\bar{C} - C_S}{J_w} = - \int_0^{y'} \frac{dy}{D + E}, \quad (S2.2)$$

where C_S is the concentration at the sediment-water interface. Introducing the dimensionless height $y^+ = \frac{yu_*}{\nu}$, Equation S2.2 reads as:

$$\frac{\bar{C} - C_S}{J_w} = - \int_0^{y^{+'}} \frac{\nu}{u_*} \frac{dy^+}{D + E}. \quad (S2.2b)$$

Defining the dimensionless concentration $C^+ = \frac{(\bar{C} - C_S)u_*}{J_w}$ (Equation 2.5), we obtain Equation 2.6:

$$C^+ = - \int_0^{y^{+'}} \frac{dy^+}{\frac{1}{Sc} + \frac{E}{\nu}}, \quad (S2.3)$$

where $Sc = \frac{\nu}{D}$ is the Schmidt number.

To obtain the general scaling law of the oxygen vertical distribution (Equation 2.8), Equation S3 is split up in two regions: the vertical distance from the sediment-water interface to the dimensionless diffusive boundary layer height δ_{DBL}^+ , and from δ_{DBL}^+ to $y^{+'}$:

$$-C^+ = \int_0^{\delta_{DBL}^+} \frac{dy^+}{\frac{1}{Sc} + \frac{E}{\nu}} + \int_{\delta_{DBL}^+}^{y^{+'}} \frac{dy^+}{\frac{1}{Sc} + \frac{E}{\nu}}. \quad (S2.4)$$

In the first integral of Equation S2.4 (i.e. very close to the sediment-water interface), the turbulent eddy diffusivity, E , can be neglected. Away from the sediment-water interface, the second integral, the turbulent transport is dominant, and hence $\frac{1}{Sc}$ can be neglected. After these simplifications we obtain:

$$-C^+ = \int_0^{\delta_{DBL}^+} \frac{dy^+}{\frac{1}{Sc}} + \int_{\delta_{DBL}^+}^{y^{+'}} \frac{dy^+}{\frac{E}{v}}. \quad (S2.5)$$

where $\frac{E}{v} = 9 \cdot 10^{-5}(\alpha_f y^+)^4$ (Figure 2.3), and $\alpha_f = 16 \cdot \exp(-21Re_{\eta_B})$ (Figure S2.3). Equation S2.5 can be integrated analytically:

$$C^+ = \delta^+ Sc + \frac{1}{23.6 \exp(-84Re_{\eta_B})} \left(\frac{1}{\delta_{DBL}^{+3}} - \frac{1}{y^{+'3}} \right). \quad (S2.6)$$

Equation S2.6 is identical to Equation 2.8b with $B = \frac{1}{23.6 \exp(-84Re_{\eta_B})} \approx 0.05 \exp(84Re_{\eta_B})$. If $y^{+'} < \delta_{DBL}^+$, the second integral of Equation S2.4 becomes zero and the remaining first integral up to $y^{+'}$ corresponds to Equation 2.8a.

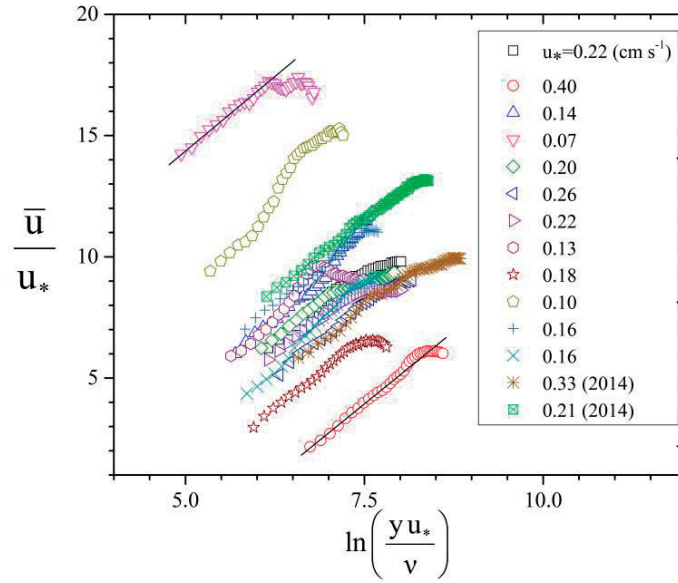


Figure S2.1: Near-sediment profiles of time-averaged nondimensional velocity (\bar{u}/u_*) measured by the Aquadopp profiler. The vertical logarithmic distance from the sediments is depicted in viscous lengths, or “wall” units, denoted by $\frac{yu_*}{\nu}$, where y is the vertical distance, u_* is the shear velocity, and ν is the kinematic viscosity. The legend provides u_* from 12 profiles measured in 2015, and two profiles measured in 2014 (Table 2.1).

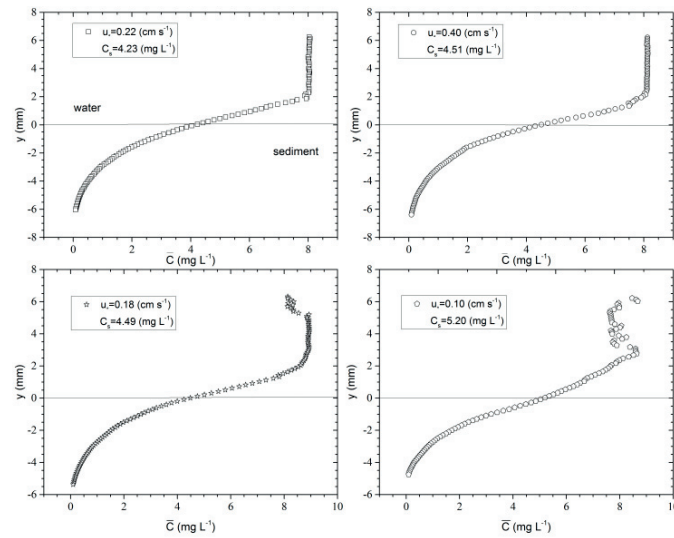


Figure S2.2. Examples of four oxygen microprofiles under varying turbulent conditions. The sediment-water interface is set to $y = 0$ (fine lines). u_* is the friction velocity, and C_s the oxygen concentration at the sediment-water interface.

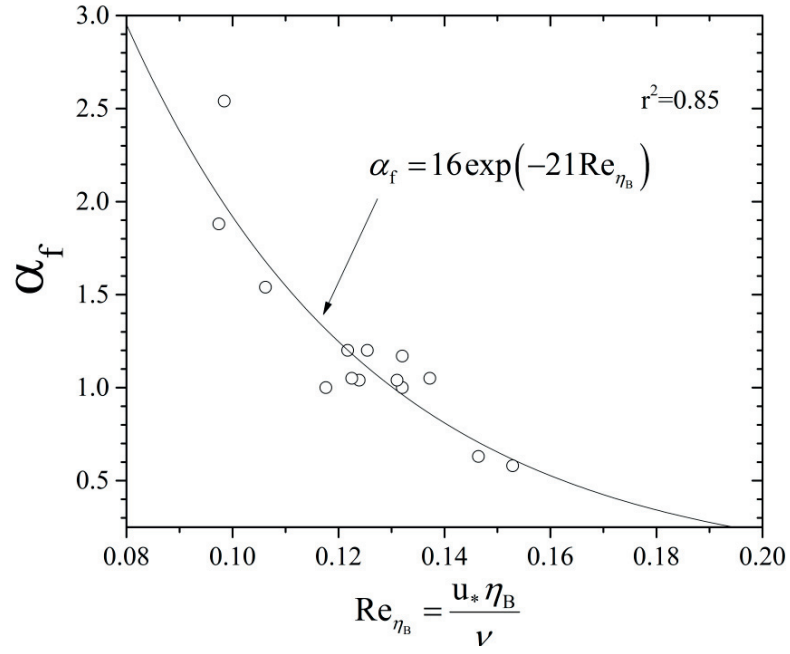


Figure S2.3: The correction function, α_f , of the eddy diffusivity above the sediment-water interface. Re_{η_B} is the Reynolds number, u_* is the friction velocity, ν the kinematic viscosity, and η_B the Batchelor microscale.

Chapter 3:

Using small-scale measurements to estimate hypolimnetic oxygen depletion in a deep lake

Robert Schwefel¹, Thomas Steinsberger^{2,3}, Damien Bouffard^{1,2}, Lee Bryant⁴, Beat Müller² and Alfred Wüest^{1,2}

¹ Physics of Aquatic Systems Laboratory - Margaretha Kamprad Chair of Environmental Science and Limnology, ENAC, EPFL, Lausanne, Switzerland

² Eawag, Swiss Federal Institute of Aquatic Science and Technology, CH-6047 Kastanienbaum, Switzerland

³ Institute of Biogeochemistry and Pollutant Dynamics, ETH Zurich, CH-8092 Zurich, Switzerland

⁴ Research Unit for Water, Environment and Infrastructure Resilience (WEIR), University of Bath, BA2 7AY Bath, United Kingdom

Submitted to *Limnology and Oceanography*.

Robert Schwefel performed the fieldwork, the analysis of the results and the writing of the manuscript. Thomas Steinsberger, Damien Bouffard, Lee Bryant and Beat Müller contributed to the fieldwork, the analysis of the results and the revision of the manuscript. Alfred Wüest contributed to the analysis of the results and the manuscript revision.

Abstract

Low oxygen concentrations in lakes and reservoirs are an ongoing environmental concern, particularly in light of increasing anthropogenic activity and climate change. The processes controlling oxygen depletion in lakes are still not completely understood and a variety of oxygen depletion models have been proposed in the past based on limited field observations. Here we present detailed field measurements of oxygen depletion processes obtained for the first time in a deep lake, Lake Geneva (Switzerland). Estimates of sediment oxygen uptake (SOU) are presented based on oxygen microprofile measurements and sediment core data of reduced substances (CH_4 , NH_4^+ , Fe(II) , Mn(II)). Comparison with long-term monitoring data allowed for an estimate of the relative importance of SOU and water column mineralization for total oxygen depletion as a function of depth. Results show a strong decrease in both SOU and water column oxygen depletion down to mid-depth of ~ 150 m. Below this depth, the total oxygen depletion increased due to an enhanced sediment area to water volume ratio. This vertical pattern of oxygen depletion is driven by (i) lake morphometry paired with increasing sediment area to water volume ratios (α), and (ii) the organic matter mineralization in the water column decreasing with depth.

3.1 Introduction

Efficient lake management is directly linked to accurately describing and modeling of physical and biogeochemical processes. Dissolved oxygen (DO) demand is one of the most important parameters for characterizing lake ecosystem health and, consequently, DO concentrations in lakes have been intensively studied since the end of the 19th century (e. g., *Thienemann* 1928, *Hutchinson* 1957). Since the middle of the last century, anthropogenic pressure resulted in eutrophication and temperature increases that negatively affect the DO budget of lakes and oceans, which is often threatened to fall below biologically acceptable DO concentrations (*Diaz* 2001, *Friedrich et al.* 2014, *North et al.* 2014).

Increasing phosphorus concentrations were first identified as the main driver of eutrophication. As a result, lake management shifted to focus on reducing the phosphorus input to lakes, often with great success (*Schindler* 2006, *Müller et al.* 2014). Several empirical models were developed to predict DO depletion rates based on phosphorus concentrations and other parameters, including temperature or lake geometry (*Rast and Lee* 1978, *Cornett and Rigler* 1979, *Livingstone and Imboden* 1996) and were tested empirically (*Cornett and Rigler* 1980, *Rippey and McSorley* 2009). However, the relationship between DO depletion and nutrient concentrations is complex and poorly understood (*Müller et al.* 2012a, *Scavia et al.* 2014). DO depletion has remained high in many lakes despite significant reduction in nutrient inputs, as shown by *Müller et al.* (2012b) for several lakes on the Swiss Plateau including Lake Geneva (the focus of this study; Figure 3.1).

Oxygen depletion is caused by mineralization of organic matter in the water column or within the upper sediments. Aerobic respiration is the dominant process for organic matter mineralization under oxic conditions. However, under anoxic conditions other electron acceptors come into play leading to the formation of reduced compounds such as CH₄, NH₄⁺, Mn(II), and Fe(II)), as in the deep-water of meromictic lakes or in anoxic sediments. These substances diffuse towards the oxic zones and are then oxidized, thereby contributing to further DO uptake. These fluxes of reduced substances can contribute significantly to DO depletion in eutrophic lakes (*Gelda et al.* 1995, *Matzinger et al.* 2010). Fluxes of reduced substances and oxic respiration depend on the mixing regime and on the availability and quality of organic matter, which can vary significantly within the waterbodies of large lakes. A schematic overview of the relevant processes for DO depletion in lakes is given in Figure 3.2.

Long-term DO depletion measurements often rely on vertical DO profiles monitored at a single location within a lake. While time-series measurements at a singular point are useful for assessing long-term trends integrated over the entire water-body, DO depletion is largely controlled by biogeochemical processes at the sediment surface which may vary considerably over the entire lake waterbody. Thus, while much work has been done to understand the various sinks of DO depletion in large lakes (*Cornett and Rigler 1979, Livingstone and Imboden 1996, Müller et al. 2012a*), there is still a lack in comprehensive identification of the involved processes. Current lake DO models use either simplified empirically derived expressions that do not quantitatively describe the complex processes upon which they are built (*Fang and Stefan 2009, Rucinski et al. 2010*) or they rely on a large number of free parameters that require calibration based on empirical field data (*Rucinski et al. 2014*). For both approaches, good knowledge of the sinks of DO depletion and its spatial variability is crucial to improving their reliability and predictive power.

In this study, we investigate the DO depletion in Lake Geneva, which is currently recovering from anthropogenic eutrophication and shows high levels of areal DO demand and periodic hypoxia in the deep hypolimnion (*Schwefel et al. 2016*). Sediment-water microprofile measurements were performed at different depths of the lake to determine the spatial variability of sediment oxygen uptake (SOU; i.e., the flux of DO from the water towards the sediment surface). Simultaneous porewater analyses of sediment cores allowed for the quantification of the fluxes of reduced substances out of the sediment. Combined with a set of long-term monitoring data from over more than 60 years, collected from the water column at the deepest location of the lake, these observations allow for a distinction between the various pathways of DO consumption as a function of depth. The aims of this study were (i) to characterize the spatial distribution and variability of DO depletion, (ii) to determine the relative importance of different organic matter mineralization pathways that control DO depletion, and (iii) to find a conceptual model that explains the observed DO depletion rates.

3.2 Methods

Study site: Lake Geneva is a deep perialpine lake situated on the border of France and Switzerland with a mean depth of 153 m, a surface area of 582 km² and a volume of 89 km³.

Once considered oligotrophic, Lake Geneva has experienced high nutrient inputs since the 1950s. Phosphorus concentrations increased from 15 mg m^{-3} around 1960 to up to 90 mg m^{-3} in the 1980s. Consequently, water transparency decreased, the phytoplankton communities shifted to species more typical for eutrophic environments, and phyto- and zooplankton biomass increased (Loizeau and Dominik 2005, Anneville and Pelletier 2000). While DO has been monitored in the deep hypolimnion since the late 1890s (e. g., Forel 1895, Delebecque 1898, Vivier 1944), low DO concentrations had never been observed prior to 1957, either with direct field measurements (Delebecque 1898, Vivier 1944) or in sediment core samples (Jenny *et al.* 2014). Since then, periods of hypoxia have been observed regularly (Savoye *et al.* 2015; Figure 3.3). Recent governmental measures to limit the phosphorus input into the lake reduced total phosphorus to the present concentrations of $\sim 20 \text{ mg m}^{-3}$. Despite the high reduction in nutrient loads, total biomass remained high and DO depletion rates and concentrations have not shown any significant trend over the last 40 years (Anneville and Pelletier 2000, Savoye *et al.* 2015, Schwefel *et al.* 2016; Figures 3.1 and 3.3).

Microprofile measurements: In total ninety-two DO profiles were measured with a MP4/8 Microprofiler (Unisense A/S) equipped with oxygen microsensors at seven different measurement campaigns between autumn 2013 and summer 2015 (Table 3.1). Measurements were performed in the western part of Lake Geneva in depth between 43 and 133 m (Table 3.1). The instrument was deployed between one and three days for each individual campaign, measurement locations and dates are shown in Figure 3.4 and summarized in Table S3.1. The Clark-type microsensors had a tip size of $100 \mu\text{m}$ with a detection limit of 0.01 g m^{-3} and a response time of $< 8 \text{ s}$. The spatial resolution of the measurements is limited by the diameter of the sensor tip. An RBR concerto datalogger (RBR Ltd, Ottawa) equipped with an oxygen optode (Aanderaa Data Instruments) as well as a temperature and pressure sensor was attached to the microprofiler frame and positioned outside of the diffusive boundary layer (DBL) $\sim 25 \text{ cm}$ above the sediment to provide background time series of DO concentrations in the bottom boundary layer (BBL). To calibrate the oxygen microsensors in the field, we performed a two-point, linear calibration with the *in-situ* data from the optode as the upper reference point and the anoxic sediment as the lower reference point.

Table 3.1: Summary of the microprofile measurement results. Sediment oxic zone is defined as zone, in which the oxygen concentrations stays above 0.1 g m^{-3} .

Number	Depth [m]	# of profiles	SOU [$\text{g}_{\text{DO}} \text{ m}^{-2} \text{ d}^{-1}$]	DBL thickness [mm]	Sediment oxic zone [mm]	BBL temperature [°C]	BBL DO concentration [g m^{-3}]	Date
MP1	43	4	1.08 ± 0.51	1.1 ± 0.8	2.1 ± 0.1	6.6	8.8	Oct. 2013
MP2	45	12	1.08 ± 0.33	0.8 ± 0.6	2.4 ± 0.5	6.6	10.3	Mar. 2014
MP3	72	7	0.50 ± 0.11	1.5 ± 0.8	2.9 ± 0.7	6.6	10.1	May 2014
MP4	76	13	0.46 ± 0.16	1.4 ± 0.6	3.8 ± 1.0	6.4	9.4	July 2014
MP5	93	30	0.32 ± 0.16	2.0 ± 1.3	4.5 ± 0.7	6.3	8.5	Aug. 2015
MP6	109	13	0.39 ± 0.07	1.7 ± 0.4	4.3 ± 0.3	5.9	8.7	July 2014
MP7	133	13	0.21 ± 0.06	2.1 ± 0.8	5.0 ± 0.8	6.0	7.8	July 2015

Table 3.2: Flux of reduced substances in units of oxygen equivalents [$\text{g}_{\text{DO}}^{\text{eq}} \text{ m}^{-2} \text{ d}^{-1}$] using equation 3.2

	LG1	LG2	LG3	LG4	LG5	LG6	LG7	LG8	Mean
Depth [m]	40	80	120	310	310	300	200	175	
Methane	0.029	<0.001	0.003	0.035	0.051	0.039	0.005	0.056	0.027 (55%)
Ammonium	0.017	0.027	0.010	0.019	0.033	0.013	0.008	0.010	0.017 (35%)
Manganese(II)	<0.001	0.003	0.002	0.004	0.001	0.002	0.006	0.005	0.003 (6%)
Iron(II)	0.003	0.002	0.003	0.006	0.002	<0.001	0.002	<0.001	0.002 (4%)
Sum	0.049	0.032	0.018	0.064	0.086	0.055	0.021	0.071	0.049

The detection of the sediment-water interface (SWI) is important when investigating SOU. As our instrument was very slowly and continuously sinking into the sediment during the experiments, we had to perform accurate SWI detection prior to each profile. We programmed the microprofiler so that before each small scale profile, the microsensor was first lowered continuously until the DO signal was reduced to 60% of the initial DO concentration. This drop was defined as a good proxy for identifying the close proximity of the DBL. Afterwards, the sensors were raised by ~7 mm and the high-resolution DO microprofile measurements were started in typically 150-300 steps of 100 μm fully covering the DBL on the water side and the sediment oxic zone. Sediment detection and profiling lasted generally about 70 minutes and varied depending on the number of steps and the time needed for sediment detection. Final determination of the SWI was later calculated based on the gradient change in the DO profiles across the SWI that results from differing diffusivity between water and sediment.

Current measurements and modeling: Flow measurements were performed with an upward-looking 2 MHz acoustic Doppler current profiler (ADCP; Nortek Aquadopp). The ADCP was deployed closely to the microprofiler (~100 m distance) to allow for flow measurements under comparable boundary conditions. During all deployments, the vertical resolution was 5 cm. Due to the blanking distance of the ADCP, the first measurement cell was ~20 cm above the sediment. Measurements were performed in burst mode in 20 min intervals with 256-1024 measurements per burst. Due to instrument and/or deployment issues, velocity data were not available for all deployments (see Table S3.1).

The hydrodynamic conditions of the four relatively short (< 1 week) measurements periods were compared to the typical conditions in Lake Geneva by using the 3-dimensional hydrodynamic model Delft3D (Razmi *et al.* 2012). The model was validated for the year 2012 (Kiefer *et al.* submitted) and provided a map of yearly averaged speed of the BBL currents at one meter above the bottom. Over one year, we observed a clear decrease of the bottom currents with depth as shown in the contour map in Figure 3.5a and the frequency distribution at different measuring locations in Figure 3.5b. The comparison between the modeled bottom current distribution and the *in-situ* measurements indicate that at the 43-m-site, measurements were collected over comparatively quiet conditions. During the measurements at the deeper sites, the currents were close to the modelled mean bottom currents (Figure 3.5b).

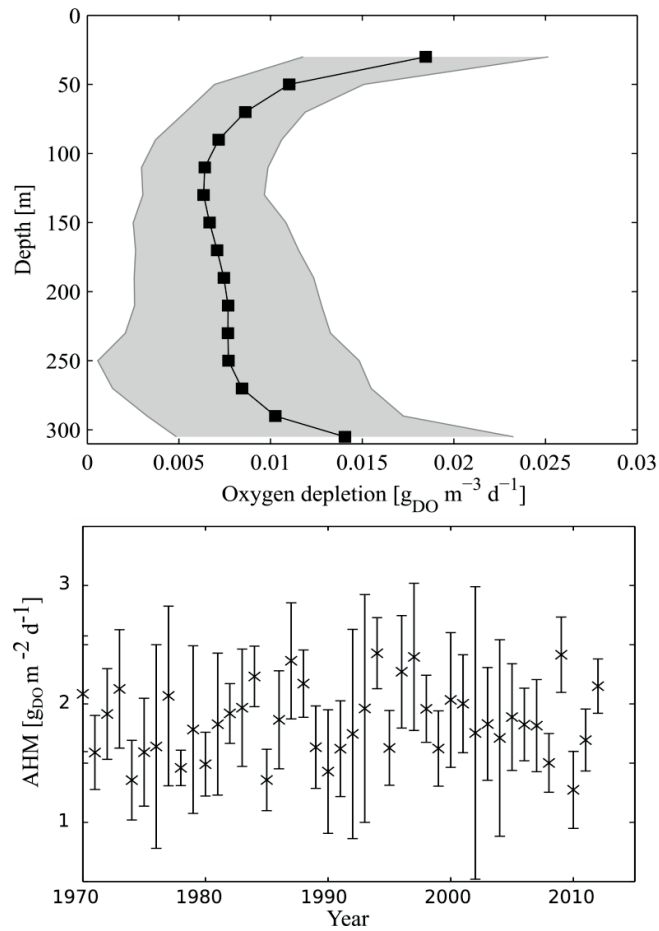


Figure 3.1: a) Mean total oxygen depletion (TOD) and standard deviation for 1970 to 2012 as a function of depth. b) Areal hypolimnetic mineralization (AHM) as a function of time for 1970 to 2012 for the hypolimnetic water below 15 m depth.

Sediment cores: A total of 16 sediment cores were collected with a UWITEC corer equipped with a PVC tube (6.5 cm inner diameter, 60 cm length) at eight different sites from 40 to 310 m depth (Figure 3.4 and Table S3.2). At each site, one core was sampled for the analysis of CH_4 via gas chromatography and a second core to measure porewater concentrations of cations and anions using capillary electrophoresis (Kuban *et al.* 2007, Torres *et al.* 2013). For porewater retrieval, PVC tubes with pre-drilled with holes of 2 mm diameter at 5 mm vertical intervals. The holes were sealed with adhesive tape prior to sampling. Immediately after retrieval, the cores were brought to the lab and 10 to 50 μL of sediment porewater were sampled by insertion of a MicroRhizon filter tube (1 mm diameter, 0.20 μm pore size; Rhizosphere Research Products, Wageningen, Netherlands) through the pre-drilled holes. Resolution of the measurements was 0.5

cm for the first 10 cm and 1 cm for the next 10 cm of the sediment. Additionally, one sample was taken in the overlying water. Measurements were performed with two portable capillary electrophoresis systems equipped with capacitive coupled contactless conductivity detectors. Cations were analyzed in all eight cores. The analysis of anions was omitted for logistical reasons in the 2014 campaign. Full separation of ions of interest (NH_4^+ , Mn(II) , and Fe(II)) was achieved within six minutes. Standard deviations of all measurements were $< 5\%$. The setup is described in detail by *Torres et al. (2013)* and *Steinsberger et al. (in prep.)*.

For the CH_4 measurements, holes of 1.2 cm diameter were drilled staggered at 1-cm vertical intervals in the sediment sampling tube and covered with adhesive tape. Immediately after retrieval, cores were sampled from top to bottom by cutting the tape and inserting a plastic syringe which had the tip cut off. Two mL of sediment was transferred into 125 mL serum flasks prefilled with 2 mL of 7 M NaOH and sealed with butyl rubber stoppers. Methane was analyzed by headspace gas chromatography (Agilent) using a 1010 Supelco Carboxene column.

Monitoring data: Since 1957, DO measurements were performed on a regular basis by the Commission International pour la Protection des Eaux du Léman (CIPEL). DO was measured along with other parameters (e.g., total phosphorus, transparency and temperature) at the deepest point of the lake (SHL2, see Figure 3.4) throughout the entire water column for eight to twelve times per year between 1957 and 1980 and ~20 times thereafter. Building on these historical data, this study focuses on the results of the measurements from the deepest location of the lake at SHL2 (46.45° N; 6.59° E; Figure 3.4) where continuous data exist between 1957 and 2012. Comparisons between SHL2 and other off-shore measurement stations show only minor variations of 6% on average with higher variability in spring compared to summer and autumn (Figure S3.1). Therefore, data from SHL2 can be considered as representative for the whole lake during stratified summer conditions.

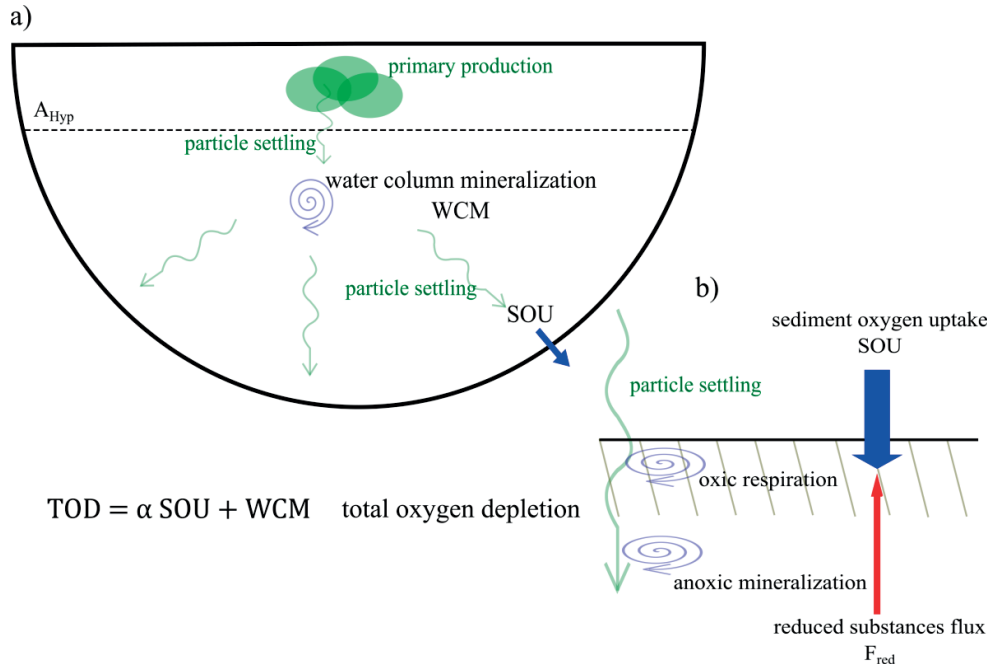


Figure 3.2: Schematic illustration of oxygen depletion processes in the lake (a) and at the sediment surface (b). TOD is the total oxygen depletion [$g_{DO} m^{-3} d^{-1}$] (Figure 3.1), SOU the sediment oxygen uptake [$g_{DO} m^{-2} d^{-1}$] which is either consumed directly by oxic respiration or indirectly by the reduced substances flux F_{red} [$g_{DO}^{eq} m^{-2} d^{-1}$]. $\alpha = -\frac{dA}{dV}$ is the sediment surface to water volume ratio [m^{-1}].

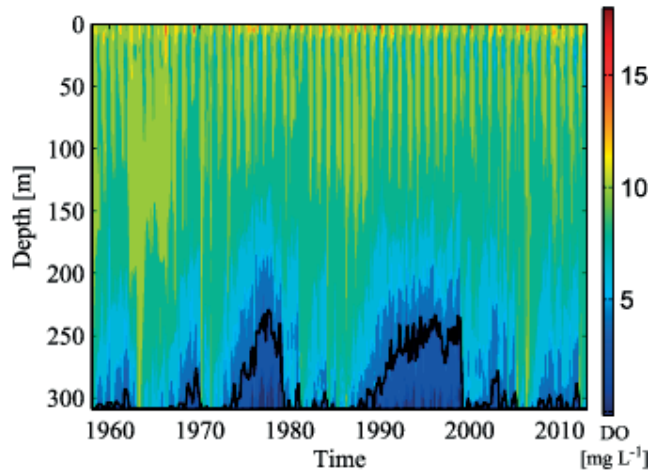


Figure 3.3: Contour plot of DO at the SHL2 location of the deepest point of Lake Geneva (1957 - 2012). The black line indicates the 4 $g m^{-3}$ contour line, which defines the limit to hypoxic conditions as dictated for fish health.

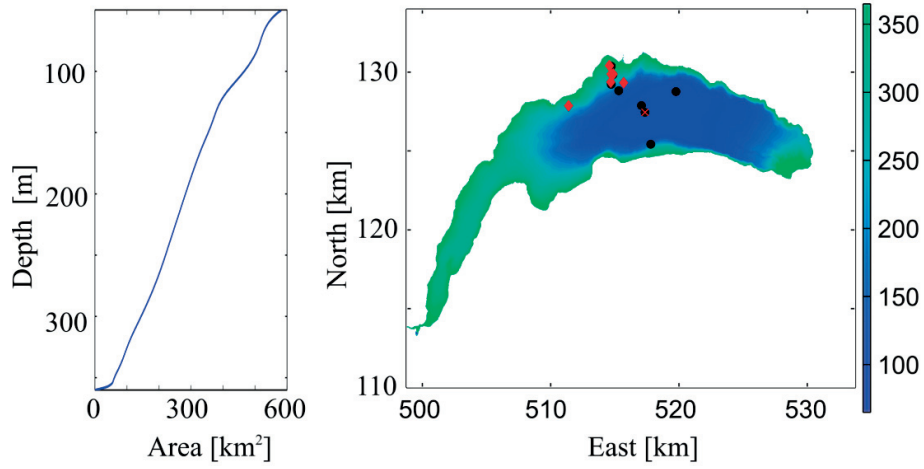


Figure 3.4: Left panel: Hypsometry of Lake Geneva. Right panel: Measurement locations, red diamonds: microprofiles (Table 3.1, MP1 and MP2 as well as MP3 and MP4 are displayed as one point as they are too close to be resolved), black circles: sediment cores (Table 3.2), red cross: long-term monitoring point SHL2.

3.3 Results

Microprofile measurements: Two typical microprofiles for 45 m and 133 m depth (Table 3.1) are shown in Figure 3.6. The SWI was determined based on the change of the gradient in the laminar region of the DO profile (*Røy et al. 2004, Bryant et al. 2010b*). The lower boundary of the sediment oxic zone was defined by the depth where DO concentrations fell below 0.1 g m^{-3} ($\sim 3 \mu\text{mol L}^{-1}$ as in *Bryant et al. 2010a*). The SOU was estimated from the waterside based on Fick's law:

$$\text{SOU} = D \frac{\partial O_2}{\partial z}, \quad (3.1)$$

where D is the temperature-dependent molecular diffusion coefficient of oxygen in water. $\frac{\partial O_2}{\partial z}$ is the DO gradient in the linear region above the SWI where z is defined positive downwards. Hence, positive values indicate fluxes into the sediment.

The BBL temperatures and DO concentrations were measured simultaneously with the microprofiles during each deployment. While BBL temperatures showed only minor differences between the single measurements, BBL DO concentrations decreased with depth and were, as expected, lower in autumn compared to spring and summer (Table 3.1). The mean DO fluxes into

the sediment, the sediment oxic zone depths as well as BBL temperatures and DO concentrations at the different measurement locations are summarized in Table 3.1. Figure 3.7 shows the variation of SOU with depth. The individually estimated SOU varied strongly during measurement sessions consisting of 4 to 30 profiles (Table 3.1). These variations can be partially explained by BBL turbulence dynamics that was also observed in other studies (*Lorke et al. 2003, Bryant et al. 2010a*). Besides temporal variations observed during an individual measurement session at particular sites, SOU showed a strong spatial variability amongst the different measurement sites with a distinct decrease with depth from $1.06 \pm 0.51 \text{ g}_{\text{DO}} \text{ m}^{-2} \text{ d}^{-1}$ at 45 m depth to only $0.21 \pm 0.06 \text{ g}_{\text{DO}} \text{ m}^{-2} \text{ d}^{-1}$ at 133 m depth. In parallel, the penetration depth of DO into the sediment oxic zone increased with depth from $\sim 2 \text{ mm}$ at 43 m depth to $\sim 5 \text{ mm}$ at 133 m depth (Table 3.1).

Sediment cores: The SOU is the flux of DO from the BBL water to the sediment surface. In the top few mm of the sediment, the DO is depleted by two processes: (i) the aerobic respiration in the sediment and (ii) the reduced substances flux from the deeper sediment (Figure 3.2). The flux of reduced substances (F_{CH_4} , F_{NH_4} , F_{Mn} , F_{Fe}) was calculated based on the concentrations gradients measured in the upper layer of the sediment cores (Figure 3.2, Figure S3.2). A one-dimensional balance model (*Müller et al. 2003*) assuming steady-state conditions in the sediment was used to estimate the species fluxes which were then converted to the flux of oxygen equivalents (*Matzinger et al. 2010*) by:

$$F_{\text{red}} = 2F_{\text{CH}_4} + 2F_{\text{NH}_4} + 0.5F_{\text{Mn}} + 0.25F_{\text{Fe}} \quad (3.2)$$

where F_{red} represents the sum of all reduced substances (estimated in $\text{mol m}^{-2} \text{ d}^{-1}$) and expressed in oxygen equivalents [$\text{g}_{\text{DO}}^{\text{eq}} \text{ m}^{-2} \text{ d}^{-1}$] by using equation (3.2).

An analysis of the reduced substances measured from the sediment cores reveals that oxic respiration is the most dominant sink of SOU in Lake Geneva. F_{red} varied from only 0.018 to $0.086 \text{ g}_{\text{DO}}^{\text{eq}} \text{ m}^{-2} \text{ d}^{-1}$ with a mean of $0.049 \pm 0.024 \text{ g}_{\text{DO}}^{\text{eq}} \text{ m}^{-2} \text{ d}^{-1}$ (Figure 3.8, Table 3.2), which is extremely small compared to medium-sized lakes with comparable eutrophication history (*Steinsberger et al. in prep.*). The F_{red} fluxes, estimated in cores from the deepest lake zones of $\sim 300 \text{ m}$, varied between ~ 0.06 and $0.09 \text{ g}_{\text{DO}}^{\text{eq}} \text{ m}^{-2} \text{ d}^{-1}$. The cores taken at sites between 40 m and 200 m depth showed generally lower F_{red} fluxes. An exception is core LG7, taken at depth 200 m, where F_{red} is comparatively high, but still very low in absolute terms. This can partially be

explained by the influence of the City of Evian close to the measurement site which could lead to locally increased organic matter concentrations due to wastewater inputs. Unfortunately, no microprofile measurements were performed close to this point as the steep bathymetry is not well suited for microprofiler stability. On sites with parallel microprofile and sediment core measurements (LG1, LG2, and LG3, Table 3.2), the flux of reduced substances was consistently less than 10% of SOU. The most dominant reduced substances were CH_4 and NH_4^+ (Table 3.2), which is consistent with measurements in other Swiss lakes (*Mazinger et al.* 2010, *Steinsberger et al.* in prep.).

BBL turbulence: During the microprofiling, the highest BBL turbulence was measured at 133 m; the lowest was at 45 m. All measurements were performed under typical hydrodynamic conditions, as shown by the comparison with the 3D-numerical model flows in the BBL (Figure 3.5b). While DO flux and DBL thickness varied at each site depending on turbulent conditions, the mean values in DO fluxes were considerably higher at the shallowest location with the lowest BBL currents. In turn, DBL thickness tended to increase with depth.

Long-term monitoring data: Since 1970, DO concentrations were measured at least once per month. For the years 1970 – 2012, these values were interpolated spatially and temporally and the areal hypolimnetic mineralization rate (AHM) [$\text{g}_{\text{DO}} \text{m}^{-2} \text{d}^{-1}$] as well as the total oxygen depletion rate (TOD) per depth layer [$\text{g}_{\text{DO}} \text{m}^{-3} \text{d}^{-1}$] were determined based on the linear decrease in DO during summer stagnation (Figure 3.1). While TOD is a measure of the DO depletion per volume in every depth layer during summer (Figure 3.2), AHM integrates the summer DO depletion over the whole hypolimnion (from the bottom to a depth of 15 m). AHM varied around a mean value of $1.34 \pm 0.34 \text{ g}_{\text{DO}} \text{m}^{-2} \text{d}^{-1}$ without any significant trend during the observed period. An analysis of the vertical structure of DO depletion rates shows that the depletion decreases with depth down to ~150 m. Below 150 m, the DO depletion increases again (Figure 3.1). At every depth, the SOU measured by the microprofiles (Figure 3.7) was significantly lower than TOD. Both, TOD estimated from the long term monitoring data as well as the SOU decreased with depth.

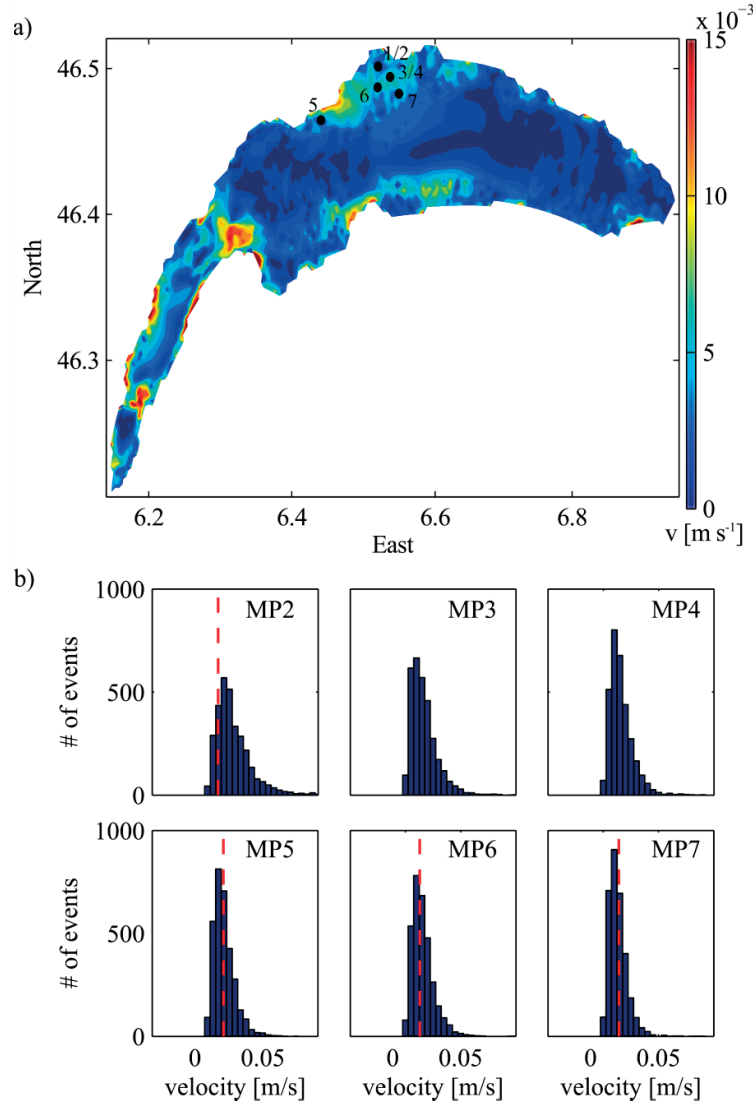


Figure 3.5: a) Contour plot of mean current speed 1 m above the sediment during the year 2012 according to the 3D hydrodynamic model DELFT 3D. The black dots give show the positions of the combined microprofile and ADCP measurements b) Histograms of the modelled current speed at the measurement sites (MP2 – MP7, for exact coordinates see Table S3.1). The red line gives the mean observed velocities during the measurements (ADCP data were not available during MP3 and MP4). For measurements MP1 MP2 and MP4, no ADCP current data were available.

3.4 Discussion

SOU and depth of sediment oxic zone: Despite a strong variability in the physical boundary conditions, all microprofile measurements showed a consistent decrease of SOU with depth (Figure 3.7). Measurement dates ranged from March to October, mostly in summer (June – August). For this reason and also due to the varying depth, DO concentration in the BBL varied between 10 and 7.8 g m⁻³. The variations in BBL temperatures were not important (~0.6 °C), since the instrument was always deployed well below the thermocline. DO fluxes are dependent on the DO difference between SWI and the BBL above the DBL. Hence, lower BBL DO concentrations directly imply lower DO fluxes into the sediment. Nevertheless, the variation of measured SOU with depth was too high to be explained solely by different BBL DO concentrations. During the measurements, the standard derivation of SOU was typically on the order of ~30% and individual measurements could be more than 100% higher than the mean values. These variations can be partially explained by the varying DBL thickness due to BBL turbulences (*Bryant et al. 2010a, Lorke et al. 2003*) and in turn higher DO fluxes into the sediments (*Bryant et al. 2010a, Bryant et al. 2010b*). However, the relationship between BBL turbulence and SOU was not as clear as that reported for other lakes (e.g., Lake Alpnach in *Bryant et al. 2010a*) and could not explain by the systematic decrease with depth. Measured differences in the averaged SOU between 43 and 133 m were ~500% while changes in BBL current speed were only ~50%. During the measurements at the shallowest site with the highest SOU, the currents and, in turn, BBL turbulence were even lower than at all other sites (Figure 3.5b).

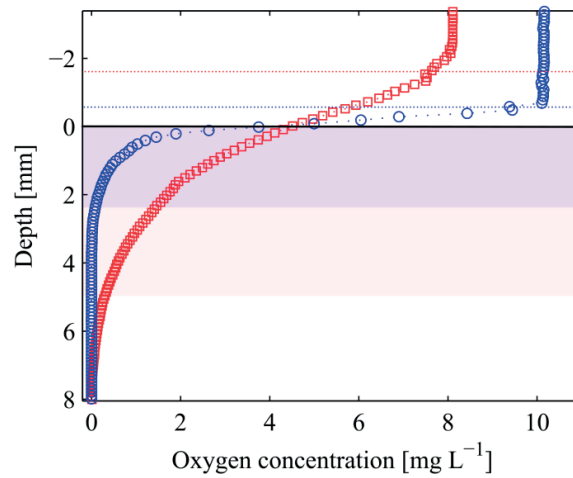


Figure 3.6: Examples of DO microprofiles at 45 m (blue) and at 133 m (red). Dotted lines show the upper end of the DBL. In color the thickness of the oxenic zone at 45 m (light blue, 2.1 mm) and at 133 m (light red, 5.1 mm).

DO depletion in the sediment depends on the amount of organic matter and its quality

(Steinsberger *et al.* in prep.). While parts of the organic material are easily degradable (labile) and quickly decompose, other parts degrade over longer time scales (Kristensen and Holmer 2001). In the upper layers, the labile fraction is decomposed quickly in the water column or precipitates quickly to the sediment of the shallower region of the lake. Consequently, the organic matter in the deeper sediments consists mainly of more refractory organic carbon and the mineralization rate decreases with increasing depth (Sobek *et al.* 2009).

The deepening of the sediment oxenic zone with increasing depth is fully consistent with this interpretation. While easily decomposing organic matter is more abundant in the shallower sediments, the decreasing SOU is a strong evidence that the deeper parts of the lake are covered with more refractory organic matter leading to lower biological activity that thus supports deeper sediment oxenic zones. A similar deepening of the oxenic zone was noticed in the study of Müller *et al.* (2003) for the eutrophic Lake Sempach and by Maerki *et al.* (2006) in Lake Baikal. Also in Lake Erie, Bouffard *et al.* (2013) reported an average SOU of $0.46 \text{ g}_{\text{DO}} \text{ m}^{-2} \text{ d}^{-1}$, whereas direct measurements in sediment cores taken from the center of the lake resulted in a SOU of only $\sim 0.2 \text{ g}_{\text{DO}} \text{ m}^{-2} \text{ d}^{-1}$ (Smith and Matisoff 2008) indicating a strong decrease in SOU with depth.

The sediment oxenic zone depth is of particular interest for fish eggs, which only survive under oxenic conditions. Given the thin oxenic zone in the top sediments, fish egg survival is not guaranteed even if DO concentrations in the overlaying water remain relatively high. Fish eggs sinking slightly into the sediment can easily experience anoxic conditions which are detrimental to their survival;

Swiss federal law requires therefore a minimum of 4 g m^{-3} DO in natural waters to alleviate this problem. In Lake Geneva, however, the lake char (*Salvelinus umbla*) population is still not able to proliferate without artificial stocking, even after decades of reoligotrophication with hypoxia occurring only rarely (Caudron *et al.* 2014). The thin sediment oxic zone observed during the current study, which was found to be prevalent particularly in the shallower hypolimnetic sediments, could explain this phenomenon.

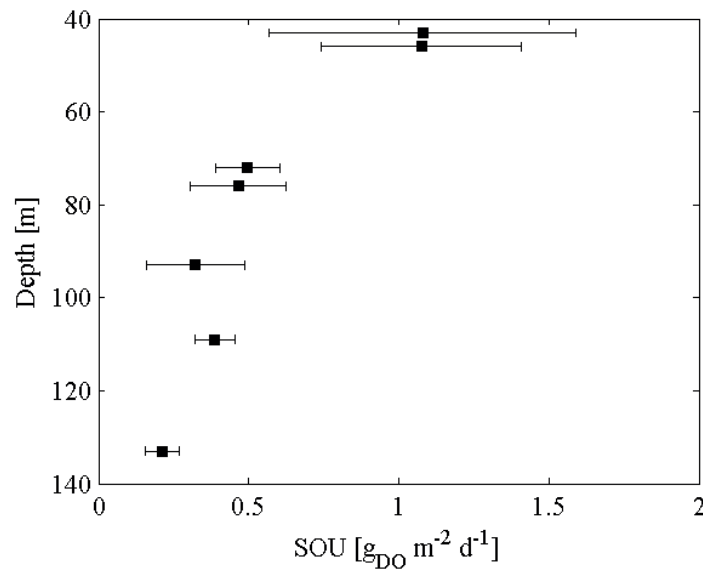


Figure 3.7: Measured SOU as function of depth. The error bars give the standard deviation of each measurement campaign (averaged values over 7 to 30 profiles).

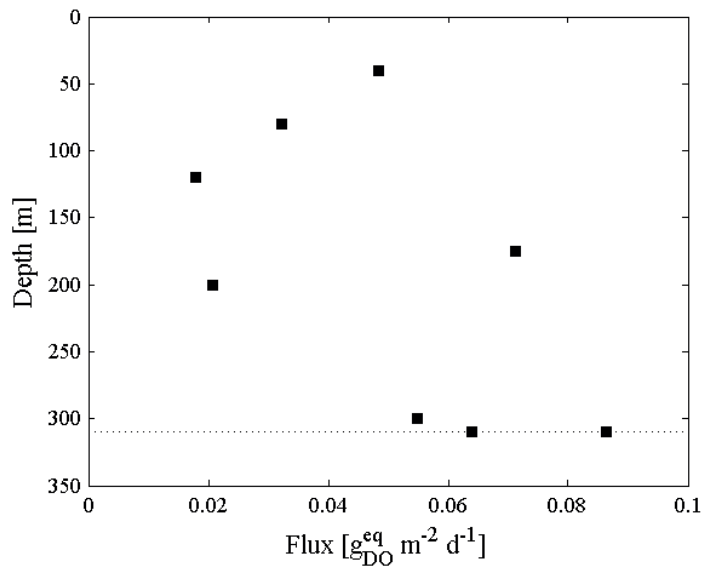


Figure 3.8: Flux of reduced substances, F_{red} , from the sediment to the water as a function of depth expressed in oxygen equivalents.

SOU is the sum of two different processes: (i) aerobic respiration in the top sediment and (ii) chemical oxidation of the flux of reduced substances, F_{red} , from the deeper sediment (Figure 3.2). In Lake Geneva, the majority of soluble, reduced substances are already oxidized within the thin oxic zone which prevents these species from diffusing into the water column. Thus, microprofile measurements represent the sum of both processes and so the individual processes are not directly identifiable from microprofiling alone. A separation is possible, however, through parallel microprofile and geochemical sediment core measurements. Three sediment cores (S1, S2, S3) were taken close enough (between 100 and 400 m distance) to the microprofile measurement sites to allow for quantification of the fraction of total SOU attributed to oxidation of reduced substances flux. At 40 m depth, F_{red} was less than 5 % of SOU (Figure 3.8). This fraction increases with increasing depth, but was still below 10 % even at the lowest site. The averaged F_{red} of the eight cores (Table 3.2) was $0.049 \text{ g}_{\text{DO}}^{\text{eq}} \text{m}^{-2} \text{d}^{-1}$ or only 3.6 % of the total AHM of $1.34 \text{ g}_{\text{DO}} \text{m}^{-2} \text{d}^{-1}$ (see below).

In summary, the reduced substances play only a minor role for AHM in Lake Geneva despite a high primary production. *Müller et al.* (2012a) reported a relative contribution of up to 80% of

the AHM in several small- or medium-sized lakes. They also found a direct relationship between the relative importance of reduced substances, mean hypolimnion depth and the organic carbon content in the sediments (*Steinsberger et al.* in prep.). Deeper hypolimnia of lakes correspond to larger DO reservoirs and smaller sediment surface to water volume ratios (α). The mean hypolimnion depth of Lake Geneva is much higher than in the lakes discussed in *Müller et al.* (2012a) and hypoxic conditions are found only occasionally in the deepest layers; hence, the contribution of F_{red} to SOU is low. The deep sediment oxic zone in the deeper hypolimnion of Lake Geneva confirms that organic matter mineralization is largely completed in the upper oxic zone of the lake and oxic respiration is the dominant pathway of organic matter mineralization. Consequently, the fluxes of reduced substances are very low. The results of this deep lake study are in perfect agreement with the observations in the shallow lakes and logically explain that the very high AHM rate in Lake Geneva is a consequence of the large deep hypolimnetic reservoir of DO which facilitates persistently high DO concentrations available for the mineralization of settled organic matter. In summary, as deep lakes are less likely to become anoxic above the sediment, they favor the more efficient process of oxic respiration for mineralization.

Water column mineralization: Oxygen depletion can also be quantified by the monthly DO profiles measured by CIPEL. The mean AHM calculated below a depth of 15 m (corresponding to a hypolimnion area of 534 km²; i.e., 92 % of the surface) between 1970 and 2012 was $1.34 \pm 0.34 \text{ g}_{\text{DO}} \text{ m}^{-2} \text{ d}^{-1}$. With a depletion period during summer of ~ 180 days, this corresponds to an annual loss of $1.29 \times 10^5 \text{ t}$ of DO per summer stratification period. Assuming a Redfield ratio of 138 moles of O₂ per 106 mineralized moles of carbon C (*Redfield* 1958), this corresponds to a mineralization rate of $370 \text{ mg C m}^{-2} \text{ d}^{-1}$. Graham et al. (2016) reported an annual gross sedimentation flux of organic matter between 285 and $595 \text{ mg C m}^{-2} \text{ d}^{-1}$ for the years 2009 and 2010, which is in excellent agreement with these estimates based on the DO consumption.

While the volume-averaged AHM is in good agreement with the expectations based on the organic matter flux, it gives no information about the vertical distribution of the DO depletion. In Figure 3.1, the variation of TOD during summer with depth is shown. TOD decreases rapidly in the first 100 m, stays constant over ~ 150 m, and then increases again towards the maximum depth of the lake (Figure 3.1). According to *Livingstone and Imboden* (1996), TOD can be separated into contributions proportional to (i) the water volume and (ii) the sediment surface. While the areal contribution depends on lake geometry, namely on the sediment surface to water

volume α (Livingstone and Imboden 1996), the volumetric contribution is independent from the morphology. The strong increase in α with depth explains the increase in TOD below 250 m. The model of Livingstone and Imboden (1996), however, assumes the volumetric and areal fraction of the TOD to be constant over the hypolimnion and, therefore, cannot explain the decrease in the upper layers. The trend of SOU decreasing with depth, as shown in Figure 3.7, partially explains the decreasing TOD. However, even if SOU is subtracted from TOD, the remaining fraction, which can now be interpreted as water column mineralization (WCM), still shows a decreasing trend in the upper hypolimnion. As the quality of organic matter does not significantly differ between the water column and the sediment, it is reasonable to assume that the decrease in WCM with depth is also caused by an decrease in easily degradable organic matter.

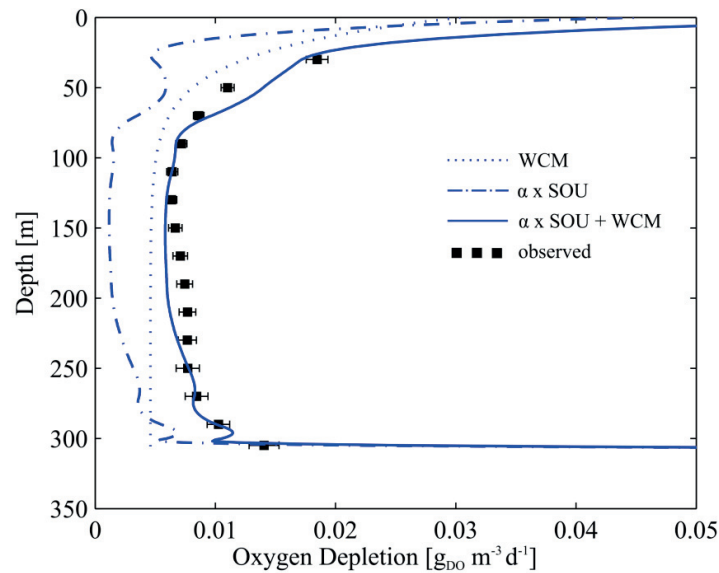


Figure 3.9: Total oxygen depletion (TOD) as function of depth and contributions of the water column mineralization (WCM) and sediment oxygen uptake (SOU). α is the sediment surface to volume ratio.

Conceptual model of oxygen depletion: The observed variations of the SOU and TOD with depth build the foundation of a conceptual model of DO depletion based on the deductive model of *Livingstone and Imboden* (1996). As described in their study, TOD can be separated in a water-volume-proportional term, WCM [$\text{g m}^{-3} \text{d}^{-1}$], and a sediment area-proportional term, SOU [$\text{g}_{\text{DO}} \text{m}^{-2} \text{d}^{-1}$]:

$$\text{TOD} = \text{WCM} + \alpha \text{SOU} \quad (3.3)$$

where α [m^{-1}] again is the sediment surface to water volume ratio (Figure 3.2).

Our analysis of SOU and TOD shows that both terms are substantially decreasing with depth. Assuming that the DO depletion rate is a sum of (i) an exponentially decreasing contribution caused by easily degradable organic material and (ii) a refractory contribution of slowly degrading organic matter which does not significantly vary over depth, SOU and WCM can be described as:

$$\text{SOU} = S_1 + S_2 e^{\frac{-(z-z_0)}{z_\tau}} \quad (3.4)$$

$$\text{WCM} = W_1 + W_2 e^{\frac{-(z-z_0)}{z_\tau}} \quad (3.5)$$

where S_1 and W_1 are the contribution of the slowly degrading part of the organic matter and S_2 and W_2 describe the contribution of the fast degrading fraction at the lower end of the productive zone (depth z_0 ; here set to 30 m). z_τ is the depth where the contribution of the fast degrading part is reduced to $1/e$ of the value at z_0 . The degradation depth scale z_τ is assumed to be the same for WCM and SOU, as the decrease in amount and quality of organic matter is identical for the water column and the sediment.

The parameters S_1 , S_2 and z_τ were determined based on the experimental results of the microprofile measurements. Afterwards, SOU was subtracted from the mean TOD values determined by the long term data. Equation (3.5) was then fitted to the residual. The best fit was found for $S_1 = 0.25 \text{ g m}^{-2} \text{d}^{-1}$; $S_2 = 1.45 \text{ g m}^{-2} \text{d}^{-1}$; $W_1 = 0.0046 \text{ g m}^{-3} \text{d}^{-1}$; $W_2 = 0.0078 \text{ g m}^{-3} \text{d}^{-1}$ and $z_\tau = 25.1 \text{ m}$. In Figure 3.9, the model result is shown in comparison to the values of the monitoring data.

Since the model relies on several free parameters (S_1 , S_2 , W_1 , W_2 and z_τ), the exact quantification of an individual parameter is complicated given the relatively large variations in the data.

However, the model is able to reproduce TOD and allows for separation of the volumetric and

areal contributions. The model deviates in regions with large gradients of α , namely near 50 m and at maximum depth. At these depths, the increased SOU is reduced by the effect of turbulent vertical diffusion. In theory, equations (3.3) to (3.5) are only valid for non-diffusive water columns. However, this is not always strictly fulfilled, especially in deep layers where turbulent diffusion and DO gradients are comparatively large.

Between 100 and 250 m depth, the proposed model approximates TOD with a root mean square error of only 7%. Larger deviations are observed above and below. Below 250 m, the error is mainly caused by the neglect of vertical diffusion. Diffusion leads to a net flux of DO from regions with low depletion to regions with higher depletion. Since the highest depletion rates are expected in the deepest layers with high values for α , neglecting diffusion leads to an underestimate of SOU in these regions, as seen in Figure 3.9. Similarly, the local bathymetry with an increase in α around 50 m leads to an overestimation in the model above ~100 m. The increased mixing due to gyre formation and basin-scale internal waves may also explain parts of the deviations since the resulting DO transport to the deeper layers is not considered.

According to this simplified model, 69% of TOD takes place in the interior of the water column while 31% occurs at the sediment surface. These results compare well with values found in the literature. *Bouffard et al.* (2013) found SOU to be responsible for 51-53% of the TOD for Lake Erie (maximum depth: 64 m). *Beutel et al.* (2007) reported 40-50% for the San Vicente Reservoir in California (maximum depth: 58 m). In general, the importance of SOU decreases with lake depth since smaller values of α favor mineralization in the water column. Consequently, the AHM in small-to-medium sized lakes can be explained completely by SOU as exemplified by *Müller et al.* (2012a).

3.5 Conclusions

The different contributors to the total oxygen depletion (TOD) in Lake Geneva were measured and conceptually explained. For the first time, sediment oxygen uptake (SOU) was measured autonomously at deep sediment surfaces of lakes via microprofiling. In parallel, sediment cores were retrieved to measure the flux of reduced substances from deeper sediment layers into the water column. The findings were complemented by more than 40 years of oxygen monitoring data.

- The SOU rate decreased from $\sim 1 \text{ g}_{\text{DO}} \text{ m}^{-2} \text{ d}^{-1}$ at 43 m to only $\sim 0.2 \text{ g}_{\text{DO}} \text{ m}^{-2} \text{ d}^{-1}$ at 133 m. Conversely, as SOU decreases, the thickness of the sediment oxic zone increases. This observation can be attributed to decreasing availability of labile organic carbon. Besides the implications for the oxygen budget of the whole lake, the varying SOU and the corresponding sediment oxic zone are highly relevant for the lake ecosystem as fish egg survival depends on oxic conditions in the upper sediment. Within the sediment, the flux of reduced substances was extremely low at all locations. This confirms that oxic respiration of organic carbon, as opposed to oxidation of reduced substances originating from anoxic mineralization, is the dominant pathway of DO consumption in deep lakes.
- The analysis of long-term monitoring data suggests that the water column mineralization (WCM) shows a similar decrease with depth. A conceptual model explains the variation of the TOD with depth based on parametrizations for SOU, WCM, and lake hypsometry.
- Based on the developed conceptual model, the relative importance of SOU and WCM can be estimated. Compared to shallow lakes, the relative importance of WCM ($\sim 70\%$ of TOD) is high. This agrees with the expectation that SOU becomes less important with increasing lake depth and, in turn, decreasing sediment surface to water volume.
- The exponential decrease of oxygen depletion in the upper hypolimnion of Lake Geneva provides evidence of the important role of the quality of organic matter for oxygen depletion processes and carbon cycling. Detailed analysis of the fraction of labile and refractory organic matter in different depths of the lake could further improve the understanding of oxygen depletion in deep lakes.

Acknowledgements

The authors would like to thank Adrien Gaudard, Patrick Kathriner, Sébastien Lavanchy, Vincent Nouchi, Love Råman Vinnå, Katrina Schuler, and Michael Schurter for their help during the field measurement campaigns. The long-term monitoring data were provided by the Commission International pour la Protection des Eaux du Léman (CIPEL) and the Information System of the SOERE OLA (<http://si-ola.inra.fr>), INRA Thonon-les-Bains. The first author was supported by the Swiss National Science Foundation grants 200021_146652 and 200020_165517. The second author was supported by the Swiss National Science Foundation grants 200021_146234.

References

- Anneville, O., and J. P. Pelletier. 2000. Recovery of Lake Geneva from eutrophication: quantitative response of phytoplankton. *Arch. Hydrobiol.* **148**: 607–624. doi:10.1127/archiv-hydrobiol/148/2000/607
- Beutel, M., I. Hannoun, J. Pasek, and K. B. Kavanagh. 2007. Evaluation of hypolimnetic oxygen demand in a large eutrophic raw water reservoir, San Vicente Reservoir, Calif. *J. Environ. Eng.* **133**: 130–138. doi:10.1061/(ASCE)0733-9372(2007)133:2(130)
- Bouffard, D., J. D. Ackerman, and L. Boegman. 2013. Factors affecting the development and dynamics of hypoxia in a large shallow stratified lake: Hourly to seasonal patterns. *Water Resour. Res.* **49**: 2380–2394. doi:10.1002/wrcr.20241
- Bryant, L. D., C. Lorrai, D. McGinnis, A. Brand, A. Wüest, and J. C. Little. 2010a. Variable sediment oxygen uptake in response to dynamic forcing. *Limnol. Oceanogr.* **55**: 950–964. doi:10.4319/lo.2009.55.2.0950
- Bryant, L. D., D. F. McGinnis, C. Lorrai, A. Brand, J. C. Little, and A. Wüest. 2010b. Evaluating oxygen fluxes using microprofiles from both sides of the sediment-water interface. *Limnol. Oceanogr. Meth.* **8**: 610–627. doi:10.4319/lom.2010.8.0610
- Caudron, A., E. Lasne, C. Gillet, J. Guillard, and A. Champigneulle. 2014. Thirty years of reoligotrophication do not contribute to restore self-sustaining fisheries of Arctic charr, *Salvelinus alpinus*, in Lake Geneva. *Fish. Res.* **154**: 165–171. doi:10.1016/j.fishres.2014.01.023
- Cornett, R. J., and F. H. Rigler. 1979. Hypolimnetic oxygen deficits: their prediction and interpretation. *Science* **205**: 580–581. doi:10.1126/science.205.4406.580
- Cornett, R. J., and F. H. Rigler. 1980. The areal hypolimnetic oxygen deficit: An empirical test of the model. *Limnol. Oceanogr.* **25**: 672–679. doi:10.2307/2835755
- Delebecque, A. 1898. *Les lacs français*, Typographie Chamerot et Renouard.
- Diaz, R. J. 2001. Overview of hypoxia around the World. *J. Environ. Qual.* **30**: 275–281. doi:10.2134/jeq2001.302275x
- Fang, X., and H. G. Stefan. 2009. Simulations of climate effects on water temperature, dissolved oxygen, and ice and snow covers in lakes of the contiguous United States under past and future climate scenarios. *Limnol. Oceanogr.* **54**: 2359–2370.

- Forel, F. 1895. *Le Léman: Monographie Limnologique. Tome II. Mécanique, Hydraulique, Thermique, Optique, Acoustique, Chimie*, Lausanne, F. Rouge.
- Friedrich, J., F. Janssen, D. Aleynik, and others. 2014. Investigating hypoxia in aquatic environments: diverse approaches to addressing a complex phenomenon. *Biogeosciences* **11**: 1215–1259. doi:10.5194/bg-11-1215-2014
- Gelda, R. K., M. T. Auer, and S. W. Effler. 1995. Determination of sediment oxygen demand by direct measurement and by inference from reduced species accumulation. *Mar. Freshwater Res.* **46**: 81–88. doi:10.1071/MF9950081
- Graham, N.D., D. Bouffard, J.-L. Loizeau. 2016. The influence of bottom boundary layer hydrodynamics on sediment focusing in a contaminated bay, *Environ. Sci. Pollut. Res.* doi:10.1007/s11356-016-7715-9
- Hutchinson, C. E. 1957. *A Treatise of Limnology. Vol. 1 Geography, Physics and Chemistry*, Wiley, New York, New York, USA.
- Jenny, J.-P., F. Arnaud, B. Alric, J.-M. Dorioz, P. Sabatier, M. Meybeck, and M.-E. Perga. 2014. Inherited hypoxia: A new challenge for reoligotrophicated lakes under global warming. *Global Biogeochem. Cy.* **28**: 1413–1423. doi:10.1002/2014GB004932
- Kiefer, I., A. Wüest, D. Odermatt, M. Riffler, and D. Bouffard. 2017. Are surface temperature and chlorophyll in a large deep lake related? An analysis using satellite imagery. Submitted to *Limnol. Oceanogr.*
- Kristensen, E., and M. Holmer. 2001. Decomposition of plant materials in marine sediment exposed to different electron acceptors (O_2 , NO_3^- , and SO_4^{2-}), with emphasis on substrate origin, degradation kinetics, and the role of bioturbation. *Geochim. Cosmochim. Acta* **65**: 419–433. doi:10.1016/S0016-7037(00)00532-9
- Kubáň, P., H. T. A. Nguyen, M. Macka, P. R. Haddad, and P. C. Hauser. 2007. New fully portable instrument for the versatile determination of cations and anions by capillary electrophoresis with contactless conductivity detection. *Electroanal.* **19**: 2059–2065. doi:10.1002/elan.200703908
- Livingstone, D. M., and D. M. Imboden. 1996. The prediction of hypolimnetic oxygen profiles: a plea for a deductive approach. *Can. J. Fish. Aquat. Sci.* **53**: 924–932. doi:10.1139/f95-230
- Loizeau, J.-L., and J. Dominik. 2005. The history of eutrophication and restoration of Lake Geneva. *Terre et Environnement* **50**: 43–56.

- Lorke, A., B. Müller, M. Maerki, and A. Wüest. 2003. Breathing sediments: The control of diffusive transport across the sediment-water interface by periodic boundary-layer turbulence. *Limnol. Oceanogr.* **48**: 2077–2085. doi:10.2307/3597808
- Maerki, M., B. Müller, and B. Wehrli. 2006. Microscale mineralization pathways in surface sediments: A chemical sensor study in Lake Baikal. *Limnol. Oceanogr.* **51**: 1342–1354. doi:10.2307/3841181
- Matzinger, A., B. Müller, P. Niederhauser, M. Schmid, and A. Wüest. 2010. Hypolimnetic oxygen consumption by sediment-based reduced substances in former eutrophic lakes. *Limnol. Oceanogr.* **55**: 2073–2084. doi:10.4319/lo.2010.55.5.2073
- Müller, B., Y. Wang, M. Dittrich, and B. Wehrli. 2003. Influence of organic carbon decomposition on calcite dissolution in surficial sediments of a freshwater lake. *Water Res.* **37**: 4524–4532. doi:10.1016/S0043-1354(03)00381-6
- Müller, B., L. D. Bryant, A. Matzinger, and A. Wüest. 2012a. Hypolimnetic oxygen depletion in eutrophic lakes. *Environ. Sci. Technol.* **46**: 9964–9971. doi:10.1021/es301422r
- Müller, B., L. Och, and A. Wüest. 2012b. Entwicklung des Phosphorhaushalts und der Sauerstoffzehrung im Sempacher- und Baldeggersee. EAWAG report.
- Müller, B., R. Gächter, and A. Wüest. 2014. Accelerated water quality improvement during oligotrophication in peri-alpine lakes. *Environ. Sci. Technol.* **48**: 6671–6677. doi:10.1021/es4040304
- North, R. P., R. L. North, D. M. Livingstone, O. Köster, and R. Kipfer. 2014. Long-term changes in hypoxia and soluble reactive phosphorus in the hypolimnion of a large temperate lake: Consequences of a climate regime shift. *Glob. Change Biol.* **20**: 811–823. doi:10.1111/gcb.12371
- Rast, W., and G. F. Lee. 1978. Summary analysis of the North American (US portion) OCED eutrophication project: Nutrient loading - lake response relationships and trophic state indices. U.S. Environmental Protection Agency, Corvallis Oregon.
- Razmi, A. M., D. A. Barry, R. Bakhtyar, D. Le, A. Dastgheib, U. Lemmin, and A. Wüest. 2013. Current variability in a wide and open lacustrine embayment in Lake Geneva (Switzerland). *J. Great Lakes Res.* **39**: 455–465. doi:10.1016/j.jglr.2013.06.011
- Redfield, A. C. 1958. The biological control of chemical factors in the environment. *Am. Sci.* **46**: 205–221.

- Rippey, B., and C. McSorley. 2009. Oxygen depletion in lake hypolimnia. *Limnol. Oceanogr.* **54**: 905–916.
- Røy, H., M. Huettel, and B. B. Jørgensen. 2004. Transmission of oxygen concentration fluctuations through the diffusive boundary layer overlying aquatic sediments. *Limnol. Oceanogr.* **49**: 686–692. doi:10.4319/lo.2004.49.3.0686
- Rucinski, D. K., D. Beletsky, J. V. DePinto, D. J. Schwab, and D. Scavia. 2010. A simple 1-dimensional, climate based dissolved oxygen model for the central basin of Lake Erie. *J. Great Lakes Res.* **36**: 465–476.
- Rucinski, D. K., J. V. DePinto, D. Scavia, and D. Beletsky. 2014. Modeling Lake Erie’s hypoxia response to nutrient loads and physical variability. *J. Great Lakes Res.* **40**: 151–161.
- Savoye, L., P. Quetin, and A. Klein. 2015. Evolution physico-chimique des eaux du Léman, données météorologiques, apports par les affluents au Léman et au Rhône à l’aval de Genève. *Rapp. Comm. int. prot. eaux Léman contre pollut, campagne 2014*: 21-51.
- Scavia, D., J. David Allan, K. K. Arend, and others. 2014. Assessing and addressing the re-eutrophication of Lake Erie: Central basin hypoxia. *J. Great Lakes Res.* **40**: 226–246. doi:10.1016/j.jglr.2014.02.004
- Schwefel, R., A. Gaudard, A. Wüest, and D. Bouffard. 2016. Effects of climate change on deep-water oxygen and winter mixing in a deep lake (Lake Geneva)—Comparing observational findings and modeling. *Water Resour. Res.* doi:10.1002/2016WR019194
- Schindler, D. W. 2006. Recent advances in the understanding and management of eutrophication. *Limnol. Oceanogr.* **51**: 356–363. doi:10.4319/lo.2006.51.1_part_2.0356
- Smith, D. A., and G. Matisoff. 2008. Sediment oxygen demand in the central basin of Lake Erie. *J. Great Lakes Res.* **34**: 731–744. doi:10.1016/S0380-1330(08)71614-9
- Sobek, S., E. Durisch-Kaiser, R. Zurbrügg, N. Wongfun, M. Wessels, N. Pasche, and B. Wehrli. 2009. Organic carbon burial efficiency in lake sediments controlled by oxygen exposure time and sediment source. *Limnol. Oceanogr.* **54/6**, 2243-2254.
- Steinsberger, T., M. Schmid, A. Wüest, R. Schwefel, B. Wehrli, and B. Müller. 2017. Organic carbon mass accumulation rate regulates the flux of reduced substances from deep lake sediments. *Environ. Sci. Technol.*, in prep.
- Thienemann, A. 1928. *Der Sauerstoff im eutrophen und oligotrophen See: ein Beitrag zur Seetypenlehre*, E. Schweizerbart.

- Torres, N. T., P. C. Hauser, G. Furrer, H. Brandl, and B. Müller. 2013. Sediment porewater extraction and analysis combining filter tube samplers and capillary electrophoresis. *Environ. Sci. Process. Impacts* **15**: 715–720. doi:10.1039/c3em00068k
- Vivier, P. 1944. Température et oxygène dissous dans le Léman français. *Travaux du laboratoire d'hydrobiologie de l'Université de Grenoble* **20**: 25–35.

Supporting information for chapter 3: Using small-scale measurements to estimate hypolimnetic oxygen depletion in a deep lake

**Robert Schwefel¹, Thomas Steinsberger^{2,3}, Damien Bouffard^{1,2}, Lee Bryant⁴, Beat Müller²
and Alfred Wüest^{1,2}**

¹ Physics of Aquatic Systems Laboratory - Margaretha Kamprad Chair of Environmental Science and Limnology, ENAC, EPFL, Lausanne, Switzerland

² Eawag, Swiss Federal Institute of Aquatic Science and Technology, CH-6047 Kastanienbaum, Switzerland

³ Institute of Biogeochemistry and Pollutant Dynamics, ETH Zurich, CH-8092 Zurich, Switzerland

⁴ Research Unit for Water, Environment and Infrastructure Resilience (WEIR), University of Bath, BA2 7AY Bath, United Kingdom

Introduction

Table S3.1 and S3.2 summarize details about the microprofile and sediment core measurements.

Figure S3.1 describes the variability of oxygen measurements at five different measurement stations in Lake Geneva 1976-1981 and Figure S3.2 shows the concentration of reduced substances measured by sediment pore water analysis.

Table S3.1: Details about the microprofile measurements

Nr.	Depth	Coordinates	# of profiles	ADCP	Date
MP1	43	6.516° E / 46.505° N	4	No	25.10.2013
MP2	45	6.515° E / 46.506° N	12	Yes	11. – 12. 03. 2014
MP3	72	6.519° E / 46.496° N	7	No	21. – 23. 05. 2014
MP4	76	6.523° E / 46.496° N	13	No	14. – 15. 07. 2014
MP5	93	6.545° E / 46.486° N	30	Yes	27. – 29.08.2015
MP6	109	6.519° E / 46.487° N	13	Yes	17. – 18. 07. 2014
MP7	133	6.545° E / 46.486° N	13	Yes	15. – 16. 07. 2015
Total	43 to 133		92	4	7 times

Table S3.2: Details about the sediment core measurements

Nr.	Depth	Coordinates	Date
LG1	40	6.520 °E / 46.505 °N	15.07.2014
LG2	80	6.522 °E / 46.495 °N	15.07.2014
LG3	120	6.520 °E / 46.484 °N	16.07.2014
LG4	310	6.581 °E / 46.461 °N	16.07.2014
LG5	310	6.589 °E / 46.453 °N	13.07.2015
LG6	300	6.652 °E / 46.477 °N	14.07.2015
LG7	200	6.535 °E / 46.477 °N	15.07.2015
LG8	175	6.601 °E / 46.416 °N	15.07.2015

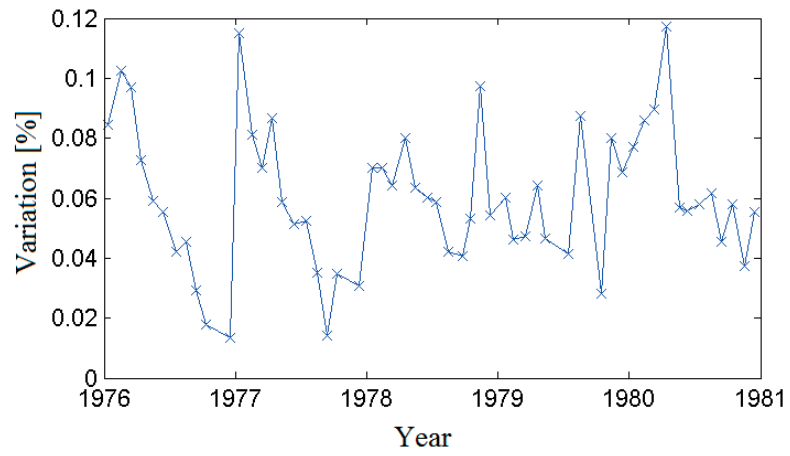


Figure S3.1: Coefficient of variation for the oxygen data measured at five different stations (SHL1, SHL2, CRG3, CRG23 and CRG24) for 1976 - 1981.

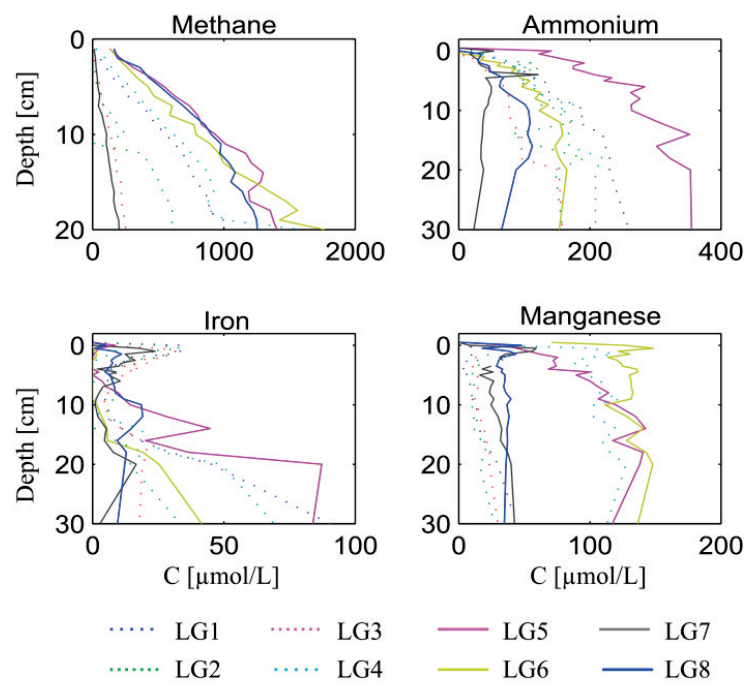


Figure S3.2: Concentration of reduced substances as function of depth.

Chapter 4:

Effects of climate change on deep-water oxygen and winter mixing in a deep lake (Lake Geneva) – Comparing observational findings and modeling

Robert Schwefel¹, Adrien Gaudard², Alfred Wüest^{1,2}, Damien Bouffard¹

¹ Physics of Aquatic Systems Laboratory, Margaretha Kamprad Chair, Ecole Polytechnique Fédérale de Lausanne, Institute of Environmental Engineering, CH-1015 Lausanne, Switzerland.

² Eawag, Swiss Federal Institute of Aquatic Science and Technology, Surface Waters – Research and Management, Kastanienbaum, Switzerland.

Water Resources Research **52**(11)

Robert Schwefel performed the modelling, the analysis of the field data and model results and the writing of the manuscript. Adrien Gaudard performed the model calibration and contributed to the analysis of the results and the revision of the manuscript. Damien Bouffard and Alfred Wüest contributed to the analysis of the results and the manuscript revision.

Abstract

Low concentrations of dissolved oxygen remain a global threat to the ecological health of lakes and reservoirs. In addition to high nutrient loads, climate-induced changes in stratification and mixing represent another anthropogenic threat resulting in decreased deep-water oxygen levels. The analysis of 43 years of monitoring data from Lake Geneva shows a decreasing trend neither in the areal hypolimnetic mineralization rate, nor in extent of hypoxia. Instead, hypoxic conditions are predominantly controlled by deep mixing in winter and much less by the trophic variations over the past decades. To reproduce winter mixing, the one-dimensional hydrodynamic model SIMSTRAT was specially adapted to deep lakes and run for several climate scenarios. The simulations predicted a decrease in the maximum winter mixing depth from an average of ~172 m for 1981–2012 to ~136 m and ~127 m in response to predicted atmospheric temperatures between 2045–2076 and 2070–2101 according to the IPCC scenario A1B. Concurrently, events with complete homogenization of temperature and oxygen in winter will decrease by ~50%. Consequently, the hypolimnetic oxygen concentrations will significantly decrease. These results demonstrate that changes in deep mixing can have stronger impact than eutrophication on the deep-water oxygen levels of oligomictic lakes.

4.1 Introduction

Among the various parameters used to monitor the health of lake ecosystems, dissolved oxygen remains of uttermost importance. During the 20th century, hypoxia in lakes and oceans increased significantly due to eutrophication caused by anthropogenic nutrient inputs (e.g. *Diaz* 2001, *Farley* 2012, *Friedrich et al.* 2014). Thus, initial lake management efforts focused on reducing nutrients and in turn, many empirical models were proposed to quantify oxygen depletion utilizing nutrient loading and lake morphometry (e. g. *Cornett and Rigler* 1979, *Matthews and Effler* 2006, *Müller et al.* 2012). Although the use of these models often facilitated meaningful solutions in the form of nutrient load reduction and often led to an increase in water quality, the relation between phosphorus and oxygen depletion in lakes is still not completely understood (*Gächter and Müller* 2003).

The effect of global warming on water quality of lakes and reservoirs and on oxygen renewal, in particular, is currently a critical concern (*Fang and Stefan* 2009, *Foley et al.* 2012, *Zhang et al.* 2015). Average lake surface temperature increases of 0.01 to 0.1 °C yr⁻¹ have been observed in the recent past (*Schneider and Hook* 2010, *Shinoda et al.* 2011, *O'Reilly et al.* 2015) and a further increase is predicted (*Schmid et al.* 2014). A major effect of global warming is to increase the duration of summer stratification. *Foley et al.* (2012) analyzed four decades of data from a small temperate lake in England and observed an average increase of 38 days in the duration of summer stratification. This change led to an increase in hypolimnetic anoxia, despite the fact that the rate of oxygen depletion decreased during the assessed four decades. Besides the extent of the stratified season, the maximal depth of convective mixing in winter (i.e. “winter mixing”) also plays a key role for oxygen renewal in deep lakes. Therefore, climate-induced reductions in the intensity of winter mixing directly affect the oxygen budget. *Livingstone et al.* (2006) and *North et al.* (2014) found an increase in stratification and hypoxia in Lake Zurich based on data dating back to 1949. Furthermore, *Straile et al.* (2003) reported a decrease in deep-water oxygen renewal due to reduced winter mixing in Lake Constance. *Zhang et al.* (2015) observed similar trends in a deep reservoir in China. *Jankowski et al.* (2006) and *Straile et al.* (2010) investigated the effect of extraordinary warm periods and concluded that increased thermal stratification will have an impact on the deep-water oxygen content.

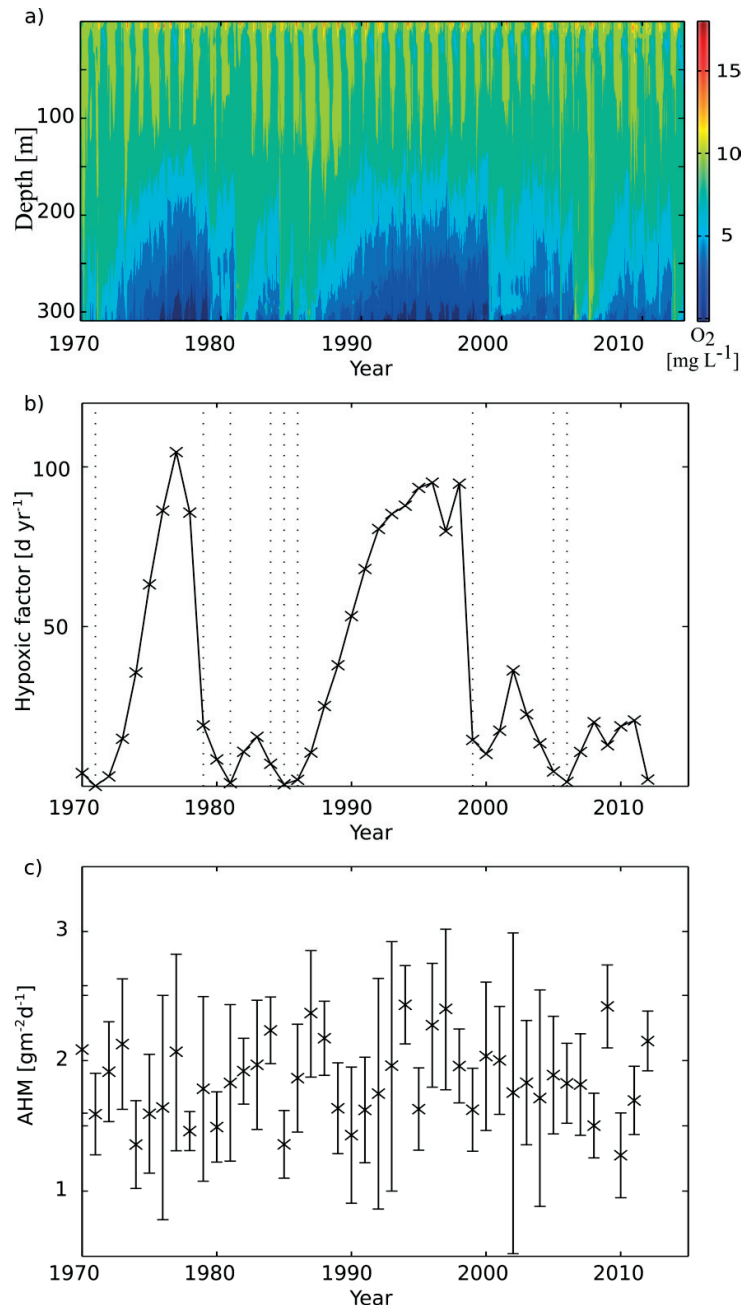


Figure 4.1: a) Contour plot of oxygen concentration 1970–2012. b) Hypoxic factor HF 1970–2012. The concept of the HF (Nürnberg, 2002) is explained in the methods chapter. The threshold oxygen concentration to calculate HF is $4\ mg\ L^{-1}$. The dashed lines represent winter mixing reaching below 270 m. c) Areal hypolimnetic mineralization rate (AHM; depth > 15 m) for the period 1970–2012.

Few studies, so far, have modeled the impact of climate change on winter mixing and deep-water oxygen budget. *Fang and Stefan* (2009) simulated the oxygen dynamics of 27 generically designed types of lakes at 209 different hypothetical locations in the USA meant to be representative for typical temperate lakes. For the expected conditions, the authors also predicted the effects of a two-fold increase in CO₂ concentration in the atmosphere. Their study focused on rather shallow lakes (depth < 24 m), with annually occurring complete winter mixing. *Fink et al.* (2014) and *Perroud and Goyette* (2012) used horizontally averaged one-dimensional k-ε turbulence models (*Goudsmit et al.* 2002) to predict the impact of climate change on the deep waters of Lakes Constance and Geneva. These studies, however, focused on heat budget and lake-atmosphere coupling. *Matzinger et al.* (2007) assessed the combined effects of atmospheric warming and different nutrient loads on the oxygen budget and temperature structure of Lake Ohrid. The authors concluded that even under decreasing nutrient inputs, hypoxic conditions in the deep-water would drastically expand if the air temperature increases at the current rate during the next decades as the lake would become meromictic with a permanently anoxic deep layer. *Sahoo et al.* (2013) predicted the same for Lake Tahoe where deep mixing and deep-water oxygen concentration will decrease drastically according to numerical simulations based on different IPPC emission scenarios.

We consider Lake Geneva as an ideal water body to investigate the impact of deep winter mixing on hypoxia. Lake Geneva is warm monomictic with irregularly occurring complete winter mixing, thereby leading to hypolimnetic oxygen levels which are highly sensitive to mixing. The extent of hypoxia as well as deep-water oxygen levels showed strong fluctuations over the last 40 years (Figures 4.1a and 4.1b). Nevertheless, the measured oxygen depletion remained high, despite a drastic reduction in phosphorus concentration from ~90 to ~20 µg L⁻¹ between 1980 and 2010 (*Savoye et al.* 2015, *Müller et al.* 2014). In response to the decreasing nutrient input, a subsequent decrease in the areal hypolimnetic mineralization rate (AHM) of organic matter in the hypolimnion was expected. The AHM describes the mineralization of organic matter in the hypolimnion and is identical to the areal hypolimnetic oxygen depletion rate under oxic conditions (*Matzinger et al.* 2010). However, the AHM oscillated around a mean of $1.34 \pm 0.34 \text{ g O}_2 \text{ m}^{-2} \text{ d}^{-1}$ (calculated as oxygen depletion during summer stagnation below a constant depth of 15 m) without any significant trend over the last 40 years (Figure 4.1c). We therefore hypothesize

that the amount of oxygen resupply during winter mixing events is the governing factor controlling the extent and strength of hypoxia in deep hypolimnia.

To verify this hypothesis, we analyzed 43 years of temperature and oxygen data with focus on (i) water column stability, (ii) deep mixing, and (iii) the occurrence and severity of hypoxia. We also assess possible future changes by numerical modeling based on regional climate predictions (*CH2011* 2011) and varying water clarity. The calibrated model provides essential information for investigating the effect of future climate changes on deep-water mixing and oxygen budgets.

4.2 Methods

4.2.1 Study site

Lake Geneva is a deep perialpine lake situated between France and Switzerland (46.45° N, 6.52° E, Figure S4.1) at an altitude of 372 m. With a volume of 89 km³ and a surface area of 580 km², it is the largest freshwater lake in Western Europe. Lake Geneva is a warm monomictic lake with deepest seasonal mixing in late February / early March. Due to its maximum depth of 309 m and mild temperatures, the lake never freezes in winter, and complete winter overturns occur irregularly (every fifth year on average). Between 1983 and 2000, the mean annual surface temperature increased by ~1 °C with seasonally increases of up to 2 °C in summer (*Gillet and Quélin* 2006, *Molinero et al.* 2007). The length of the stratification period consequently increased (*Anneville et al.* 2013).

Lake Geneva is still recovering from its eutrophic past. Once considered as an oxygen-rich oligotrophic lake (*Forel* 1895, *Vivier* 1944), the trophic state turned to eutrophic due to high phosphorus input after 1950 (*Lachavanne* 1980). Until 1980, phosphorus concentration increased by a factor of seven and caused decreasing water transparency, changes in phytoplankton and zooplankton composition and low oxygen concentrations in the deep hypolimnion (*Loizeau and Dominik* 2005). Oxygen measurements were only occasionally performed before 1957, but all measurements showed consistently high oxygen concentrations even in the deepest layers (*Forel* 1895, *Delebecque* 1898, *Vivier* 1944). Despite a reduction in phosphorus, hypoxic conditions still appear occasionally in the deep layers and AHM remained high.

4.2.2 Measurements and analysis of lake profiles

Oxygen and temperature profiles are measured regularly since 1957 at point SHL2 (46.45° N; 6.59° E; Figure S4.1) by the Commission Internationale pour la Protection des Eaux du Léman (CIPEL). Sampling frequencies were 6 to 8 times per year before 1970, monthly between 1970 and 1980 and 18 to 20 times per year after 1980. The number of sample depths per profile varied between 12 and 20. The vertical resolution was 2.5 to 10 m down to 30 m depth, followed by 50 m between 50 and 250 m depth and again finer below 250 m (mostly at 275, 290, 300, 305 and 309 m). Details concerning the sampling methodology are annually published in the scientific reports of CIPEL, the most recent one is *Savoye et al. (2015)*.

Temperature and oxygen profiles were interpolated vertically and temporally to one meter and one day resolution using cubic spline interpolation. Afterward, water density (ρ) was estimated from temperature data; and the Schmidt stability (S), a measure of the stability of the overall stratification, was calculated:

$$S = \frac{1}{A_0} \sum_{z=0}^{z_{max}} (z - z_*) (\rho(z) - \rho_*) A(z) \Delta z, \quad (4.1)$$

where A_0 is the lake surface area, $\rho(z)$ and $A(z)$ are the density and area at depth z , varying from 0 (lake surface) to z_{max} (maximal depth) by $\Delta z = 1$ m and. z_* is the volumetric mean depth defined as

$$z_* = \frac{1}{V} \sum_{z=0}^{z_{max}} z A(z) \Delta z \quad (4.2)$$

with the lake volume V . ρ_* is the mean density (defined equivalent to z_*).

In this study, we use Nürnberg's hypoxic factor HF (*Nürnberg 2002*) to quantify hypoxia. It combines information about the annual temporal and spatial extent of hypoxia based on measured oxygen profiles and lake geometry and is defined as

$$HF = \frac{1}{1 \text{ year}} \sum_{t_i=0}^{1 \text{ year}} \left(\frac{A_i}{A_0} \right) \Delta t_i \quad (4.3)$$

where A_i denotes the area under which the oxygen concentration falls below a predefined critical value during the time Δt_i . Accordingly, HF [d yr^{-1}] describes the relative lake area, under which hypoxic conditions are observed multiplied by the duration of the hypoxic conditions in the year considered. An HF of 365 d yr^{-1} means that the complete lake volume is hypoxic throughout the year. A value of 100 d yr^{-1} could either mean that the lake was hypoxic the entire year below an

area equal to 27 % (100/365) of the surface area or that the complete lake was hypoxic for 100 d yr⁻¹ (or any combination of the two). To distinguish hypoxic from oxic water, a threshold oxygen level needs to be defined. Here we chose 4 mg L⁻¹ justified by local water quality regulations, based on minimally tolerable oxygen concentration for fish egg survival (*Müller et al.* 2012, *Savoye et al.* 2015). Using other thresholds (*Nürnberg* 2002, *North et al.* 2014) would not significantly change our findings.

Table 4.1. Parameters Used in SIMSTRAT Model. Details in *Goudsmit et al.* (2002).

Parameter	Value Used in This Study		Description
p ₁	1.09		Correction for absorption of infrared radiation
p ₂	0.90		Correction for sensible heat flux
C ₁₀	0.0017		Wind drag coefficient 10 m above water
α	Summer: 0.035	Winter: 0.009	Fraction of wind energy transferred to seiche energy
q	1.25		Distribution coefficient for seiche energy

The maximal depth of deep convective winter mixing (hereafter called mixing depth) was determined based on the vertical structure of the oxygen and temperature profiles during the winters 1970–2012. Data before 1970 were omitted since the temporal resolution was considered as too coarse. Uncertainty in the mixing depth estimation depends on the vertical resolution of the profiles and is usually large for mixing depth shallower than 250 m, where the vertical resolution reaches 50 m between 50 and 250 m depth. Independent from this study, mixing depth is calculated since 1978 by CIPEL and published in the annual reports (e.g. *Savoie et al.* 2015 for 2014). A comparison shows only minor differences.

4.2.3 One-dimensional model

4.2.3.1 The numerical model SIMSTRAT

In the present study, the one-dimensional (1D) model SIMSTRAT (*Goudsmit et al.* 2002) was used (Version 2015). It combines a buoyancy-extended k- ϵ -model with an internal seiche model to estimate the vertical diffusivity as function of time and depth. SIMSTRAT was already applied to medium- to large-sized lakes for different purposes (*Peeters et al.* 2002, *Matzinger et al.* 2007, *Fink et al.* 2014).

In the past decades, several 1D model approaches have been developed and were able to reproduce thermal structures of lakes with high accuracy (e.g. *Imberger et al.* 1978, *Burchard et al.* 1999). *Perroud et al.* (2009) compared the performance of four such 1D models in predicting the temperature structure of Lake Geneva. Among them, SIMSTRAT performed best and showed a satisfactory reproduction of temperature profiles and thermocline variability. However, the 2009 version of SIMSTRAT tends to overestimate deep-water mixing and temperatures in the deep layers. *Perroud and Goyette* (2012) found a systematical deviation of +0.5 °C for the deeper hypolimnion of Lake Geneva throughout the year. This is caused by systematic overestimation of the turbulent kinetic energy transferred by the internal seiche, which results in too large downward fluxes of heat during winter. The model transfers a constant fraction of the wind energy into internal seiching. In reality, the efficiency of this transfer is dependent on the internal wave period and, in turn, on the density stratification (*Patterson et al.* 1984). To force internal seiching efficiently, the wind has to blow in a consistent direction for a time of ideally one-quarter of the seiching period. The longer the period, the more unlikely this condition is met. In turn, this period is a function of geometry and stratification (*Bouffard and Boegman* 2012). In Lake Geneva, the period of the most dominant Kelvin wave varies from 70 h in mid-summer to

110 h in early spring and much larger values during weakly stratified winter periods (*Bouffard and Lemmin* 2013). A more realistic parameterization of the internal seiching of the 1D model has to take the strength of the stratification into account. The easiest approach, used in this study, is to use two different parameters α for the energy transfer depending on the season. Values of α used in this study for winter (November to March), and summer (April to October) are listed in Table 4.1.

4.2.3.2 Model forcing

Meteorological data: Air temperature, cloud cover, solar radiation, vapor pressure and wind speed and direction were obtained from the meteorological station Pully (46.52° N, 6.67° E, MeteoSwiss). The data are available from 1981–2013 on ten minutes and hourly time increments. A comparison between model runs with ten minutes and hourly resolution reveals only minor differences because internal waves dominate the hypolimnion dynamics and time scales of several hours are necessary to generate them. Subsequently, hourly forcing was chosen.

Light absorption: The absorption of shortwave-radiation in SIMSTRAT is calculated by Lambert-Beer-law:

$$H_S(z) = G(1 - r_s)\exp(-\epsilon_{\text{abs}}z). \quad (4.4)$$

where G is the ground solar radiation [W m^{-2}] and r_s its reflection. We estimated ϵ_{abs} [m^{-1}] by daily interpolation of monthly to bimonthly measured Secchi depth data (z_{SD}) provided by CIPEL and by using the empirical relation

$$\epsilon_{\text{abs}} = k z_{\text{SD}}^{-1}. \quad (4.5)$$

During model calibration, $k = 1.4$ turned out to be the best value for Lake Geneva.

Inflow and outflow: The primary inflow to Lake Geneva is the Rhône River with a mean discharge of $185 \text{ m}^3 \text{ s}^{-1}$ which is responsible for 70 to 75% of total inflow. Other contributors include Dranse, Aubonne, Venoge, and several other small rivers. Recent multibeam survey confirms the existence of groundwater inflows but their role remain marginal as recently shown with a giant (100 m diameter) pockmark in the nearby Lake Neuchâtel (*Reusch et al.* 2015). The mean residence time is ~ 11.6 yr and therefore, the in- and outflows were neglected, after testing that the thermal structure of Lake Geneva was only little affected by this assumption. Since *Pilotti et al.* (2014) showed that water residence time is expected to increase with changing

climate, this assumption is also justified for model runs with increased air temperature. However, the Rhône inflow still acts as a small additional source of deep-water oxygen during periods of flood-induced turbidity underflows (*Loizeau and Dominik 2000, Fink et al. 2016*).

Model calibration: Using CIPEL temperature monitoring data from 1981–2012, we optimized the model parameters p_1 , p_2 , C_{10} , α and q (Table 4.1) by minimizing the root-mean-square error (RMSE)

$$\text{RMSE} = \sqrt{\frac{1}{M} \sum_{i=1}^M (T_i^m - T_i^o)^2} \quad (4.6)$$

between measurements and model results (M is the total number of measurements, T_i^m is the modeled temperature at time “ i ”, and T_i^o is the observed temperature for measurement i). The calibration was repeated for varying absorption coefficients k (Equation 4.5). The lowest RMSE were found for $k = 1.4$, which was close to $k = 1.3$ used by *Fink et al. (2014)* for Lake Constance. A detailed description of the function of the calibrated parameters is provided in the SI (Text S4.1). To achieve the most realistic reproduction, the parameter α was set different for summer and winter and the value for winter (Table 4.1) was further adapted to reproduce the temperatures of the deepest layers accurately.

4.2.3.3 Climate change

Potential future local atmospheric temperatures were estimated from *CH2011* (2011) according to the A1B emission scenario (balanced use of fossil and renewable energy) of the Intergovernmental Panel on Climate Change (*IPCC 2013*). To address the local impact of global climate change, different regional downscaling algorithms of the global model were applied in *CH2011* (2011). The most probable air temperature change at Lake Geneva was estimated by averaging the predicted changes of four meteorological stations around the lake (Pully, 46.52° N, 6.67° E; Montreux-Clarens, 46.45° N, 6.90° E; Genève-Cointrin 46.25° N, 6.13° E; Nyon-Changins 46.4° N, 6.23° E). For each station, the mean of five different global climate models using ten different regional downscaling chains was determined (details in *CH2011* 2011).

In total, we investigated nine different model simulations. The comparable reference “A0” uses the meteorological forcing for the years 1981–2012. Model runs B0 and C0 simulate the lake stratification for the 2045–2076 and 2070–2101 predicted conditions. B0 and C0 are constructed by adding the mean temperature changes predicted by *CH2011* (2011) to the reference

temperature (Figure S4.2). As for cloud cover and wind speed no clear trends are predicted, only the change of air temperature is considered. The temperature additions differed depending on the season and were higher in summer with a maximum around August. Because the lake model uses local meteorological data, the temperatures given by regional climate models are not necessarily representative for the location of the lake. Since we add the average temperature increases between present conditions and future climate scenarios (Figure S4.2), we assume that the variability in temperatures and the bias between regionally modeled and local temperatures do not change significantly in the future.

In addition to temperature changes, we also investigated the effect of altered light absorption on the thermal structure of the lake (Table 4.2). In the model runs A+, B+ and C+, we investigated the combined effect of increased light absorption (+10% increase) and changing air temperatures (which were identical to the scenarios A0, B0 and C0, respectively). In scenario A-, B- and C- the absorption was decreased by the same amount. The SI contains further details about the absorption scenarios (Text S4.3).

Table 4.2. Summary of the Model Runs Employed in this Study.

Temperature Water Transparency	Recent Past 1981 - 2012	Predicted 2045 - 2076	Predicted 2070 - 2101
Increased light absorption	A+	B+	C+
Measured light absorption	A0	B0	C0
Decreased light absorption	A-	B-	C-

4.2.4 Oxygen model

The oxygen concentration was reproduced based on the results of the hydrodynamic model SIMSTRAT. Oxygen was simulated in the mixed (upper) and stratified (lower) layers of the lake. To estimate the impact on the deep part of the lake, the deepest 50 m were simulated as third (deep) layer. The depth of the upper end of the thermocline defined the base of the upper layer.

To ensure that all the primary production occurs in the upper layer we also defined a minimum thickness of 30 m for this layer.

In the upper layer, the change of oxygen $\frac{dC_{ul}}{dt}$ was modeled as

$$\frac{dC_{ul}}{dt} = c_1 k [C_{sat}(T, t) - C_{ul}] + c_2 \text{Min}(t) 1.036^{(T-20^\circ\text{C})} P_{\max} \text{Chl}(t) - c_3 \text{VOD}(z, t) \quad (4.7)$$

where the first term on the right-hand side describes the gas exchange with the atmosphere, followed by the oxygen production, and the oxygen depletion by respiration and organic matter decomposition. c_1 , c_2 and c_3 are calibration parameters ($c_1 = 1.85$, $c_2 = 0.08$, $c_3 = 0.72$). k describes the wind-dependent gas exchange velocity according to *Cole and Caraco* (1998), $C_{sat}(T)$ the saturation concentration. The oxygen production was calculated according to *Fang and Stefan* (2009) based on measured chlorophyll-a (Chl in g m^{-3}) profiles. P_{\max} (9.6 g O_2 per g Chl and per h) describes the maximal oxygen production as given in *Fang and Stefan* (2009); $\text{Min}(t)$ is the light limitation. The light limitation was considered proportional to the day length and modified by the calibration parameter c_2 (see Text S4.2). The factor $1.036^{(T-20^\circ\text{C})}$ accounts for the temperature dependency of oxygen production. Since Chl data were not available for the whole measurement period, we used the years 2007-2012 to get averaged Chl concentration with a representative annual variation and used these averaged data for the period before 2007. For the model runs representing the future climate, we used the same Chl concentrations as in model run A0. This assumption is probably an oversimplification, since increasing temperatures as well as decreasing nutrient loads lead to a change in biomass production. However, the maximal oxygen production takes place in summer and leads to an oversaturation in the surface layer. Therefore, an increasing production leads directly to an increased loss to the atmosphere. The oxygen concentration in the deep layer is less affected. One should even expect a decrease in deep-water oxygen, since increased biomass productions leads to an increase in hypolimnetic oxygen depletion. However, the oxygen depletion in the hypolimnion (Figure 4.1c) showed no significant trend in the last 40 years despite important changes in nutrient loads and temperature.

The time and depth dependent oxygen depletion rate (VOD in $\text{g O}_2 \text{ m}^{-3} \text{ d}^{-1}$) is based on the oxygen decrease in the hypolimnion during the summers 1970-2012 estimated from the CIPEL monitoring data. In winter, the oxygen depletion is expected to be lower than in summer. During model calibration, a reduction by 50% gave reasonable results and was used during all model

runs. Unfortunately, no simple method is available to determine winter depletion based only on monthly CTD-data.

In the lower and deep layers, no oxygen production takes place and water is isolated from the atmosphere. Therefore, oxygen depletion remains the only relevant process:

$$\frac{dC_{ll}}{dt} = -c_3 \cdot \text{VOD}(z, t). \quad (4.8)$$

The output of SIMSTRAT was daily averaged and allowed the thickness of the upper and lower layer to be calculated. For each day, the oxygen concentrations of the three layers were determined based on the oxygen levels of the previous day and the changes in the layer volumes. Finally, the changes in concentration during the day were calculated according to the equations (4.7) and (4.8). The model includes exchange between upper and lower layer implicitly due to the change of the layer thicknesses, the diffusion between lower and deep layer was explicitly calculated with an optimized exchange coefficient of $2 \cdot 10^{-7} \text{ ms}^{-1}$.

If the upper layer increases by a volume ΔV between the time steps $n-1$ and n , the new concentration at timestep n (C_n^{ul}) is calculated as

$$C_n^{ul} = \frac{1}{V_n^{ul}} (C_{n-1}^{ul} V_{n-1}^{ul} + C_{n-1}^{ll} \Delta V) \quad (4.9)$$

where C_n^{ul} and C_n^{ll} are the concentrations of the upper and lower layer and V_n^{ul} the volume of the upper layer at time step n . If the mixing reaches below 260 m, the lower layer disappears and the oxygen is distributed between the deep layer and the upper layer. If the mixing reaches to maximum depth, the whole lake is considered as one mixed layer.

The change in oxygen concentration caused by river inflows or outflows is neglected. The SI contains more details about the parametrization of oxygen sinks and sources in the proposed model (Text S4.2 and Figures S4.3 and S4.4).

4.3 Results

4.3.1 Field observations

4.3.1.1 Stability and deep-water mixing

The thermal structure of Lake Geneva is depicted by seasonal stratification with a thermocline depth of ~15 m in spring, which continually deepens during summer and autumn. Seasonal water-temperature fluctuations are high at the thermocline and only gradual, around ~5.7 °C, in the deep hypolimnion. Winter mixing varied between complete mixing (309 m) and mixing depths of only ~50 m with an average of 179 ± 20 m. During February and March winter mixing reached deepest and the maximum mixing depth correlated strongly with the Schmidt stability during this season (Figure 4.2). Winter mixing depth was strongly correlated ($r^2 = 0.73$) with the mean air temperature (Figure 4.3 and Figure S4.5). In contrary, mixing depth is only weakly correlated with winter wind speed ($r^2 = 0.29$). No full mixing event occurred when the Schmidt stability was larger than 50 kg m^{-1} (Figure 4.2) during February and March. Over 43 years of observations, complete winter mixing occurred during ten winters (dotted lines in Figure 4.1b), seven of them during 1981–2012, which is the period numerically modeled in this study.

4.3.1.2 Hypoxia

Since 1970, the oxygen concentrations in the deep layers of Lake Geneva decline regularly below the threshold of 4 mg L^{-1} (Figure 4.1). Hypoxic conditions were also observed between 1960 and 1970, most pronounced 1969 (*Loizeau and Dominik* 2005). Before 1960, hypoxic conditions were detected neither with direct field observations (*Forel* 1895, *Delebeque* 1898, *Vivier* 1944) nor via analysis of sediment cores (*Jenny et al.* 2014). During the last 40 years, HF varied from 0 to more than 100 d yr^{-1} , with a mean of 34 d yr^{-1} . The estimated HF corresponds to a hypoxic volume between 0 and 12 km^3 or up to 12% of the total volume. As expected, HF strongly decreased during winters with complete mixing. During two periods (1971 to 1979 and 1986 to 1999), no complete winter mixing occurred and HF rose as high as 104 d yr^{-1} in 1977 and 95 d yr^{-1} in 1996 (Figure 4.1b).

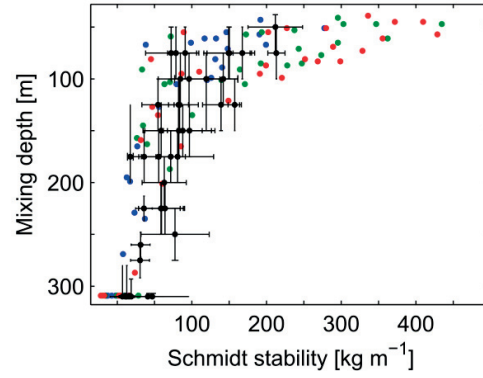


Figure 4.2: Winter mixing depth as a function of mean winter Schmidt stability (February and March). The observed depths (1981-2012, black) are compared to the model results for the reference scenario A0 (blue), scenario B0 (green), and scenario C0 (red).

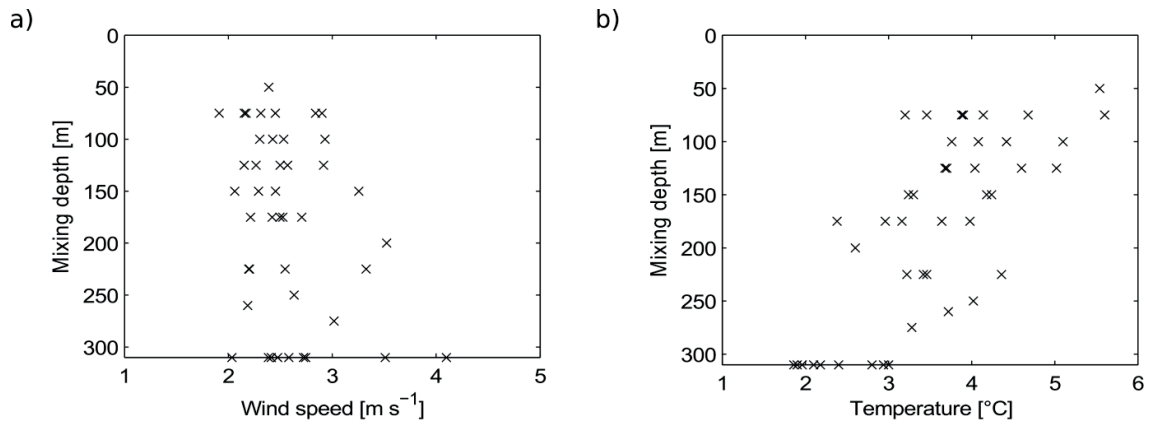


Figure 4.3: Measured mixing depth dependence of mean wind (a) and air temperature (b) during winters of 1970–2012. In the SI, a more detailed figure is given labeling each data point with its corresponding time (Figure S4.5).

4.3.2 Model results

4.3.2.1 Thermal structure and deep-water mixing

The optimized version of SIMSTRAT reproduced mean temperatures and the thermal structure of Lake Geneva well. The modeled volume-averaged mean temperature was 6.68 °C and very close to the measured value of 6.74 °C. Time series of the modeled and measured lake temperatures are shown in Figures 4.4a and 4.4b, and a contour plot is given in the SI (Figure S4.6). The seasonal evolution of the thermal structure is reproduced with a RMSE of ~2 °C in the thermocline region and better than 0.5 °C in the deeper layers. While the RMSE is low in the deep layers and no systematic bias is observed (Figures 4.4c and 4.4d), the larger differences in the thermocline are caused by baroclinic displacements, such as by internal seiches or gyres (*Lemmin and D'Adamo 1997*), which are apparent in the *in-situ* measurements but cannot be reproduced with a 1D model. The small RMSE demonstrates the success of our internal seiche parameterization using two seasonal wind energy transfer parameters (Table 4.1). Note that not only the bottom temperature, but also Schmidt stability (Figure 4.5) and deep-water mixing are very well reproduced. The averaged modeled mixing depth of 172 m was in excellent agreement with the observed mixing depth of 179 ± 20 m. However, the model shows still an overestimation during very cold winters (nine years with complete winter mixing instead of seven). In winters without complete overturn, the mixing was underestimated (113 m instead of 143 m). The original code using a single value for wind energy transfer ($\alpha = 0.025$) resulted in a 10% higher RMSE. While there was almost no improvement in the upper layers, the RMSE below 300 m improved by almost 30%.

4.3.2.2 Effects of atmospheric warming on lake temperatures

In the model runs B0 and C0 (Table 4.2), the previously validated model is now forced with increased air temperatures according to the predictions by *CH2011* (2011) for the period 2045–2076 (B0) and 2070–2101 (C0). The change in the seasonally modeled lake temperatures relative to the reference is shown in Figures 4.6b and 4.6c. We observe a temperature increase over the entire water column. However, the surface water temperature increases faster than the hypolimnion water (1.5 °C warming in the top layer compared to 0.7 °C in the deepest layer for B0; as well as ~2 °C and ~1 °C for C0), leading to an overall stronger temperature stratification. The temperature increase had a comparable pattern in the past (Figure 4.6a), although the

absolute observed temperature increase between 1957 and 2012 was less than the model prediction for the end of the century.

4.3.2.3 Effects of atmospheric warming on stratification and mixing

To quantify the stability in winter, we estimated the average Schmidt stability during February and March (S_{Winter}) as well as the depth of deepest convective mixing (Table 4.3) based on the modeled temperatures. Relative to the reference A0, the mean S_{Winter} doubled for B0, from 71 to 146 kg m^{-1} , and increased further to 179 kg m^{-1} for C0 (Table 4.3). Consequently, the mean mixing depth was reduced from 172 m to 136 m and 127 m for B0 and C0, respectively, which corresponds to reductions of ~21% and ~26% in mixing depth. The number of winters with complete mixing decreased with increasing temperatures from nine (A0) to four (C0) (Table 4.3; Figure 4.7).

Table 4.3: Comparison of Modeling Results with Measured Values of Winter Mixing and Stratification.

Period	Mean Winter Mixing Depth [m]	Winters With Complete Mixing	Schmidt Stability in Winter [kg m^{-1}]
1981 - 2012 (measured)	179	7 (22%)	80
1981 - 2012 (A0)	172	9 (28%)	71
2045 - 2076 (B0)	136	6 (19%)	146
2070 - 2101 (C0)	127	4 (13%)	179

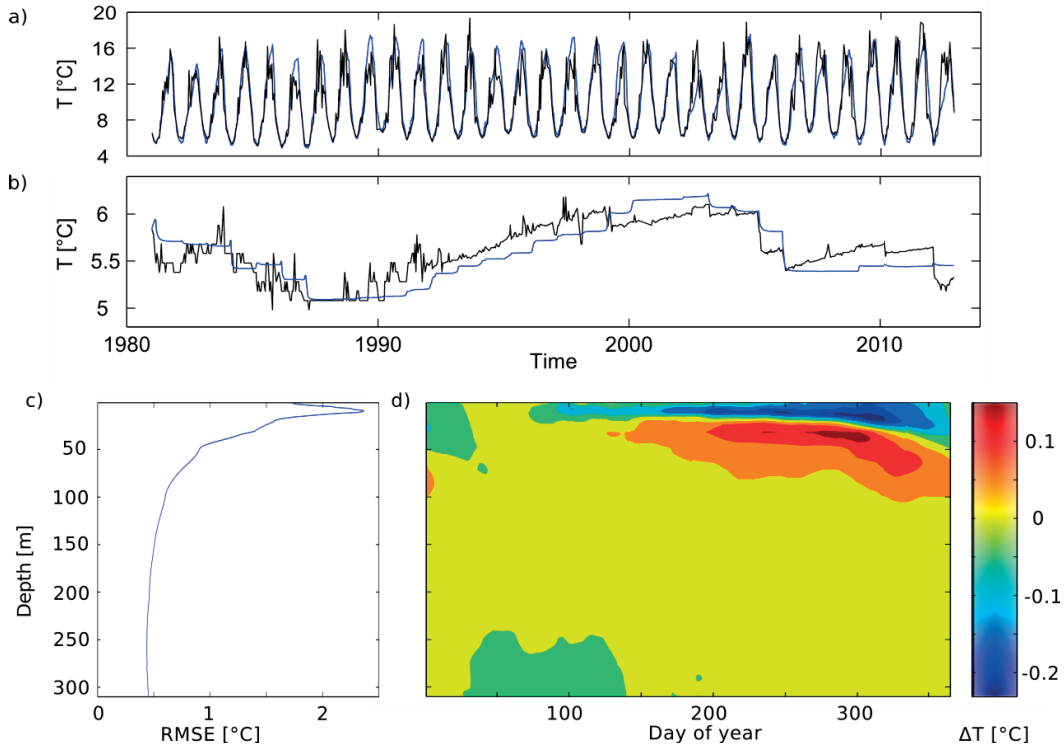


Figure 4.4: Modeled (blue) and measured (black) temperatures 1981–2012 at a) 15 m depth and b) 250 m depth. c) Root mean square error of modeled temperature output. While there are considerable differences in the thermocline (as baroclinic displacements are considered in the observations but not in the model), the modeled deep-water temperature is in good agreement with measurements. d) Deviation of the mean annual modeled temperatures from the measured mean values (1981–2012).

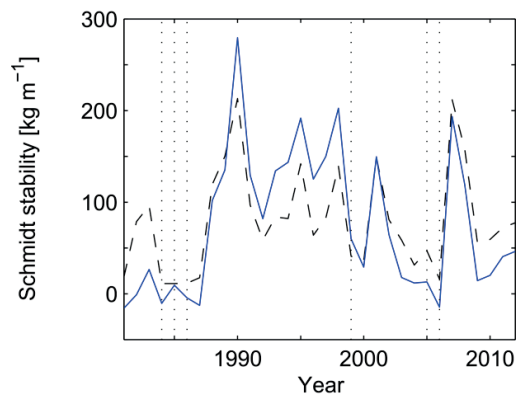


Figure 4.5: Mean Schmidt stability in February and March: measurements (black, dashed) 1981–2012 compared to simulation results for the reference scenario A0 (blue). Dotted lines indicate the winter mixing events reaching below 270 m depth (Table 4.3).

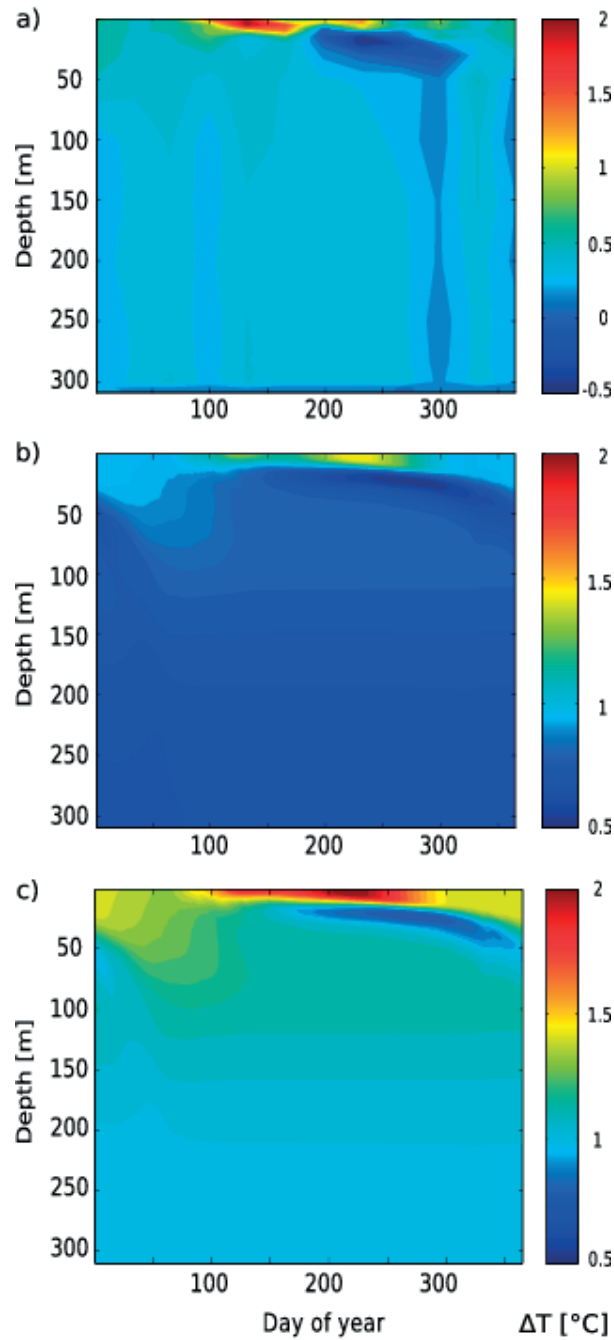


Figure 4.6: Increase in mean water column temperatures in the recent past and future: a) difference between the last 25 years (1988–2012) and the first 25 years of observation (1957–1981); b) predicted difference between the model averages for model run B0 (temperatures representative for 2060) and the reference scenario A0 (1981–2012); c) predicted difference between model results for model run C0 (temperatures representative for 2085) and reference scenario A0. Note the different scale of a) compared to b) and c).

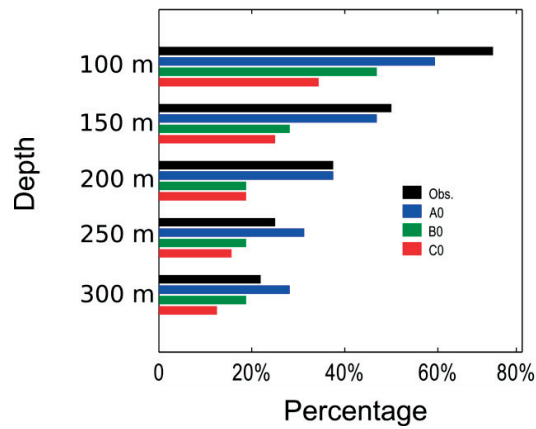


Figure 4.7: Percentage of occurrence of winter mixing reaching deeper than 100 / 150 / 200 / 250 / 300 m, respectively, for the three scenarios A0 (blue), B0 (green) and C0 (red) compared to the observations (1981–2012, black). 100% corresponds to 32 winters (Table 4.3)

4.3.2.4 Effects of water transparency

Besides the effect of increasing atmospheric temperature, we investigated the effect of variable transparency on the thermal structure of Lake Geneva (Table 4.2). The relevant model parameter is the short wave absorption coefficient, which depends on Secchi depth and in turn on particle concentration. With increased light absorption, the thermocline becomes more stable and mean lake temperature and mixing depth decrease (Table 4.4). In turn, less absorption leads to a slightly warmer lake with a less stable thermocline. The largest temperature changes are discovered below the thermocline with up to ± 0.5 °C at the end of autumn (Figures S4.7a and S4.7b). In total, the mean temperature differences between changed absorption (A-, A+) and reference (A0) were only ± 0.1 °C. In B+ and C+, where increased absorption was combined with higher air temperature, the suppression of lake warming below the thermocline was amplified (Figure S4.7d). In turn, reduced absorption (B- and C-) leads to an enhanced warming in this region (Figure S4.7c). The differences in mean temperature were about ± 0.1 °C between B+ / B- versus B0 and C+ / C- versus C0, respectively. Overall, we suggest that lower transparency cools the lake and strengthens the thermocline while higher transparency has the opposite effect.

4.3.2.5 Effects of atmospheric warming on oxygen concentrations

The oxygen model coupled to SIMSTRAT allows for estimating the impact of climate change on the oxygen budget. The comparison of the model results with the oxygen concentrations measured between 1981 and 2012 showed that the general trend in oxygen is very well reproduced (Figure 4.8). The variability between summer and winter is slightly lower in the model compared to the measurements. Particularly in 2007, the model predicts a too little oxygen gain in spring. This disagreement can be partially explained by the hydrodynamic model, which tends to underestimate the mixing in warm winters. In the following analysis, year 2007 is excluded, and additional oxygen was added to match the measured concentrations in January 2008 for the model run A0. The same amount of oxygen was added in B0 and C0. For the reference period A0, the model predicts an average oxygen production of $1.57 \cdot 10^5 \text{ t yr}^{-1}$ and a depletion of $-1.29 \cdot 10^5 \text{ t yr}^{-1}$. The gas exchange with the atmosphere was a net sink of oxygen ($-0.28 \cdot 10^5 \text{ t yr}^{-1}$). However, atmospheric exchange acts as oxygen source in winter and as sink in summer while the other components are always either sinks (depletion) or sources (production). The RMSE of the modelled oxygen concentration was 0.51 mg L^{-1} in model run A0.

The simulations B0 and C0 revealed a general decrease in oxygen. The annual mean oxygen concentration of the entire lake fell from 8.99 to 8.48 mg L^{-1} for B0 and 8.30 mg L^{-1} for C0 (Figure 4.9a). While the decrease in the mean concentration was minor, the impact on the deepest layer was much stronger. Here, the model run A0 predicts a mean value of 6.02 mg L^{-1} (measured value: 5.59 mg L^{-1}), which dropped by almost 25% to 5.01 mg L^{-1} in model run B0 and 4.60 mg L^{-1} in run C0. Consequently the fraction of values lower than 4 mg L^{-1} increased by more than 25% in model run C0, indicating longer periods of hypoxic conditions (Figure 4.9b).

Table 4.4. Modeled Mixing Depth [m] for Increased (+) and Reduced (-) Light Absorption

Period	Mixing Depth Reference [m]	Mixing Depth Stronger Absorption [m]	Mixing Depth Weaker Absorption [m]
1981 - 2012	172 (A0)	167 (A+)	177 (A-)
2045 - 2076	136 (B0)	128 (B+)	138 (B-)
2070 - 2101	127 (C0)	119 (C+)	130 (C-)

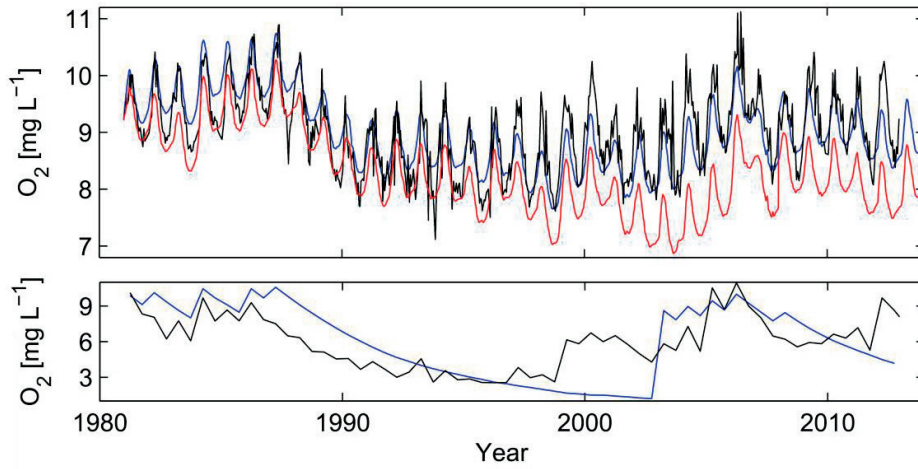


Figure 4.8: Simulated mean oxygen concentrations over the entire lake for model run A0 (blue) and C0 (red) compared to the measured oxygen concentration (black). In the lower panel, the measured (black) and simulated (model run A0, blue) oxygen concentrations for the lowest 50 m are shown.

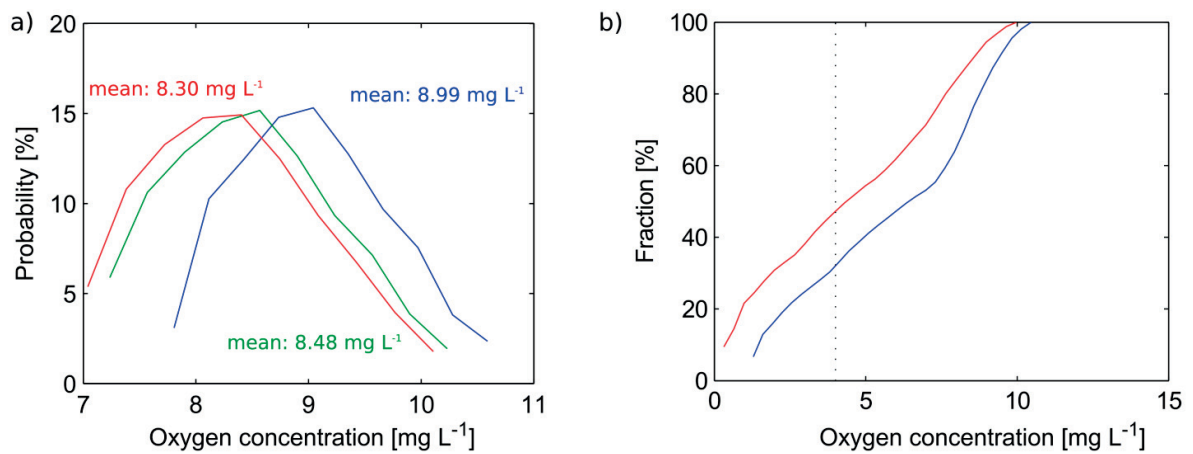


Figure 4.9: (a) Probability distribution of oxygen content of Lake Geneva for simulations A0 (blue), B0 (green) and C0 (red). The numbers show the annual mean concentration. There is a trend to lower concentrations for the simulations with higher air temperatures. (b) Cumulative sum of the oxygen concentration in the deep layer (lowest 50 m) for the model runs A0 (blue) and C0 (red). Values below the dotted lines (4 mg L^{-1}) show hypoxic conditions.

4.4. Discussion

4.4.1 Modeling deep winter mixing

The modified SIMSTRAT model provides a good estimate of deep mixing during winter (Table 4.3). The previous model version with constant wind-to-seiche energy transfer overestimated the mixing depth and predicted complete mixing in more than 50% of all winters. With the newly adapted parameterization, the simulated stability S_{Winter} is remarkably close to the observations (Figure 4.5). Consequently, the mean simulated winter mixing depth of 172 m is close to the observed value of 179 m (Table 4.3). The number of complete winter mixing events is overestimated (9 versus 7) although some of these events were very short. In contrast, the model underestimates the mixing during winters with shallow mixing depth. We explain this deviation with the temperature dependence of the energy transfer to internal waves. The transfer is more effective during warmer winters, when the internal seiche period remains shorter. Using the same parameterization for every winter thus leads to a mixing depth overestimation during cold winters and an underestimation during warm winters. Nevertheless, our simple approach reproduces the temperature pattern and mixing behavior without bias and with a low RMSE especially in the deep layers as shown in Figure 4.4d.

4.4.2 Effect of climate change on lake warming and stratification

Lake warming under higher atmospheric temperature was clearly apparent in all simulations (Figures 4.6b and 4.6c). The simulated lake warming is even stronger in the future than the previously observed trends based on systematic temperature measurements since 1957 (Figure 4.6a). Consequently, lake stratification becomes stronger. The annual mean Schmidt stability increases from 1250 kg m⁻¹ (A0) to 1490 kg m⁻¹ (B0) and 1590 kg m⁻¹ (C0). Not only the increased temperature gradient between epilimnion and metalimnion, but also increased mean temperatures lead to this stability increase. The volumetric averaged lake temperature over the reference period was 6.7 °C. This value increased to 7.5 °C for B0 and 7.9 °C for C0. The Schmidt stability (equation 4.1) is dependent on the density difference due to temperature gradients and temperature change per se, as expressed by

$$\frac{\partial \rho}{\partial T} = -\rho \alpha_{\text{th}}(T), \quad (4.10)$$

as the thermal expansivity α_{th} increases with temperature. Therefore, increasing temperatures cause higher stability even when gradients do not change. For Lake Geneva, the predicted increase in temperature between 1997 and 2035 is typically 1.5 °C in the upper part of the thermocline and 0.5 °C in the deep-water. For typical summer conditions (22.5 °C at 7 m depth and 8.5 °C at 25 m), this results in an increase of the temperature gradient from 0.78 to 0.83 °C m⁻¹ (6.4%), whereas the mean thermal expansivity increases from $1.52 \cdot 10^{-4}$ to $1.62 \cdot 10^{-4}$ °C⁻¹ (6.6%). Both effects thus have a comparable impact on the increase in stability.

With increased air temperatures, warming is less pronounced between 25 and 75 m depth during the second half of the stratification period. This minimum in warming is caused by the stronger summer stratification, which reduces the warming just below the thermocline. Since this phenomenon occurs mainly in late summer and autumn, it is irrelevant during the period of deep winter mixing.

Compared to climate warming the effects of transparency on the hypolimnion temperature are small. The biggest effect is visible in the thermocline, which deepened with decreasing absorption. The effect on the mixing depth was only marginal (Table 4.4). This is fundamentally different in shallow lakes with smaller hypolimnia. There, water quality was found to be a significant factor affecting the thermal structure (*Snucins and Gunn 2000, Persson and Jones 2008*). Details about the effect of water transparency are given in the SI (Text S4.3).

4.4.3 Implication for deep-water mixing and oxygen budget

The Schmidt stability in late winter (February and March) is strongly correlated with the mixing depth, both for the observations as well as for the model simulations (Figure 4.2). The shape of the curve in Figure 4.2 is similar for all investigated model runs. For B0 and C0, model results are shifted to shallower mixing depths and higher stabilities. The mean Schmidt stability increased for B0 and C0 and, in turn, winter mixing depth decreased (Figures 4.2 and 4.7).

The model predicts a decrease of the mean mixing depth from 172 m (reference A0) to 136 m (B0) and 127 m (C0), respectively. Seven full overturns were observed in the simulation period which corresponds to 22% of all winters (e.g. one every four to five winters, Figure 4.7). This value decreased to six (19%) for the period 2045–2076, although the model seems to overestimate extreme mixing events. For 2070–2101 the number was further reduced to four (i.e. one every 8 winters, 13%). Hence, the frequency of deep-water reoxygenation will be reduced by

a factor of two by the end of the century according to our model results. Furthermore, the duration of unstratified winter periods will be shorter in the future (defined as the period in which the temperature difference in the top 50 m is less than 3 °C). From 125 days for the period 1981–2012, the duration decreased to 118 days (-6%) for 2045–2076 and to 115 days (-8%) for 2070–2101.

Our study predicts complete winter mixing events even for the warmest scenario while *Matzinger et al.* (2007) and *Sahoo et al.* (2013) predicted both a complete halt of winter mixing in their studies. While the deep hypolimnion shows a constant temperature increase during periods without complete mixing, the epilimnion experiences strong seasonal fluctuations (Figures 4.4a and 4.4b). Although a warmer lake tends to be more stable (thermal expansivity α_{th} ; equation 4.10), the hypolimnion continuously warms in absence of mixing and becomes susceptible for deep mixing in extraordinary cold winters. While *Matzinger et al.* (2007) use a constant temperature ramp-up to predict future air temperature, our study kept the observed temperature fluctuations between 1981 and 2012 in addition to the warming trend. With this realistic temperature variability, extraordinary cold winters and complete deep mixing still occur. Local climate conditions, which dictate a stronger temperature increase in summer compared to winter (*CH2011* 2011; Figure S4.2), also favor occasional winter mixing.

A comparison of the model results of the runs (A-, B-, C-) with (A+, B+, C+) demonstrates that the effect of sunlight absorption on mixing depth is marginal. The higher absorption has the strongest effect at the end of the stratification period in autumn. At the end of winter, when deep mixing occurs, the temperature difference between the different absorption scenarios was not more than ± 0.1 °C. The predicted difference in mixing depth of ~ 5 m between A0 and A+ / A-, respectively (Table 4.4), was seven times smaller than the differences due to air temperature increase (from A0 to B0). The beginning of the unstratified winter period was later by negligible degree. Similar to the mixing depth, this effect was marginal (change of 1 day only) and caused no relevance for the oxygen budget.

To estimate the impact of deep mixing on oxygen concentration, we set up a simplified three-box oxygen model. Despite its substantial simplifications, the proposed model was able to reproduce the trends in oxygen concentration between 1981 and 2012 (Figure 4.8). The difference between oxygen production and consumption was about $0.28 \cdot 10^5$ t yr⁻¹, which directly relates to the net oxygen flux to the atmosphere and the net carbon burial in the sediment. Assuming the Redfield

ratio (*Redfield* 1958) of 138 mol of O₂ per 106 mol of carbon (C), this corresponds to a net burial of 14 g C m⁻² yr⁻¹, which is produced in the upper layer but not consumed and accumulates in the sediments without contribution to the oxygen depletion. This flux is in good agreement with core-based estimates of net sediment accumulation of 11 g C m⁻² yr⁻¹ in Lake Geneva (*Span et al.* 1990, *Loizeau et al.* 2012). In addition, the net oxygen system production of 1.57·10⁵ t yr⁻¹ corresponds to carbon gross sedimentation, i.e., a total biomass production of 79 g C m⁻² yr⁻¹, which is fully consistent with the estimate of *Graham et al.* (2016). The oxygen depletion of -1.29·10⁵ t yr⁻¹ corresponds to 1.23 g O₂ m⁻² d⁻¹ for a stagnation duration of 180 days (only slightly lower than the estimate of 1.34 g O₂ m⁻² d⁻¹ based on CIPEL measurements; Figure 4.1c). The oxygen budget terms are in excellent agreement with independent observations in Lake Geneva and confirm that the model realistically reproduces the relevant processes.

To estimate the effects of changing climatic conditions, we focused on the simulations without considering the negligible effect of light absorption (Table 4.4). The mean deep-water oxygen concentration decreases by 6% for B0 and by 8% for C0. However, the variability of oxygen content in the lake will be larger, especially in winter. While there will be still large amounts of oxygen after complete mixing events, the concentrations will be lower during episodes without deep mixing (Figure 4.9a). For this reason, the variations in the deep layer are much larger than the changes of the average oxygen level. For the layer of the lowest 50 m above maximum depth, the model predicted concentrations below 4 mg L⁻¹ in 31% of the simulation period in the reference scenario A0. In model run C0, this fraction increased to 39%, which corresponds to an increase by 25% (Figure 4.9b). Since complete winter mixing will still occur even with the strongest climate warming (Tables 4.3 and 4.4), we do not expect the deepest layer to be depleted entirely. Even for the strongest warming, the lake is still able to reoxygenize during particularly cold winters, but less often than in the past.

As we assume constant oxygen depletion, possible changes in oxygen production, mineralization or gas exchange were not addressed. Decreasing oxygen consumption rates as well as an increased oxygen supply in winter due to stronger winds could improve the oxygen concentration. However, no trend in oxygen depletion was apparent since 1970 and stronger wind speeds could simultaneously increase sediment oxygen uptake (*Bryant et al.* 2010).

4.5 Conclusions

The analysis of 43 years of combined oxygen and temperature data in the deepest part of Lake Geneva demonstrated that hypoxic conditions occur regularly in its deep layers. As no decreasing trend in hypolimnetic oxygen depletion (currently at $1.34 \text{ g O}_2 \text{ m}^{-2} \text{ d}^{-1}$) nor in the hypoxic factor (average 34 d yr^{-1} , varying between 0 and 120 d yr^{-1}) were observed, hypoxia was found to depend on winter air temperatures and subsequent deep winter mixing.

Deep-water temperatures of Lake Geneva were realistically simulated using an improved version of a one-dimensional k-epsilon model specially adapted to deep lakes. The model successfully reproduces the observed trends in deep convective winter mixing in the lake. Using the proposed model, future changes in the lake thermal structure were predicted for various locally downscaled IPCC A1B climate scenarios. The results show a strong decrease in the mean winter mixing depth from 172 m to 136 m (for 2045-2076) and 127 m (for 2075-2101). At the end of the century, complete deep homogenization in winter will decrease by $\sim 50\%$ but will not cease completely. After long periods of stratification, extraordinary cold winters still lead to a homogenization of the lake. In additional model simulations, the effect of light absorption was investigated. The results confirmed that stronger light absorption results in cooler hypolimnia, however, with minor effects on lake stratification and winter mixing.

As a consequence of the reduced mixing, our model predictions show that average oxygen concentrations in the hypolimnion will decrease by the end of the century by $\sim 8\%$. Moreover, the deepest layers are expected to experience an increase in hypoxic conditions by more than 25% due to reduced winter mixing and fewer complete mixing events. Since independent simulations of other deep lakes predicted a regime shift from oligomictic to meromictic with even more severe consequences for the oxygen budget, predicting the mixing behavior under climate-induced forcing remains an important challenge for lake modeling.

Acknowledgments

We are thankful to the following institutions for the important data support: The CH2011 data we obtained from the Center for Climate Systems Modeling (C2SM, <http://www.ch2011.ch>); oxygen and lake temperature data were provided by the Commission Internationale pour la Protection des Eaux du Léman (CIPEL) and the Information System of the SOERE OLA (<http://si-ola.inra.fr>),

INRA Thonon-les-Bains. Meteorological data used in this study are archived and distributed by the Swiss Federal Office of Meteorology and Climatology, MeteoSwiss (obtained via IDAWEB, see <http://www.meteoswiss.admin.ch/home/services-and-publications/beratung-und-service/data-portal-for-teaching-and-research.html>). The source code of SIMSTRAT can be obtained from the authors; an online publication is planned for the future.

We thank Miki Hondzo, Lee Bryant and the anonymous reviewers for the valuable comments on the manuscript. The first author was funded by the Swiss National Science Foundation grants 200021_146652 and 200020_165517.

References

- Anneville, O., M. Beniston, N. Gallina, C. Gillet, S. Jacquet, and M. Perroud. 2013. L’empreinte du Changement climatique sur le Léman. *Arch. Sci.* 66: 157–172.
- Burchard, H., K. Bolding, and M.R. Villarreal. 1999. GOTM, a general ocean turbulence model: Theory, implementation and test cases. Space Applications Institute.
- Bouffard, D., and L. Boegman. 2012. Basin-scale internal waves. In *Encyclopedia of Lakes and Reservoirs*. Springer Netherlands, 102–107.
- Bouffard, D., and U. Lemmin. 2013. Kelvin waves in Lake Geneva. *J. Great Lakes Res.* 39: 637–645. doi:10.1016/j.jglr.2013.09.005
- Bryant, L. D., C. Lorrai, D. McGinnis, A. Brand, A. Wüest, and J. C. Little. 2010. Variable sediment oxygen uptake in response to dynamic forcing. *Limnol. Oceanogr.* 55: 950–964. doi:10.4319/lo.2009.55.2.0950
- CH2011. 2011. Swiss Climate Change Scenarios CH2011. C2SM, Zurich.
- Cole, J. J., and N. F. Caraco. 1998. Atmospheric exchange of carbon dioxide in a low-wind oligotrophic lake measured by the addition of SF₆. *Limnol. Oceanogr.* 43: 647–656. doi:10.4319/lo.1998.43.4.0647
- Cornett, R. J., and F. H. Rigler. 1979. Hypolimnetic oxygen deficits: Their prediction and interpretation. *Science* 205: 580–581. doi:10.1126/science.205.4406.580
- Delebecque, A. 1898. *Les lacs français*. Typographie Chamerot et Renouard.
- Diaz, R. J. 2001. Overview of Hypoxia around the World. *J. Environ. Qual.* 30: 275–281. doi:10.2134/jeq2001.302275x

- Fang, X., and H. G. Stefan. 2009. Simulations of climate effects on water temperature, dissolved oxygen, and ice and snow covers in lakes of the contiguous United States under past and future climate scenarios. *Limnol. Oceanogr.* 54: 2359–2370.
- Farley, M. 2012. Eutrophication in fresh waters: An international review, p. 258–270. In *Encyclopedia of Lakes and Reservoirs*. Springer.
- Fink, G., M. Schmid, and A. Wüest. 2014. Large lakes as sources and sinks of anthropogenic heat: Capacities and limits. *Water Resour. Res.* 50: doi:10.1002/2014WR015509. doi:10.1002/2014WR015509
- Fink, G., M. Wessels, and A. Wüest. 2016. Flood frequency matters: Why climate change degrades deep-water quality of peri-alpine lakes. *J. Hydrol.* 540: 457–468. doi:10.1016/j.jhydrol.2016.06.023
- Foley, B., I. D. Jones, S. C. Maberly, and B. Rippey. 2012. Long-term changes in oxygen depletion in a small temperate lake: effects of climate change and eutrophication. *Freshwater Biol.* 57: 278–289. doi:10.1111/j.1365-2427.2011.02662.x
- Forel, F. 1895. *Le Léman: Monographie Limnologique*. Tome II. Mécanique, Hydraulique, Thermique, Optique, Acoustique, Chimie, Lausanne, F. Rouge.
- Friedrich, J., F. Janssen, D. Aleynik, and others. 2014. Investigating hypoxia in aquatic environments: diverse approaches to addressing a complex phenomenon. *Biogeosciences* 11: 1215–1259. doi:10.5194/bg-11-1215-2014
- Gächter, R., and B. Müller. 2003. Why the phosphorus retention of lakes does not necessarily depend on the oxygen supply to their sediment surface. *Limnol. Oceanogr.* 48: 929–933. doi:10.4319/lo.2003.48.2.0929
- Gillet, C., and P. Quétin. 2006. Effect of temperature changes on the reproductive cycle of roach in Lake Geneva from 1983 to 2001. *J. Fish Biol.* 69: 518–534. doi:10.1111/j.1095-8649.2006.01123.x
- Goudsmit, G. H., H. Burchard, F. Peeters, and A. Wüest. 2002. Application of $k-\epsilon$ turbulence models to enclosed basins: The role of internal seiches. *J. Geophys. Res.* 107: 3230. doi:10.1029/2001JC000954
- Graham, N., D. Bouffard, J.-P. Loizeau. 2016. What goes up, must come down: Implications of bottom boundary layer hydrodynamics and sediment focusing for a contaminated bay. *Environ. Sci. Pollut. R.*, doi 10.1007/s11356-016-7715-9

- Imberger, J., I. Loh, B. Hebbert, and J. Patterson. 1978. Dynamics of reservoir of medium size, J. Hydraul. Div. 104(5): 725–743.
- IPCC. 2013. Climate Change 2013: The Physical Science Basis. Contribution of Working Group I to the Fifth Assessment Report of the Intergovernmental Panel on Climate Change. Cambridge University Press.
- Jankowski, T., D. M. Livingstone, H. Bührer, R. Forster, and P. Niederhauser. 2006. Consequences of the 2003 European heat wave for lake temperature profiles, thermal stability, and hypolimnetic oxygen depletion: Implications for a warmer world. *Limnol. Oceanogr.* 51: 815–819. doi:10.4319/lo.2006.51.2.0815
- Jenny, J.-P., F. Arnaud, B. Alric, J.-M. Dorioz, P. Sabatier, M. Meybeck, and M.-E. Perga. 2014. Inherited hypoxia: A new challenge for reoligotrophicated lakes under global warming. *Global Biogeochem. Cy.* 28: 1413–1423. doi:10.1002/2014GB004932
- Lachavanne, D. P. J.-B. 1980. Les manifestations de l'eutrophisation des eaux dans un grand lac profond: le Léman (Suisse). *Schweiz. Z. Hydrologie* 42: 127–154. doi:10.1007/BF02502431
- Lemmin, U., and N. D'Adamo. 1997. Summertime winds and direct cyclonic circulation: observations from Lake Geneva. *Ann. Geophys.* 14: 1207–1220. doi:10.1007/s00585-996-1207-z
- Livingstone, D. M. 2003. Impact of Secular Climate Change on the Thermal Structure of a Large Temperate Central European Lake. *Climatic Change* 57: 205–225. doi:10.1023/A:1022119503144
- Loizeau, J.-L., and J. Dominik. 2000. Evolution of the Upper Rhone River discharge and suspended sediment load during the last 80 years and some implications for Lake Geneva. *Aquat. sci.* 62: 54–67. doi:10.1007/s000270050075
- Loizeau, J.-L., and J. Dominik. 2005. The history of eutrophication and restoration of Lake Geneva. *Terre et Environnement* 50: 43–56.
- Loizeau, J.-L., S. Girardclos, and J. Dominik. 2012. Taux d'accumulation de sédiments récents et bilan de la matière particulaire dans le Léman (Suisse-France). *Arch. Sci* 65: 81–92.
- Matthews, D. A., and S. W. Effler. 2006. Long-Term Changes in the Areal Hypolimnetic Oxygen Deficit (AHOD) of Onondaga Lake: Evidence of Sediment Feedback. *Limnol. Oceanogr.* 51: 702–714. doi:10.2307/4499623

- Matzinger, A., M. Schmid, E. Veljanoska-Sarafiloska, and others. 2007. Eutrophication of ancient Lake Ohrid: Global warming amplifies detrimental effects of increased nutrient inputs. *Limnol. Oceanogr.* 52: 338–353. doi:10.4319/lo.2007.52.1.0338
- Matzinger, A., B. Müller, P. Niederhauser, M. Schmid, and A. Wüest. 2010. Hypolimnetic oxygen consumption by sediment-based reduced substances in former eutrophic lakes. *Limnol. Oceanogr.* 55: 2073–2084. doi:10.4319/lo.2010.55.5.2073
- Mazumder, A., and W. D. Taylor. 1994. Thermal structure of lakes varying in size and water clarity. *Limnol. Oceanogr.* 39: 968–976. doi:10.4319/lo.1994.39.4.0968
- Molinero, J. C., O. Anneville, S. Souissi, L. Lainé, and D. Gerdeaux. 2007. Decadal changes in water temperature and ecological time series in Lake Geneva, Europe—relationship to subtropical Atlantic climate variability. *Clim. Res.* 34: 15–23. doi:10.3354/cr034015
- Müller, B., L. D. Bryant, A. Matzinger, and A. Wüest. 2012. Hypolimnetic oxygen depletion in eutrophic lakes. *Environ. Sci. Technol.* 46: 9964–9971. doi:10.1021/es301422r
- Müller, B., R. Gächter, and A. Wüest. 2014. Accelerated water quality improvement during oligotrophication in peri-alpine lakes. *Environ. Sci. Technol.* 48: 6671–6677. doi:10.1021/es4040304
- North, R. P., R. L. North, D. M. Livingstone, O. Köster, and R. Kipfer. 2014. Long-term changes in hypoxia and soluble reactive phosphorus in the hypolimnion of a large temperate lake: Consequences of a climate regime shift. *Glob. Change Biol.* 20: 811–823. doi:10.1111/gcb.12371
- Nürnberg, G. K. 2002. Quantification of oxygen depletion in lakes and reservoirs with the Hypoxic Factor. *Lake Reserv. Manage.* 18: 299–306. doi:10.1080/07438140209353936
- O'Reilly, C. M., S. Sharma, D. K. Gray, and others. 2015. Rapid and highly variable warming of lake surface waters around the globe. *Geophys. Res. Lett.* 42: 2015GL066235. doi:10.1002/2015GL066235
- Patterson, J. C., P. F. Hamblin, and J. Imberger. 1984. Classification and dynamic simulation of the vertical density structure of lakes. *Limnol. Oceanogr.* 29: 845–861. doi:10.4319/lo.1984.29.4.0845
- Peeters, F., D. M. Livingstone, G.-H. Goudsmit, R. Kipfer, and R. Forster. 2002. Modeling 50 years of historical temperature profiles in a large central European lake. *Limnol. Oceanogr.* 47: 186–197.

- Perroud, M., S. Goyette, A. Martynov, M. Beniston, and O. Anneville. 2009. Simulation of multiannual thermal profiles in deep Lake Geneva: A comparison of one-dimensional lake models. *Limnol. Oceanogr. Meth.* 54: 1574–1594.
- Perroud, M., and S. Goyette. 2012. Interfacing a one-dimensional lake model with a single-column atmospheric model: 2. Thermal response of the deep Lake Geneva, Switzerland under a $2 \times \text{CO}_2$ global climate change. *Water Resour. Res.* 48: doi:10.1029/2011WR011222. doi:10.1029/2011WR011222
- Persson, I., and I. D. Jones. 2008. The effect of water colour on lake hydrodynamics: a modelling study. *Freshwater Biol.* 53: 2345–2355. doi:10.1111/j.1365-2427.2008.02049.x
- Redfield, A. C. 1958. The biological control of chemical factors in the environment. *Am. Sci.* 46: 205–221.
- Reusch, A., M. Loher, D. Bouffard, and others. 2015. Giant lacustrine pockmarks with subaqueous groundwater discharge and subsurface sediment mobilization. *Geophys. Res. Lett.* 42: 3465–3473. doi:10.1002/2015GL064179
- Savoye, L., Quetin, P., and A. Klein. 2012. Rapport Commission International pour la Protection des eaux du Léman, Campagne 2014: Évolution physico-chimique des eaux du Léman (Éléments majeurs). Commission International pour la Protection des Eaux du Léman (CIPEL).
- Schmid, M., S. Hunziker, and A. Wüest. 2014. Lake surface temperatures in a changing climate: A global sensitivity analysis. *Climatic Change* 124: 301–315. doi:10.1007/s10584-014-1087-2
- Schneider, P., and S. J. Hook. 2010. Space observations of inland water bodies show rapid surface warming since 1985. *Geophys. Res. Lett.* 37: L22405. doi:10.1029/2010GL045059
- Shimoda, Y., M. E. Azim, G. Perhar, M. Ramin, M. A. Kenney, S. Sadraddini, A. Gudimov, and G. B. Arhonditsis. 2011. Our current understanding of lake ecosystem response to climate change: What have we really learned from the north temperate deep lakes? *J. Great Lakes Res.* 37: 173–193.
- Sahoo, G. B., S. G. Schladow, J. E. Reuter, R. Coats, M. Dettinger, J. Riverson, B. Wolfe, and M. Costa-Cabral. 2012. The response of Lake Tahoe to climate change. *Climatic Change* 116: 71–95. doi:10.1007/s10584-012-0600-8

- Snucins, E., and G. John. 2000. Interannual variation in the thermal structure of clear and colored lakes. *Limnol. Oceanogr.* 45: 1639–1646. doi:10.4319/lo.2000.45.7.1639
- Span, D., D. Arbouille, H. Howa, and J.-P. Vernet. 1990. Variation of nutrient stocks in the superficial sediments of Lake Geneva from 1978 to 1988. *Hydrobiologia* 207: 161–166. doi:10.1007/BF00041453
- Straile, D., K. Jöhnk, and H. Roszknecht. 2003. Complex effects of winter warming on the physicochemical characteristics of a deep lake. *Limnol. Oceanogr.* 48: 1432–1438. doi:10.4319/lo.2003.48.4.1432
- Straile, D., O. Kerimoglu, F. Peeters, M. C. Jochimsen, R. Kümmerlin, K. Rinke, and K.-O. Rothaupt. 2010. Effects of a half a millennium winter on a deep lake—a shape of things to come? *Glob. Change Biol.* 16: 2844–2856.
- Vivier, P. 1944. Température et oxygène dissous dans le Léman français. *Travaux du laboratoire d'hydrobiologie de l'Université de Grenoble* 20: 25–35.
- Wüest, A., and A. Lorke. 2003. Small-scale hydrodynamics in lakes. *Ann. Rev. Fluid Mech.* 35: 373–412. doi:10.1146/annurev.fluid.35.101101.161220
- Zhang, Y., Z. Wu, M. Liu, J. He, K. Shi, Y. Zhou, M. Wang, and X. Liu. 2015. Dissolved oxygen stratification and response to thermal structure and long-term climate change in a large and deep subtropical reservoir (Lake Qiandaohu, China). *Water Res.* 75: 249–258. doi:10.1016/j.watres.2015.02.052

Supporting information for chapter 4:

Effects of climate change on deep-water oxygen and winter mixing in a deep lake (Lake Geneva) – Comparing observational findings and modeling

Robert Schwefel¹, Adrien Gaudard², Alfred Wüest^{1,2}, Damien Bouffard¹

¹ Physics of Aquatic Systems Laboratory, Margaretha Kamprad Chair, Ecole Polytechnique Fédérale de Lausanne, Institute of Environmental Engineering, CH-1015 Lausanne, Switzerland.

² Eawag, Swiss Federal Institute of Aquatic Science and Technology, Surface Waters – Research and Management, Kastanienbaum, Switzerland.

Introduction

Text S4.1 and S4.2 give a more detailed description of the model parameters used in the hydrodynamic model and the sinks and sources included in the oxygen box model. Text S4.3 provides details about the model forcing of the simulations with altered light absorption coefficients and a discussion on the results. Figure S4.1 provides a map of Lake Geneva, Figure S4.2 visualizes the temperature increase applied for the model runs B0/B+/B- and C0/C+/C-. Figures S4.3 and S4.4 illustrate the oxygen box model: S4.3 gives the schematics of the applied sinks and sources and S4.4 shows the oxygen depletion measured in Lake Geneva which was used to determine the sink term in the model. Figure S4.5 is a more detailed version of Figure 4.3 in the main text, labelling each data point with the corresponding year. Figure S4.6 compares the results of the hydrodynamic model SIMSTRAT with the measurements. Figure S4.7 shows the changes in modeled temperature due to altered transparency.

Text S4.1 Parameters used for the calibration of the hydrodynamic model SIMSTRAT

Goudsmit et al. (2002) provides a detailed description of the hydrodynamic model. Here we focus on the parameters we used for calibration, namely p_1 , p_2 , C_{10} , α and q .

p_1 and p_2 are parameters modifying radiation and the sensible heat flux at the lake surface. They have to be calibrated for every lake separately and correct for local phenomena (e.g. shadowing) and potential systematic bias of the meteorological stations.

p_1 is modifying the infrared radiation from sky:

$$H_A = p_1(1 - r_A)E_a\sigma T_A^4.$$

Here, r_A is the reflection of infrared radiation at the water surface, E_a the emissivity of infrared radiation from the atmosphere, σ the Stefan-Boltzmann constant and T_A the absolute air temperature measured in K.

p_2 affects the flux of sensible and latent heat:

$$H_C = -p_2 B f_u (T_w - T_A)$$

$$H_E = -p_2 f_u (e_w - e_a).$$

H_C and H_E are the flux of sensible and latent heat, B is the Bowen coefficient and f_u a transfer function dependent on wind speed and temperature difference between air and water. T_w and T_A are the temperatures at the water surface and in air, e_a is the water vapor pressure of the atmosphere, e_w the water vapor saturation pressure at the temperature of the lake water surface.

For Lake Geneva, we found the values $p_1 = 1.09$, $p_2 = 0.90$.

C_{10} is the wind drag coefficient, which determines the shear stress at the lake surface:

$$\begin{pmatrix} \tau_{surf,x} \\ \tau_{surf,y} \end{pmatrix} = C_{10} \rho_{air} \sqrt{u_{10}^2 + v_{10}^2} \begin{pmatrix} u_{10} \\ v_{10} \end{pmatrix}.$$

Where u_{10} and v_{10} are the velocities in x and y direction and ρ_{air} the density of air. In reality, C_{10} is not a constant, but a function of the wind speed with decreasing values up to a wind speed of $\sim 5 \text{ m s}^{-1}$ and increasing values for wind speeds $> 5 \text{ m s}^{-1}$ (Wüest and Lorke 2003). As introducing a

wind-dependent drag coefficient did not improve the model results, we chose a constant value of $C_{10} = 0.0017$ for our study.

The parameters α and q are used for the energy transfer from wind to the internal seiche motion. α parametrizes, how effective wind energy can be transferred into internal wave energy, q determines the vertical distribution of the transformation of seiche energy into turbulent kinetic energy. The total energy of the seiche motion is defined as

$$\frac{dE_{\text{Seiche}}}{dt} = PW - LS.$$

PW is the production of seiche energy by wind forcing and LS the energy loss by friction.

PW is defined as

$$PW = \alpha A_0 \rho_{\text{air}} C_{10} (u_{10}^2 + v_{10}^2)^{3/2},$$

A_0 is the surface area, the other quantities are defined as above. LS is dependent on the total amount of energy stored in the internal seiching and defined by

$$LS = -\gamma E_{\text{Seiche}}^{3/2}$$

with

$$\gamma = A_0 V_0^{-3/2} \rho_0^{-1/2} C_D.$$

$C_D = 0.002$ is the bottom drag coefficient. ρ_0 the water density and V_0 the lake volume. The part of seiche energy which is not dissipated in the molecular sublayer is then transferred to turbulent kinetic energy and given by

$$P_{\text{Seiche}}(z) = \frac{1 - 10\sqrt{C_D}}{\rho_0 c A_{\text{boundary}}} N^2 q \frac{1}{A} \frac{dA}{dz} \gamma E_{\text{Seiche}}^{3/2}.$$

A_{boundary} represents the total bottom area, N^2 the stratification and A the sediment area at depth z . c is a normalization constant. For the physical motivation of the definition of γ and P_{Seiche} , we refer to the original paper by *Goudsmit et al.* (2002).

Text S4.2 Sinks and sources for the oxygen model

S4.2.1 Gas exchange:

The gas exchange with the atmosphere is described by:

$$\frac{dC_{\text{water}}}{dt} = c_1 k [C_{\text{sat}}(T, t) - C_{\text{water}}(t)]$$

where C_{water} [g m^{-3}] is the oxygen concentration in the water at the surface, C_{sat} [g m^{-3}] the saturation concentration at temperature T , and k the exchange velocity. Different parameterizations of the gas exchange velocity exist. The parametrization of *Cole and Caraco* (1998) is used here, since it was validated on a low-wind lake and thus more suitable than other parameterizations mostly focusing on ocean conditions with very high wind speeds. In this parameterization, k [cm h^{-1}] is described as:

$$k [\text{cm h}^{-1}] = \left(\frac{Sc}{600}\right)^{-\frac{2}{3}} (2.07 + 0.215 u_{10}^{\text{abs}1.7}).$$

Here, Sc is the temperature dependent dimensionless Schmidt number for oxygen (not to be confused with the Schmidt stability) and u_{10}^{abs} the wind speed at 10 m height in m s^{-1} .

Due to the large lake size and the complex surrounding alpine topography, the wind speed at the lake shore meteorological station is not representative for the whole lake (*Lemmin and D'Adamo* 1997). We rather corrected the time series of wind data with the reanalyzed meteorological data taken at the lake center (provided by the meteorological model COSMO-2). The correction is done for the period 2008 - 2015 and then applied to the entire time series. This correction is thought to minimize the effect of the inherent difference in wind speed due to the change of roughness between land and water.

S4.2.2 Oxygen production:

The oxygen production by photosynthesis can be described as (Fang and Stefan, 2009):

$$\frac{dC_{\text{water}}}{dt} = c_2 1.036^{T-20^\circ\text{C}} P_{\text{max}} \text{Min}(t) \text{Chl}(t)$$

where $\text{Chl}(t)$ [g m^{-3}] is the concentration of chlorophyll-a, P_{max} the maximal production of $9.6 \text{ g O}_2 (\text{g Chl})^{-1} \text{ h}^{-1}$ and $1.036^{T-20^\circ\text{C}}$ a correction for the water temperature. $\text{Min}(t)$ describes the light limitation determined by Haldane kinetics. Chl data were not available for the whole measurement period, but only for the period 2007-2013 at the location of the deepest point of the

lake. Therefore, we decided to use the mean annual Chl concentration instead of a real time-series to calculate production for years before 2006. This might cause problems during years with extreme Chl concentrations caused by algae blooms, but reproduces the general pattern quite well. Chl concentration was averaged over 30 m, so light limitation is not only dependent on the incoming light, but also on the distribution of Chl and Secchi depth. To overcome these problems, we described the light limitation in our model solely based on the day length with a maximum in summer and minimum in winter, the other limiting effects were taken into account with the calibration factor c_2 . Given these simplifications, the seasonal variation of the production is probably well reproduced through the variation of Chl and day length, but the absolute value of the production and possible annual variations e.g. due to algae blooms are not reproducible. The model parameter c_2 was used during model calibration in order to minimize the error between measurements and model and to balance oxygen production and consumption realistically.

S4.2.3 Oxygen depletion:

Oxygen depletion takes place at the sediment surface through oxic respiration as well as oxidizing the reduced substances diffusing out of the sediment. In the water column oxygen is consumed by respiration and organic matter degradation. In our model, the empirically determined oxygen depletion rate was used to describe all oxygen consumption processes. This rate was determined based on over 40 years of measurements. While the mean hypolimnetic value expressed in areal units was $1.34 \text{ g m}^{-2} \text{ d}^{-1}$ or $0.0086 \text{ g m}^{-3} \text{ d}^{-1}$ in volumetric units, the depletion rate was found to be varying over depth, decreasing down to 150 m but increasing below (Figure S4.4). We therefore used a depth dependent depletion instead of the mean value and the depletion in each layer was calculated in every time-step depending on the layer thickness and the season. In summer, the calculated depletion during summer was used. During winter, the depletion was set to 50% of the depletion during summer.

Text S4.3: Details on the model runs with changed absorption.

S4.3.1 Model Forcing

In addition to temperature changes, we also investigated the effect of altered transparency on the thermal structure of the lake (Table 4.2). Light absorption can be parameterized by Secchi depth and is largely caused by particle concentration. Since the beginning of systematic monitoring, the Secchi depth is observed to decrease in Lake Geneva. This is attributed to an increased lake primary production during periods of high nutrient inputs, which reversed since 2000.

Observations showed a dependency of stratification on particle content in several lakes due to changing absorption (*Mazumder and Taylor 1994, Snucins and Gunn 2000, Persson and Jones 2008*). A detailed description of the future development of light absorption would be beyond the scope of this study, but to estimate the effect of changing absorption on winter mixing, we included model runs simulating lower and higher light absorption than under present conditions (Table 4.2). The lower absorption simulations represent the conditions in the early 1960es (model runs A-, B- and C-), whereas the higher absorption simulations (A+, B+, C+) represent an increased biomass compared to the present. To infer the trend in absorption during the monitoring period of 1957–2012, a robust linear regression was used for every season separately. In the simulations labeled with “-”, the trend in absorption for 1957 to 2012 was removed, representing a clearer lake with Secchi depth representative of the pre-eutrophication period before 1957. To estimate the effect of a more eutrophic lake, the absorption was increased by the same amount for the simulations labelled with “+”. The mean change in absorption was 12% with higher variations in winter and spring compared to summer and autumn.

S4.3.2 Results and Discussion

As expected, the volume-averaged lake temperature becomes slightly cooler in simulation A+ (Figure S4.7a). The sunlight is absorbed closer to the lake surface while the layers below receive less heat. Consequently, the surface temperature rises and causes higher longwave emission to the atmosphere. The increased heat loss causes a net cooling of the whole water body. In contrast, volume-averaged lake temperature increases slightly in A-, since light can penetrate deeper into the water (Figure S4.7b). The strongest effect was visible in the thermocline region, where a higher absorption causes a shallower and stronger thermocline. *Persson and Jones (2008)* made similar observations on the medium-sized Swedish Lake Erken. While the change in thermocline

height was comparable to our study, the impact on the whole lake is much stronger in shallow lakes with small hypolimnia.

During late summer and autumn, the most pronounced changes were observed. During this period, the thermal structure is also highly affected by changes in air temperature (Figure 4.6b and 4.6c). The cooling below the thermocline observed in the measurements (Figure 4.6a) can therefore be interpreted as a combination of increased air temperatures and plankton-induced turbidity.

Since 2000, the transparency, as observed by Secchi depth measurements, started to increase again, probably in response to the decrease in phosphorus levels (*Savoye et al.*, 2015). Our results suggest that such improvements of the water quality will lead to higher volume-averaged lake temperatures while the surface temperatures slightly decrease or stay constant. However, compared to the estimated changes in air temperature, the effect of changing light absorption on the thermal structure of Lake Geneva is small. This is not valid for small or medium-sized lakes, where light absorption might have a significant impact due to their smaller hypolimnion volume (*Persson and Jones* 2008, *Snucins and Gunn* 2000).

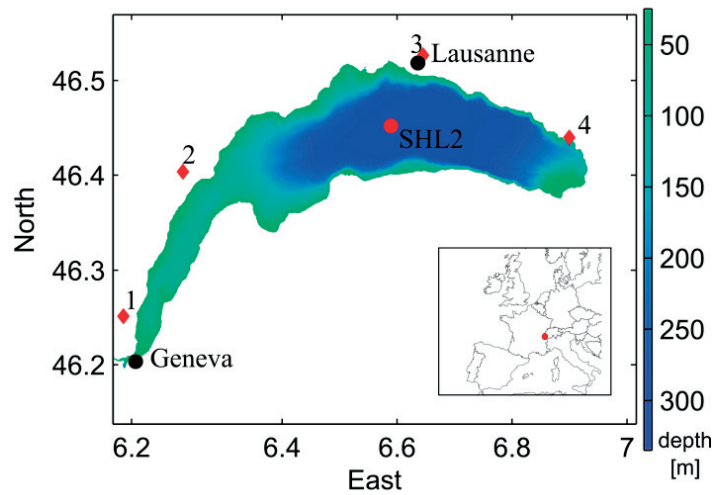


Figure S4.1: Map of Lake Geneva. The red circle shows the location of the measurement station SHL2 (46.45° N, 6.59° E; deepest point of the lake). Black circles show large cities, red diamonds symbolize meteorological stations used in this study (1: Genève-Cointrin, 2: Nyon-Changins, 3: Lausanne-Pully, 4: Montreux-Clarens).

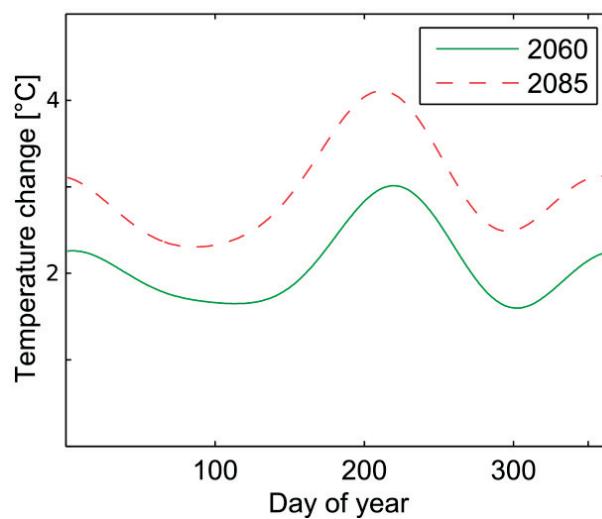


Figure S4.2: Air temperature increase relative to the reference period (1980–2009) at Lake Geneva for the IPCC A1B-scenario according to *CH2011* (2011) (green solid line: 2045–2074, red dashed line: 2070–2099). To estimate the local temperature increase, the predicted changes for four different stations around Lake Geneva were averaged.

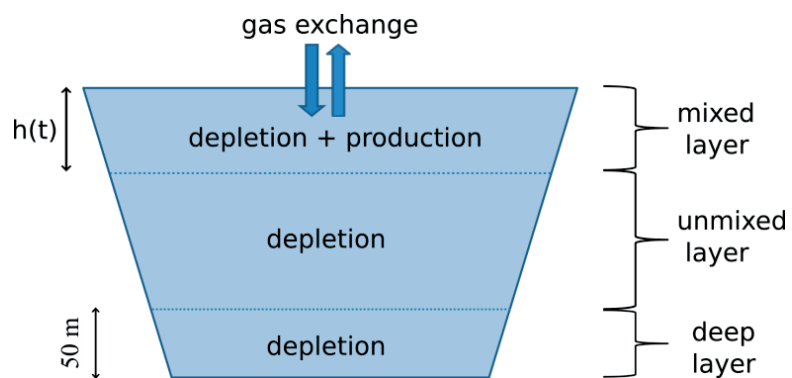


Figure S4.3: Scheme of the oxygen model. The mixed layer is in contact with the atmosphere. Production takes place only in the mixed layer, depletion over the entire depth. The size of the mixed layer is determined by the hydrodynamic model but is at least 30 m.

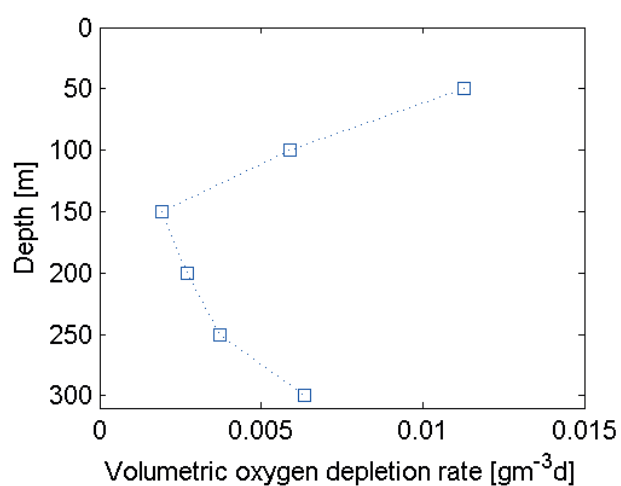


Figure S4.4: Volumetric oxygen depletion rate as a function of depth.

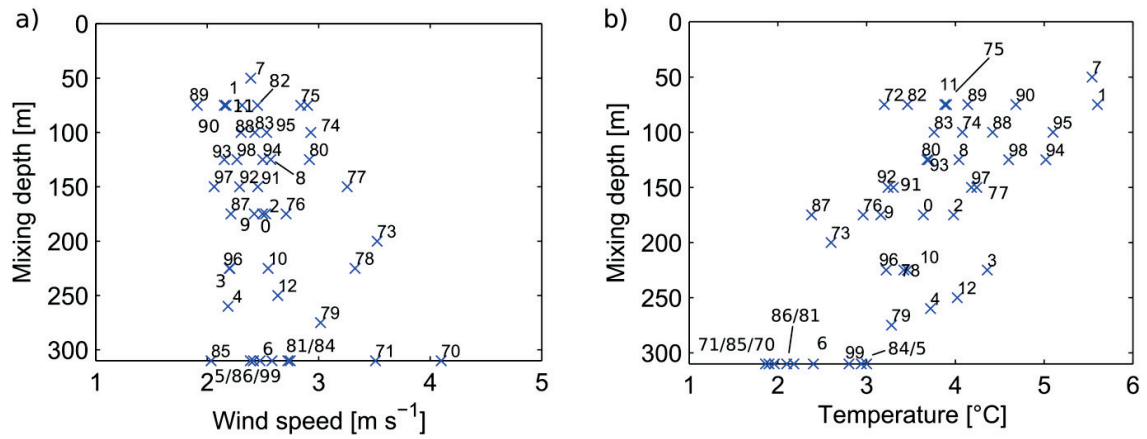


Figure S4.5: Measured maximum mixing depth in dependency of mean wind (a) and air temperature (b) during winters of 1970–2012. The numbers refer to the years for which the temperatures and wind speeds are averaged from December of the preceding year to March of the labelled year.

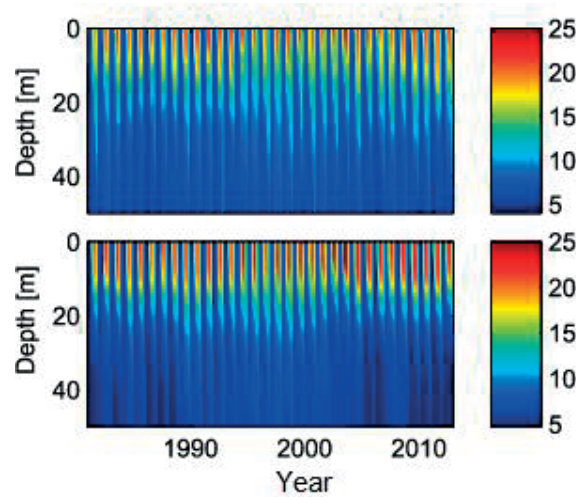


Figure S4.6: Temperature [$^{\circ}\text{C}$] of the uppermost 50 meter of Lake Geneva 1981–2012. Upper panel: measured; lower panel: simulated (model run A0).

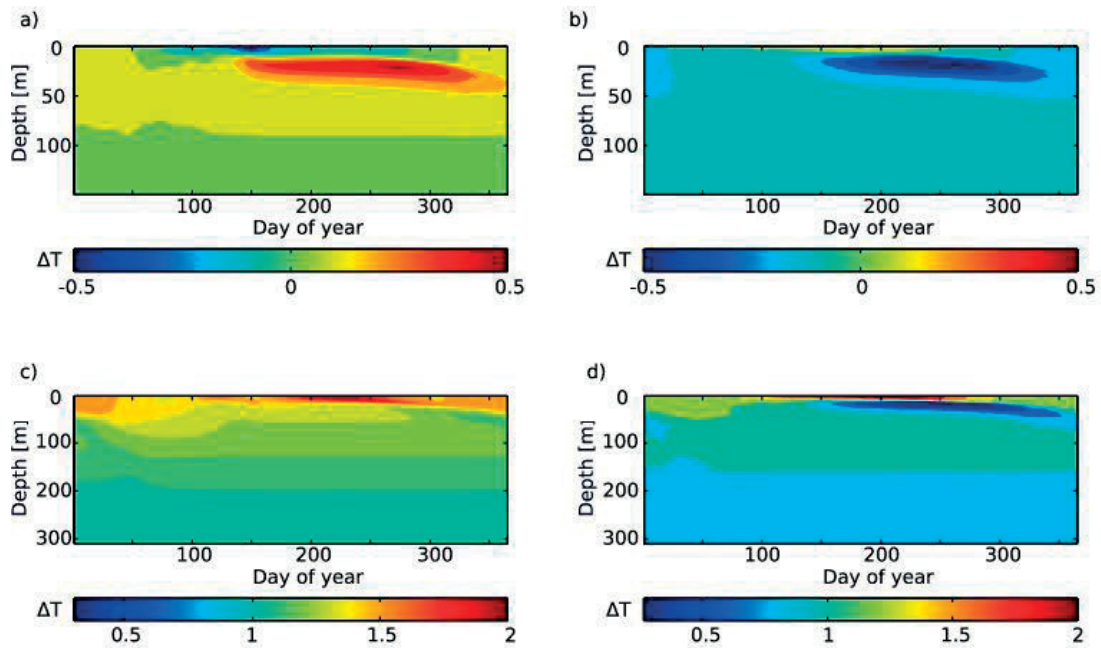


Figure S4.7. Effect of light absorption on water column temperature: The upper two contours show the temperature difference between the model scenarios A- (a, less absorption) and A+ (b, more absorption) relative to the reference scenario A0. As the changes below 100 m depth are homogenous, the graph shows only the top 150 m. The lower two contours display the temperature difference between the model scenarios C- (c, less absorption) and C+ (d, more absorption) for strongly increased temperatures as by 2085 (C in Table 4.2) compared to the reference scenario A0.

Chapter 5:

Modelling oxygen depletion in lakes

Abstract

Long-term monitoring data of dissolved oxygen from four Swiss lakes differing in size and depth were analyzed to determine the vertical variability of oxygen depletion. The results allow to separate at each depth the contribution from sediment oxygen uptake and mineralization in the water column. While the areal hypolimnetic oxygen depletion rate increases with increasing lake volume, the volumetric oxygen depletion decreases. In all observed lakes, oxygen depletion decreased with depth in the upper hypolimnion while it increases again in the lowest parts. The decrease in the upper layer is attributed to the decreasing amount of easily degradable organic matter whereas the increase in the lower layer is caused by increasing sediment to volume ratio. In parallel, the relative importance of sediment processes tends to decrease with lake volume. Based on these observational findings, a 1D-oxygen model coupled to a hydrodynamic model was developed and run for the years 2009 and 2010 on Lake Geneva under varying boundary conditions. The model was able to reproduce the mean oxygen concentration of the lake with a root mean square error of 0.36 g m^{-3} . Results under varying climatic conditions show that Lake Geneva is expected to experience increased hypoxic conditions in the deep water. A reduction of the depletion rate by 40 % would be necessary to counterbalance the effect of climate change on the total oxygen concentration.

5.1 Introduction

Oxygen depletion is important for the ecological health of lake ecosystems. Excessive depletion rates in stratified waters, driven by high mineralization rates of organic matter, can cause hypoxic conditions threatening the ecosystem by stressing the biological communities thereby affecting economical use with potential fish yield reduction and increase in treatment of drinking water supply.

Since almost a century, oxygen concentrations in lakes are recognized as an indicator of the trophic state (e.g. *Thienemann* 1928) and the total mineralization rate was believed to be mainly a function of the amount of degradable organic matter. Later studies showed that the connection between organic matter and oxygen depletion is less direct than assumed by the early investigators: Additional properties such as lake depth, hypolimnion oxygen concentration or lake hydrodynamics turned out to be highly relevant for oxygen depletion processes. Hence, empirical models to predict hypolimnetic oxygen depletion rates based on lake depth, nutrient inputs and temperature were developed (*Lasenby* 1975, *Rast and Lee* 1978, *Cornett and Rigler* 1979, *Molot et al.* 1992) and empirically tested (*Cornett and Rigler* 1980, *Rippey and McScorey* 2009). However, early oxygen depletion models used approaches based on statistical analysis without a conceptual understanding of the underlying processes. However, these data-driven models helped to identify the relevant parameters controlling oxygen depletion processes. *Livingstone and Imboden* (1996) used a more deductive model which explains the dependence of oxygen depletion rates on lake depth conceptually with the changing sediment to volume ratio and separated the total oxygen depletion (TOD) in a bathymetry-dependent sediment oxygen uptake (SOU) and a fraction which represents the mineralization of the organic matter in the water column and does not depend on the bathymetry (Water column mineralization; WCM). *Schwefel et al.* (2016) expanded this model by taking the variability of organic matter mineralization with depth into account. A conceptual model of oxygen depletion based on depth dependent SOU and WCM was able to reproduce the oxygen depletion rate in Lake Geneva and allowed to quantify the contribution of sediment oxygen uptake to the total oxygen depletion.

Here we analyze the oxygen depletion rates of four different lakes (Lake Biel, Lake Constance, Lake Geneva, and Lake Neuchâtel) and determine the relative importance of SOU and WCM. The analysis of lakes with varying size and trophic state will answer the question (1) whether the patterns found in *Schwefel et al.* (2017b) for Lake Geneva are universally valid and (2) whether a

systematic dependency of SOU or WCM with lake depth or other relevant trends in the oxygen depletion rates over the observation periods are identifiable. The results for Lake Geneva as well as the findings of Schwefel et al. (2017a) are used to calibrate a one-dimensional oxygen model to reproduce oxygen distribution over depth and time. This model was then run under varying boundary conditions to describe the sensitivity of the oxygen concentrations in the hypolimnion to climate-induced changes in air temperature and changing oxygen production and depletion rates to quantify expected future changes in the oxygen budget.

5.2 Oxygen depletion in lakes

5.2.1 Measurement sites

Lake Biel (47.104° N, 7.798° E) is a small monomictic lake in Western Switzerland. It has a surface area of 37.8 km², a volume of 1.1 km³ and maximal depth of 74 m (mean depth: 29 m). The lake has a mean residence time of only ~60 d, thus, river inflows play a major role for lake hydrodynamics. Oxygen data since 2000 were analyzed in this study. The lake mixes annually in winter and experiences strong oxygen depletion during summer leading to regularly occurring hypoxias in the deepest 10 to 20 m.

Lake Neuchâtel (46.904° N, 6.843° E) is a monomictic lake situated in Western Switzerland south of Lake Biel. It has a surface area of 217.9 km², a volume of 14 km³ and a mean depth of 64 m with a maximal depth of 152 m. The mean residence time is ~8 years and consequently, river inflows play only a minor role. Oxygen data were available since 2001 and show relatively high oxygen concentrations over the whole water column. The lake mixes convectively every winter and hypoxic conditions were never observed since 2001.

Lake Constance (47.629° N, 9.374° E) is a deep lake situated between Austria, Germany and Switzerland. With a maximal length of ~50 km and a maximal width of ~12 km, its surface area is 536 km² and the volume is 48 km³. The lake has a maximal depth of 251 m with a mean depth of 90 m. The mean residence time is ~4.5 years. Oxygen data are available since 1963 showing an oligomictic lake where winter mixing does not reach to maximum depth every winter. Hypoxic conditions are rarely observed during years with incomplete mixing.

Lake Geneva (46.452° N, 6.620° E) is a deep lake between France and Switzerland. With a surface area of 580 km² and a volume of 89 km³, it is the largest lake in Western Europe. The

mean depth is 151 m and the maximum depth is 309 m. The mean residence time is ~11.6 years. Oxygen data were available since 1957. The lake only mixes completely during extraordinary cold winter (in average, every fifth year), and consequently, the deep hypolimnion experiences regularly hypoxic conditions during periods without complete winter mixing.

5.2.2 Data analysis

Oxygen profiles were available from the deepest points of all lakes in biweekly to monthly resolution. The oxygen profiles were linearly interpolated before the total oxygen content in the hypolimnion (below 15 m) was calculated based on the oxygen concentrations and lake bathymetry. The areal hypolimnetic oxygen depletion rate [$\text{g m}^{-2} \text{d}^{-1}$] was then calculated for every lake and every year as the slope of the linear decrease in total oxygen content during summer. Begin and end of the linear decrease depend on the onset and end of thermal stratification and varied from year to year and between the lakes. To investigate the vertical structure of oxygen depletion processes, the total oxygen depletion per depth layer (TOD) [$\text{g m}^{-3} \text{d}^{-1}$] was then calculated for every lake. To ensure comparability between the different lakes, TOD was calculated as the oxygen deficit during a fixed period of time (first of April and first of October). The values were averaged over 20 m.

5.2.3 Results and discussion

The AHM rates for the four different lakes are shown in Figure 5.1. The mineralization rate fluctuates strongly without any significant trend over the last ~60 years for Lake Geneva. For Lake Constance, increased values in the period between the 1970 and 1980, in which phosphorus concentrations were increased, are visible. A slight decreasing trend for Lake Biel over the last ten years ($R^2 = 0.27$) is observed, while there was no statistically significant change in Lake Neuchâtel.

The TOD showed a similar structure in all four lakes. In the deepest layers, TOD increases with depth due to a higher sediment-to-volume ratio ($\alpha [\text{m}^{-1}]$) which increases the relative contribution of the SOU. Oppositely, TOD decreases with depth in the upper layer, since easily degradable organic matter is preferably mineralized in the top layers of the water column. Below, the remaining more refractory part is used leading to lower mineralization rates. The combination of these two effects leads to a C-shaped pattern with maxima of oxygen depletion at the top and bottom of the water column and a minimum in mid-depth. (Figure 5.2). Due to its shallow depth,

this shape is not clearly visible in Lake Biel since the decreasing and increasing effects could not be clearly separated with the 20m-averages chosen in this study.

Comparisons of the total oxygen depletion of the four lakes show that the shallower lakes show in general a higher TOD. In contrast, the AHM, which measures the oxygen depletion per surface area of the lake, tends to increase with lake depth. This is in good agreement with previous studies on this topic (*Cornett and Rigler 1979, Müller et al. 2012*). Since the amount of organic matter is mainly controlled by the surface area, the oxygen depletion per volume decreases in deep lakes where the surface-to-volume ratio is lower (*Thienemann 1928*). However, the organic matter mineralization is more complete in deep lakes. In addition, the hypolimnion of deep lakes contains more oxygen which leads to a stronger oxygen gradient at the sediment-water interface and in turn a stronger SOU. Because of these two effects, the decrease of TOD with lake depth is not completely linear and AHM increases with increasing lake depth. Compared to Lake Geneva and Lake Biel, the values for Lake Constance and Lake Neuchâtel are relatively low, which is probably caused by the larger amount of organic matter available in the former, more eutrophic lakes.

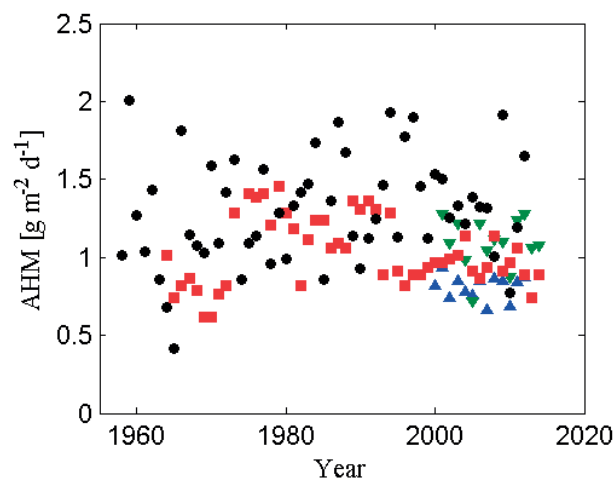


Figure 5.1: AHM as function of time for the four studied lakes: Lake Geneva (1958-2012, black circles), Lake Constance (1964-2014, red squares), Lake Neuchâtel (2001-2014, green triangles) and Lake Biel (2000-2012, blue triangles).

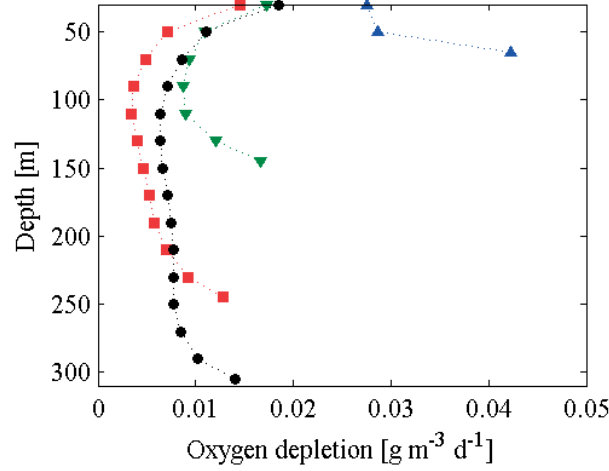


Figure 5.2: Averaged oxygen depletion between 15. April and 15. October in volumetric units as function of depth for Lake Geneva (black circles), Lake Constance (red squares), Lake Neuchâtel (green triangles) and Lake Biel (blue triangles).

Livingstone and Imboden (1996) proposed a deductive model of oxygen depletion separating the oxygen depletion into a fraction which takes place in the water column (WCM) and an areal fraction (SOU). While the volumetric fraction was constant over the whole water column, the areal fraction depended on the sediment-to-volume ratio α , which typically increases with depth. In an extension of this model, *Schwefel et al.* (2016) proposed that both contributors exponentially decreased with depth which naturally follows by assuming a constant sinking speed of organic particles and constant degradation rates. Hence, the decrease of TOD in the upper layer is taken into account and TOD is expressed as:

$$TOD = WCM + \alpha SOU \quad (5.1)$$

where

$$SOU = S_1 + S_2 e^{\frac{-(z-z_0)}{z_\tau}} \quad (5.2)$$

$$WCM = W_1 + W_2 e^{\frac{-(z-z_0)}{z_\tau}}. \quad (5.3)$$

S_1 and W_1 are the contribution of the refractory organic matter to SOU and WCM. S_2 and W_2 are the contribution of the fast-degrading organic matter at depth $z = z_0$. The fast-degrading fraction decreases exponentially with the decay length z_τ .

Numerical values of the constants S1, S2, W1, W2 and z_t , which describe the observed results given in Figure 5.2, are given in Table 5.1. It has to be noted that acceptable agreement with the measurements can be reached with different sets of parameters.

As expected, the importance of SOU is highest in Lake Biel which is the shallowest of the observed lakes and has the highest α . Consistently, the relative importance of SOU (calculated as integral over the whole water column: $\text{relative importance} = \frac{\int \alpha \cdot \text{SOU} \cdot A(z) \, dz}{\int [\alpha \cdot \text{SOU}(z) + \text{WCM}(z)] \cdot A(z) \, dz}$) decreased for Lake Constance and Lake Geneva to ~50% and ~30%, respectively (Figure 5.4). Only Lake Neuchâtel shows a very high contribution of WCM (~70%) given its relatively shallow depth compared to Lake Constance or Lake Geneva. A relatively low productivity or a high turbulence level (increasing the diffusion of oxygen and smoothing out the spatial variation of TOD) might explain this unusual behavior partially. The findings have now to be corroborated with more lakes to improve the statistics.

The experimentally found depletion rates are important for the development of numerical oxygen models. The correct prediction of oxygen concentrations in the hypolimnion largely depends on the correct parameterization of (i) turbulent transport (especially in winter) and (ii) oxygen depletion rates since the other sinks and sources of oxygen (mainly production, atmospheric exchange) only affect the epilimnion. In particular, the relative importance of SOU and WCM are important to assess the impact of increasing α on the oxygen depletion in the deepest layers. An oxygen model which takes the spatial variability of oxygen depletion based on the results of this study into account is presented in the following on the example of Lake Geneva.

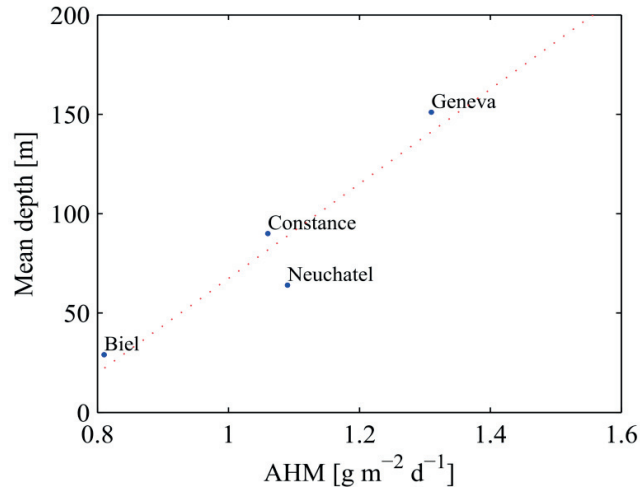


Figure 5.3: Mean areal hypolimnetic mineralization rate (AHM) as function of lake depth. Values before 2001 were omitted for Lake Biel, Lake Constance and Lake Geneva to ensure comparability.

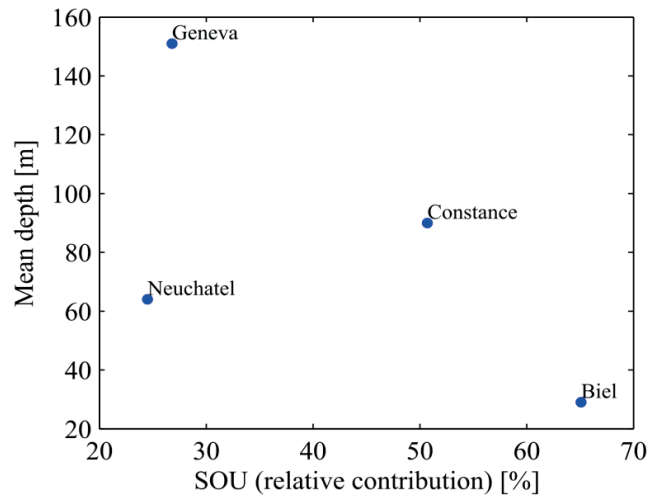


Figure 5.4: Relative contribution of sediment oxygen uptake (SOU) to the total oxygen depletion in the lake as function of lake depth. The relative contribution of SOU was calculated as

$$\text{relative contribution} = \frac{\int \alpha \cdot \text{SOU} A(z) dz}{\int [\alpha \cdot \text{SOU}(z) + \text{WCM}(z)] A(z) dz}$$

Table 5.1: The 5 parameters of equations (5.2) and (5.3) and other important quantities of the four investigated lakes. The ratio $\alpha \cdot \text{SOU}/\text{TOD}$ gives the relative importance of the oxygen depletion caused by SOU. SOU and TOD were integrated over the whole lake volume.

Parameter	Biel	Neuchâtel	Constance	Geneva
Maximal depth [m]	74	152	251	309
Volume [km ³]	1.1	14	48	89
S1 [gm ⁻² d ⁻¹]	0.15	0.12	0.20	0.25
S2 [gm ⁻² d ⁻¹]	0.40	0.55	0.89	1.45
W1 [gm ⁻³ d ⁻¹]	0.0049	0.0057	0.0015	0.0046
W2 [gm ⁻³ d ⁻¹]	0.0064	0.0060	0.0059	0.0078
z_{τ} [m]	30	18	23	25
$\alpha \cdot \text{SOU}/\text{TOD}$ [-]	64.7	24.5	50.0	26.8

5.3 Modelling oxygen in Lake Geneva

The hydrodynamic model SIMSTRAT (Goudsmit *et al.* 2002) was coupled to an oxygen model based on the experimental findings of Schwefel *et al.* (2016) and Schwefel *et al.* (2017b). The oxygen model was written in MATLAB.

5.3.1 Oxygen model

The change of oxygen in one layer at depth z of the lake per time ($\frac{\Delta O(z)}{\Delta t}$) can be described as:

$$\frac{\Delta O(z)}{\Delta t} = V(z)[Prod - WCM(z)] - V(z)\alpha(z) \left[D \frac{C(z) - C_{SWI}(z)}{\delta_{DBL}(z)} + F_{red}(z) \right] - A(z)v_T \frac{\Delta C(z)}{\Delta z} + A(z-1)v_T \frac{\Delta C(z-1)}{\Delta z} \quad \text{if } z \text{ below the surface (5.4a)}$$

or

$$\begin{aligned} \frac{\Delta O(z)}{\Delta t} = & \underbrace{A(z)k(C_{sat} - C)}_{(a)} + \underbrace{V(z)[Prod(z) - WCM(z)]}_{(b)} - \underbrace{V(z)\alpha(z)}_{(c)} \left[\underbrace{D \frac{C(z) - C_{SWI}(z)}{\delta_{DBL}(z)}}_{(d1)} + \underbrace{F_{red}(z)}_{(d2)} \right] \\ & - \underbrace{A(z)v_T \frac{\Delta C_z}{\Delta z}}_{(e)} \quad \text{if } z \text{ is surface layer (5.4b).} \end{aligned}$$

Where $O(z)$ is the oxygen content and $C(z)$ the oxygen concentration in the layer of depth z , $V(z)$ the layer volume and $A(z)$ the average surface area of layer z . C_{sat} is the saturation concentration, C_{SWI} the oxygen concentration at the sediment surface and ΔC_z the concentration difference between layer z and layer $z + 1$ ($\Delta z = 1\text{m}$). k is the gas exchange coefficient which depends on Schmidt-Number and wind speed. $Prod$ is the oxygen production and WCM is the mineralization in the water column. D is the molecular diffusivity and v_T the turbulent diffusivity. Finally, $\delta_{DBL}(z)$ is the thickness of the diffusive boundary layer between sediment and water and F_{red} the flux of reduced substances.

Part (a) of equation (5.4b) describes the exchange with the atmosphere, part (b) the oxygen production and part (e) the turbulent transport. The sum of part (c) and (d) is the TOD which consists of WCM (c) and $\alpha \cdot \text{SOU}$ (d). The SOU can be divided in the oxic respiration which depends on δ_{DBL} and the oxygen concentration above (d1) and the flux of reduced substances out of the sediment (d2).

In the model, the exchange with the atmosphere was calculated based on measured air temperatures and wind speed with a gas exchange coefficient calculated according to *Cole and Caraco* (1998). Even if this parameterization was calibrated on a lake under low wind-speed conditions, the gas exchange seemed still to be underestimated. Hence, a calibration factor was added to the gas exchange coefficient. During calibration, an increase of k by a factor of 2.0 turned out to give the best results. The production was calculated according to the equations presented in *Stefan and Fang* (1994) and measured values of chlorophyll production and transparency. The turbulent transport was estimated based on the turbulent viscosity calculated by SIMSTRAT. The SOU was determined based on the energy dissipation in each layer and the parametrization of δ_{DBL} length given in *Schwefel et al.* (2017a):

$$\delta_{DBL} = 13 \cdot \eta_B \quad (5.5)$$

Where $\eta_B = (\frac{\nu D^2}{\epsilon'})^{1/4}$ is the Batchelor length scale with the viscosity ν and ϵ' the energy dissipation in the bottom boundary layer (considered as the region with logarithmic velocity profile). While the energy dissipation ϵ is an output of SIMSTRAT, the fraction of ϵ' dissipated in the diffusive boundary layer is intrinsically not possible to determine in a one-dimensional model. However, the energy dissipation rates are considerably higher close to the boundaries where most of the energy dissipation happens (*Wüest and Lorke* 2003). Here we assumed that 80% of the total energy of each layer is dissipated in the bottom boundary. The SOU was then calculated with equation (5.5) and part (d1) of equation (5.4b). The oxygen concentration at the sediment C_{sed} was set to $C_{sed} = 0.6 C(z)$ which was close to the value of ~ 0.55 observed from microprofile measurements (*Schwefel et al.* unpublished data). The flux of reduced substances (part (d2) of equation 5.4b) in Lake Geneva is extremely low (*Steinsberger et al.* 2016, *Schwefel et al.* 2017b) and was consequently neglected. The water column mineralization was estimated based on the observational data (see *Schwefel et al.* 2017b). Since oxygen depletion rates differ in summer and winter, oxygen depletion rates were set to 50 % of the summer values between November and March. Unfortunately, no estimates of oxygen depletion during winter is available, so the reduction during winter remains a tunable parameter.

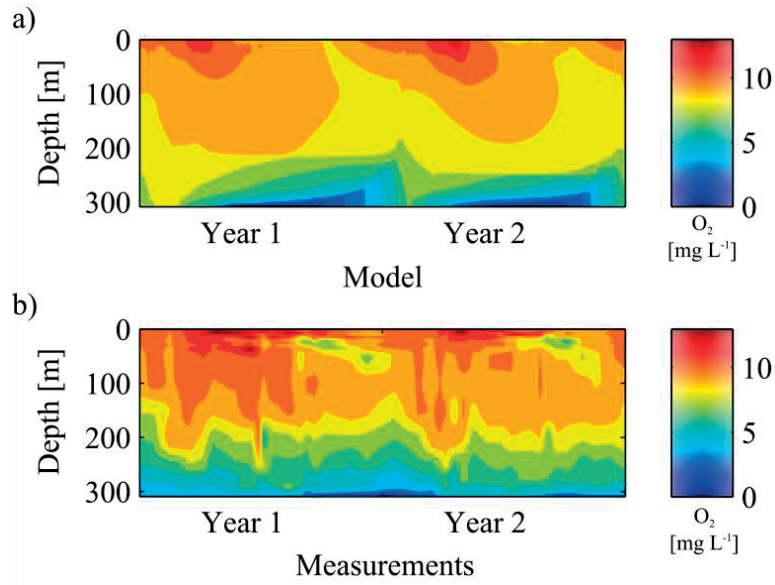


Figure 5.5: Modelled (a) and measured (b) oxygen concentrations for the years 2009 and 2010.

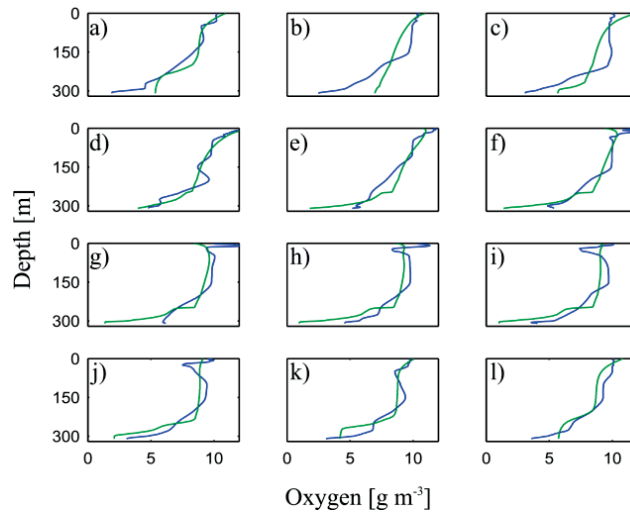


Figure 5.6: Modelled (green) and measured (blue) oxygen concentrations for the year 2010. Displayed are the interpolated values for the middle (15th day) of each month starting with a) January to l) December.

To reproduce the temperature and diffusivity of Lake Geneva, the one-dimensional hydrodynamic model SIMSTRAT was used. It is a buoyancy extended k- ϵ -model with an integrated internal seiche parameterization and was already used on Lake Geneva (*Perroud and Goyette* 2012, *Schwefel et al.* 2016) and other lakes (e.g. *Peeters et al.* 2002, *Matzinger et al.* 2007, *Fink et al.* 2014). To take the variability of the energy transfer between wind and internal waves into account, we modified the model slightly by introducing a seasonally varying parametrization for this energy transfer. Details about the model and the calibration for Lake Geneva can be found in *Schwefel et al.* (2016).

5.3.2 Results under present and future boundary conditions

The oxygen model was run for the years 2009 and 2010. A comparison between modelled and observed oxygen concentrations is shown in Figure 5.5 and 5.6. The averaged oxygen concentration is very well reproduced with a root means square error of 0.36 g m^{-3} (corresponds to $\sim 4\%$ of the observed mean value). However, the model results in average in lower oxygen concentrations (modelled mean of 9.11 g m^{-3} compared to observed mean of 9.31 g m^{-3}).

Despite the excellent agreement with the averaged oxygen values, the vertical structure of the oxygen concentrations is not perfectly resolved, especially in the lower layer during late winter and early spring and in the thermocline in summer (Figures 5.5 and 5.6). The reason is most likely an overestimation of turbulence. The averaged turbulent diffusion over all depth and times coefficient in the model is $\sim 5 \text{ cm}^2 \text{ s}^{-1}$ while long-term field observations suggest values below $1 \text{ cm}^2 \text{ s}^{-1}$ in average (*Michalski and Lemmin* 1995).

In a second run, the model was run under varied climatic forcing. The air temperature was increased to values representative for the period 2035-2074 according to the regional predictions for the IPCC climate scenario A1B (*CH2011* 2011, *IPCC* 2013). Details about the application of the regional downscaled temperature predictions for the use for SIMSTRAT on Lake Geneva can be found in *Schwefel et al.* (2016). For the oxygen model, the simulation was performed for the years 2008-2010. The first year was considered as spin-up period ensuring realistic oxygen concentrations in January 2009 which can be compared to the model run under unchanged conditions.

A comparison with the model results under unchanged conditions (Figure 5.7) shows a general decrease of oxygen concentrations which is caused mainly by increased stratification which inhibits oxygen transport to the deep layers. The volume-averaged mean oxygen decreased from 9.11 g m^{-3} to only 8.24 g m^{-3} . A reduction of the oxygen depletion (terms c and d in equation 5.4b) of $\sim 40 \%$ would be necessary to sustain mean oxygen levels which are comparable with present conditions. The impact on the deepest layers might even be stronger, since changes in stratification affect mainly the deep layer while oxygen depletion is strongest in the upper part of the lake. However, given the overestimated values for turbulent diffusion in SIMSTRAT, an estimation of the impact of climate change especially on the deepest layer is difficult.

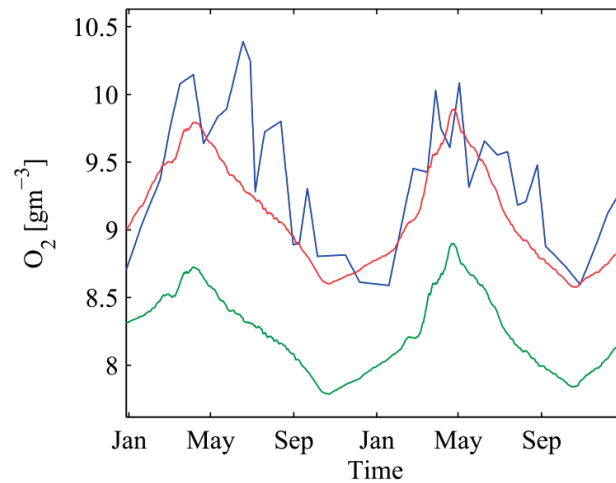


Figure 5.7: Mean volume-averaged oxygen concentrations 2010-2011 of Lake Geneva: blue: measured values, red: modelled values, green: modelled values with temperatures representative for the period 2045-2074.

5.3.3 Discussion and conclusions

While the modelled mean oxygen concentrations were very close to the observed values, the reproduction of the vertical structure remains problematic. These difficulties are caused by two different problems, (i) a probable overestimation of vertical turbulence in the hydrodynamic model SIMSTRAT and (ii) the strong depletion of very rapidly degrading organic matter settling in spring and summer.

The parameterization of WCM based on observed depletion rates between April and October (chapter 5.2) leads to incorrect results when the real depletion experiences strong seasonal variability which is mainly the case in the uppermost 50 meters of the lake during spring and summer. An addition of a third term in equation (5.3) which incorporates the very rapidly degrading organic matter could solve this issue.

However, the observed strong gradients of oxygen concentration below the thermocline are likely to be smoothed out by an overestimation of turbulent diffusion, even if the depletion itself is perfectly reproduced. In addition, an overestimation of diffusion causes too high oxygen concentrations in the deep layers of the lake, especially during late winter and spring when oxygen is transported down to the deepest layers of the lake even if a weak stratification remains in reality. This is particularly problematic since reoxygenation during winter mixing is an important research question considering the strong expected changes in air temperature forcing due to climate change (*Matzinger et al. 2007, Sahoo et al. 2013, Schwefel et al. 2016*).

Despite the remaining problems in reproducing the vertical structure, the proposed oxygen model is able to reproduce concentrations in a deep lake accurately with relatively few tunable parameters. Hence, it seems likely that it is possible that the same model can be used with relatively low calibration effort for other deep lakes in the future.

Acknowledgements

The data from Lake Geneva were provided by the Commission Internationale pour la Protection des Eaux du Léman (CIPEL) and the Information System of the SOERE OLA (<http://si->

ola.inra.fr). The data from Lake Constance were provided by the Internationale Gewässerschutzkommission für den Bodensee (IGKB), data from Lake Neuchatel and Lake Biel were obtained from the Bundesamt für Umwelt (BAFU). Meteorological data used in this study are archived and distributed by the Swiss Federal Office of Meteorology and Climatology, MeteoSwiss (obtained via IDAWEB, see <http://www.meteoswiss.admin.ch/home/services-and-publications/beratung-und-service/data-portal-for-teaching-and-research.html>). The source code of SIMSTRAT can be obtained from the authors; an online publication is planned for the future.

References

- CH2011. 2011. Swiss Climate Change Scenarios CH2011. C2SM, Zurich.
- Cole, J. J., and N. F. Caraco. 1998. Atmospheric exchange of carbon dioxide in a low-wind oligotrophic lake measured by the addition of SF₆. *Limnol. Oceanogr.* **43**: 647–656. doi:10.4319/lo.1998.43.4.0647
- Cornett, R. J., and F. H. Rigler. 1979. Hypolimnetic oxygen deficits: Their prediction and interpretation. *Science* **205**: 580–581. doi:10.1126/science.205.4406.580
- Cornett, R. J., and F. H. Rigler. 1980. The areal hypolimnetic oxygen deficit: An empirical test of the model. *Limnol. Oceanogr.* **25**: 672–679. doi:10.2307/2835755
- Fink, G., M. Schmid, and A. Wüest. 2014. Large lakes as sources and sinks of anthropogenic heat: Capacities and limits. *Water Resour. Res.* **50**: 7285–7301. doi:10.1002/2014WR015509
- IPCC. 2013. Climate Change 2013: The Physical Science Basis. Contribution of Working Group I to the Fifth Assessment Report of the Intergovernmental Panel on Climate Change. Cambridge University Press.
- Livingstone, D. M., and D. M. Imboden. 1996. The prediction of hypolimnetic oxygen profiles: a plea for a deductive approach. *Can. J. Fish. Aquat. Sci.* **53**: 924–932. doi:10.1139/f95-230
- Lasenby, D. C. 1975. Development of oxygen deficits in 14 southern Ontario lakes. *Limnol. Oceanogr.* **20**: 993–999. doi:10.4319/lo.1975.20.6.0993
- Matzinger, A., M. Schmid, E. Veljanoska-Sarafiloska, and others. 2007. Eutrophication of ancient Lake Ohrid: Global warming amplifies detrimental effects of increased nutrient inputs. *Limnol. Oceanogr.* **52**: 338–353. doi:10.4319/lo.2007.52.1.0338

- Michalski, J., and U. Lemmin. 1995. Dynamics of vertical mixing in the hypolimnion of a deep lake: Lake Geneva. *Limnol. Oceanogr.* **40**: 809–816. doi:10.4319/lo.1995.40.4.0809
- Molot, L. A., P. J. Dillon, B. J. Clark, and B. P. Neary. 1992. Predicting end-of-summer oxygen profiles in stratified lakes. *Can. J. Fish. Aquat. Sci.* **49**: 2363–2372. doi:10.1139/f92-260
- Müller, B., L. D. Bryant, A. Matzinger, and A. Wüest. 2012. Hypolimnetic oxygen depletion in eutrophic lakes. *Environ. Sci. Technol.* **46**: 9964–9971. doi:10.1021/es301422r
- Peeters, F., D. M. Livingstone, G.-H. Goudsmit, R. Kipfer, and R. Forster. 2002. Modeling 50 years of historical temperature profiles in a large central European lake. *Limnol. Oceanogr.* **47**: 186–197. doi:10.4319/lo.2002.47.1.0186
- Perroud, M., and S. Goyette. 2012. Interfacing a one-dimensional lake model with a single-column atmospheric model: 2. Thermal response of the deep Lake Geneva, Switzerland under a $2 \times \text{CO}_2$ global climate change. *Water Resour. Res.* **48**: W06522. doi:10.1029/2011WR011222
- Rast, W., and G. F. Lee. 1978. Summary Analysis of The North American (US Portion) OCED Eutrophication Project: Nutrient Loading - Lake Response Relationships And Trophic State Indices. U.S. Environmental Protection Agency Corvallis, Oregon.
- Rippey, B., and C. McSorley. 2009. Oxygen depletion in lake hypolimnia. *Limnol. Oceanogr.* **54**: 905–916. doi:10.4319/lo.2009.54.3.0905
- Sahoo, G. B., S. G. Schladow, J. E. Reuter, R. Coats, M. Dettinger, J. Riverson, B. Wolfe, and M. Costa-Cabral. 2012. The response of Lake Tahoe to climate change. *Climatic Change* **116**: 71–95. doi:10.1007/s10584-012-0600-8
- Schwefel, R., A. Gaudard, A. Wüest and D. Bouffard. 2016. Effects of climate change on deepwater oxygen and winter mixing in a deep lake (Lake Geneva): Comparing observational findings and modeling. *Water Resour. Res.* **52**(12). doi: 10.1002/2016WR019194.
- Schwefel, R., M. Hondzo, A. Wüest, and D. Bouffard. 2017a. Scaling oxygen microprofiles at the sediment interface of deep stratified waters, submitted to GRL.
- Schwefel, R., T. Steinsberger, D. Bouffard, L. Bryant, B. Müller, and A. Wüest. 2017b. Using small-scale measurements to estimate hypolimnetic oxygen depletion in a deep lake, submitted to *Limnol. Oceanogr.*
- Stefan, H. G., and X. Fang. 1994. Dissolved oxygen model for regional lake analysis. *Ecological Modelling* **71**: 37–68. doi:10.1016/0304-3800(94)90075-2

- Steinsberger, T., M. Schmid, A. Wüest, R. Schwefel, B. Wehrli, B. Müller. 2016. Organic carbon mass accumulation rate regulates the flux of reduced substances from the sediments of deep lakes. In preparation.
- Thienemann, A. 1928. Der Sauerstoff im eutrophen und oligotrophen See: ein Beitrag zur Seetypenlehre, E. Schweizerbart.
- Wüest, A., and A. Lorke. 2003. Small-scale hydrodynamics in lakes. *Ann. Rev. Fluid Mech.* **35**: 373–412. doi:10.1146/annurev.fluid.35.101101.161220

Chapter 6:

Summary and Outlook

6.1 Summary

In this thesis, oxygen depletion in lakes was studied on different scales: Small-scale microprofile measurements provided the basis for scaling of oxygen profiles close to the sediment-water-interface (SWI) and strengthened the understanding of the physical mechanisms which control the sediment oxygen uptake (chapter 2; Schwefel et al. 2016). As expected, the thickness of the diffusive boundary layer (DBL; typically order of ~ 1 mm) correlated strongly with the turbulence in the bottom boundary layer (BBL). A linear relationship between the Batchelor length scale (η_B), the length scale of the transition between molecularly controlled transport and turbulence, and DBL thickness δ_{DBL} was found ($\delta_{DBL} = 13\eta_B$). Interestingly, the eddy diffusivity E_t did not scale as predicted by flume experiments but showed a stronger dependency on the friction velocity u_* ($E_t \propto u_*^5$ instead of $E_t \propto u_*^4$). Based on the experimental findings, a scaling function for eddy viscosity and oxygen concentrations close to the SWI was proposed which is able to predict oxygen concentrations and fluxes based on hydrodynamics and few oxygen point measurements only.

Measurements at different depth in combination with sediment core analyses allowed determining relevant processes for the oxygen depletion in the hypolimnion of Lake Geneva and its vertical variability (chapter 3; Schwefel et al. 2016b). The results confirmed that oxic respiration is the main pathway of oxygen consumption at the sediment surface while oxidation of reduced substances plays only a minor role (in average, only $0.05 \text{ g m}^{-2} \text{ d}^{-1}$ or less than 5% of the mean hypolimnetic oxygen depletion). In general, sediment oxygen uptake (SOU) decreased with depth independently from the hydrodynamic conditions in the BBL most likely due to the larger amount of easily degradable organic matter in the shallower sediments. The total oxygen depletion (including SOU and mineralization in the water column) showed consequently a decrease with increasing depth from 0 to ~ 150 m. Below, an increase is observed which is caused by the increasing sediment surface to water volume ratio in the deep part of the lake. With a simple conceptual model based on *Livingstone and Imboden (1996)*, the variation of the oxygen depletion with depth can be reproduced based on few parameters describing the relative impact of refractory and easily degradable organic carbon mineralization in the sediment and in the water column. The results show, that the mineralization in the water column is responsible for $\sim 70\%$ of the total oxygen depletion while the SOU causes the remaining 30%, which is a smaller fraction

than reported in the literature for more shallow lakes (*Beutel et al.* 2007, *Müller et al.* 2012, *Bouffard et al.* 2013).

Besides oxygen depletion, the resupply of oxygen in winter is crucial for the oxygen content in the deep hypolimnion of the lake. Since Lake Geneva does not mix completely every winter, the depth of the annual winter mixing controls largely the severeness of hypoxic conditions in the deep hypolimnion. To investigate the impact of changing lake mixing in winter on the oxygen budget, a hydrodynamic model (SIMSTRAT) was used to investigate the mixing behavior of Lake Geneva under varying boundary conditions (increased air temperatures, changed transparency). The results of the hydrodynamic model were coupled to a simplified oxygen model to quantify the effects of changing mixing behavior (chapter 4). Overall, hypoxic conditions in Lake Geneva turned out to be highly dependent on the depth of deep convective mixing during winter and early spring. In model runs with increasing air temperatures according to the IPCC A1B climate scenario, the mean mixing depth in winter decreased from 172 m 1981–2012 to 136 m for conditions representative for the years 2045–2076 and ~127 m for 2070–2101. Although complete mixing events were reduced by ~50 % in the period 2070–2101, complete overturns were still observed occasionally. However, hypoxic conditions (oxygen concentrations below 4 mg L⁻¹) in the deepest layer were predicted to increase by 25% which confirms the important role of changing climatic conditions for estimating the future changes in oxygen budgets of many lakes globally.

Finally, the findings of chapter 2–4 were synthesized and generalized to other Swiss lakes (chapter 5). The variability of total oxygen depletion with depth was investigated for four different Swiss lakes (Lake Constance, Lake Geneva, Lake Neuchatel, and Lake Biel) and showed a consistent shape. Based on the scaling of SOU with BBL currents proposed in chapter 2 and the observational findings of chapter 3, a one-dimensional model for oxygen production and –depletion was developed and tested for Lake Geneva for varying boundary conditions (increased temperatures, increased production and depletion rates).

6.2 Outlook

6.2.1 Microprofile measurements

For low energetic systems, microprofile measurements are still the most efficient method to estimate oxygen fluxes at the SWI and give valuable insights in processes very close to the SWI. The measurements in Lake Geneva performed during this thesis confirmed former findings that SOU is largely controlled by the thickness of the DBL which is, in turn, controlled by BBL turbulence. However, the analysis revealed also some important differences to former measurements, e. g. in Lake Alpnach (*Bryant et al.* 2010) or coastal seas (*Wang et al.* 2016). The relatively deep oxic zone in the deeper sites of Lake Geneva (chapter 3) results in a relatively high oxygen concentration at the SWI and a strong decrease of SOU with depth with a parallel deepening of the oxic zone. While the oxygen depletion in shallow lakes can be completely described by the flux of reduced substances and oxic respiration at the sediment (*Müller et al.* 2012) based on lake-averaged parameters, the vertical structure of SOU in Lake Geneva cannot be described so easily in a similar manner. The reason for this different behavior is still not completely resolved. A detailed analysis of the organic matter content and quality at different depth with parallel microprofile measurements could give new insights to solve this open question and might enable to predict the SOU based on the amount of settling organic matter. A comparison of the results in Lake Geneva with measurements in other deep lakes would also be interesting to confirm the general validity of the observations made in Lake Geneva.

Another open point is the validity of microprofile measurements under very low and high turbulence, where the oxygen concentrations deviate from a purely diffusive behavior. So far, most studies used microprofiler to study SOU under diffusive conditions (Figure 6.1 a). Under extremely low or high turbulent conditions in the BBL, oxygen microprofile measurements show different results: In the case of extremely low turbulence conditions, peaks of several $\text{mg L}^{-1} \text{mm}^{-1}$ appear in the profiles (Figure 6.1 b). The reason for these strong fluctuations is still not completely understood. Probably they reflect small-scale variabilities in the oxygen concentration above the DBL caused e. g. by a sloping lake-bed. A better understanding of these irregularities in the oxygen profiles would help to interpret microprofile measurements e.g. to assess the validity of depletion rates measured under those extremely low-turbulent conditions.

On the other side, under extremely turbulent conditions, the assumption of completely diffusive transport above the SWI is not valid anymore in permeable sediments. Instead, advective transport has to be taken into account and the oxygen flux J is defined as:

$$J = -D \frac{\partial C}{\partial z} + v_z C. \quad (1)$$

With the diffusivity D , the oxygen concentration gradient $\frac{\partial C}{\partial z}$ and the vertical water velocity v_z .

The oxygen profiles show strong fluctuations with increased or decreased oxygen concentrations in the sediment depending on the direction of v_z (Figure 6.1 c). Measurements in a shallow lagoon in Spain showed a rapid transition between purely diffusive and advective conditions depending on the local wind forcing. An interesting research question would be to quantify more exactly the conditions where advective transport becomes dominant to identify advectively or diffusively controlled regions based on the hydrodynamic conditions.

Since in-situ measurements of SOU in lakes are still relatively rare, more measurements in lakes with differing trophic state and hydrodynamic boundary conditions would be desirable. To achieve this goal, microprofiling remains the best method to estimate SOU under low turbulent conditions where eddy correlation measurements often fail (*Brand et al.* 2008, *McGinnis et al.* 2008), even if problems as the irregular profiles shown in Figure 6.1 b might occur under extremely quiet conditions. A serious obstacle for microprofile measurements is the difficult handling under field conditions, especially in deep lakes. If the measurement site is too deep for remote control, a robust sediment detection routine is necessary and the site has to be relatively smooth and without elements which could cause sensor breaks (e. g. stones or mussels). In stony sediments, eddy correlation measurements might be easier to perform.

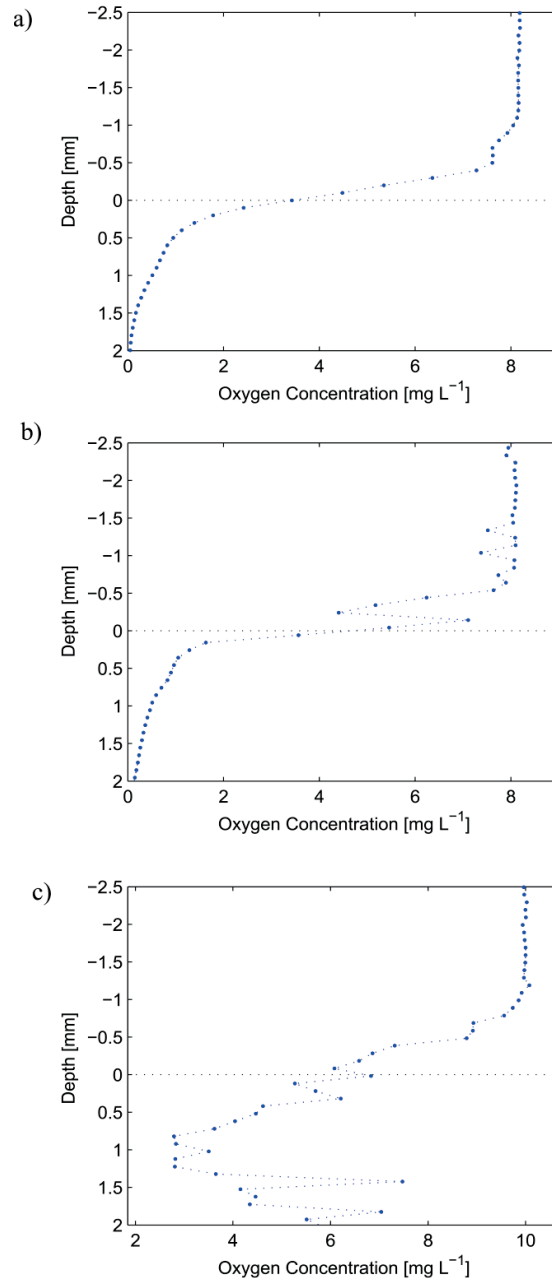


Figure 6.1: a) Typical oxygen profile in Lake Geneva (at ~43 m depth, 6.516° E / 46.505° N). b) Oxygen profile under low turbulent conditions in Lake Geneva, strong fluctuations above the sediment water interface (Depth = 0) are visible (same position as a). c) Oxygen profile under high turbulence conditions in the Laguna del Mar Menor (Spain), advective transport leads to oxygenation of the sediment.

6.2.2 Gas exchange and River intrusions

Besides the internal processes of oxygen production and depletion, the oxygen budget is also governed by external sinks and sources. In Lake Geneva, river inflows and exchange with the atmosphere are important external oxygen sinks and / or sources. In the general case, also groundwater inflows – negligible in Lake Geneva – could affect the oxygen budget.

The atmospheric exchange is generally parameterized as a function of the gradient between surface concentration or saturation and a wind-dependent gas exchange velocity. Most parameterizations were performed for ocean water under high wind-speed conditions. For quiet conditions which are more typical for lakes, the exchange velocity is less sensitive to the wind speed and also dependent on other processes such as night-time convection (*McIntyre et al.* 2010, *Dugan et al.* 2016). A recent long-term measurement of surface oxygen concentrations (*Schwefel et al.*, unpublished data) shows a daily variability of up to 60% in oxygen saturation at 25 cm depth (Figure 6.2). Hence, important questions are whether (1) the currently used gas exchange models are really appropriate for lakes and (2) whether monthly measurements at an often poorly defined point of time are representative enough for surface water model calibration.

River water is generally saturated with oxygen. Hence, the inflow of a river into an oxygen-depleted lake increases the oxygen concentrations. However, the determination of the exact intrusion depth of river water is a function of density which, in turn, depends on temperature, salinity, particle concentrations and mixing between river and lake waters. The exact amount of river water which ends up below the thermocline effectively increasing the oxygen concentrations in the hypolimnion is therefore extremely difficult to determine (first calculations were performed by *Thorez* 2016). Including a realistic river intrusion model in one or three-dimensional oxygen models would greatly improve their performance, especially for lakes with shorter residence times or river inflows with high particle concentrations.

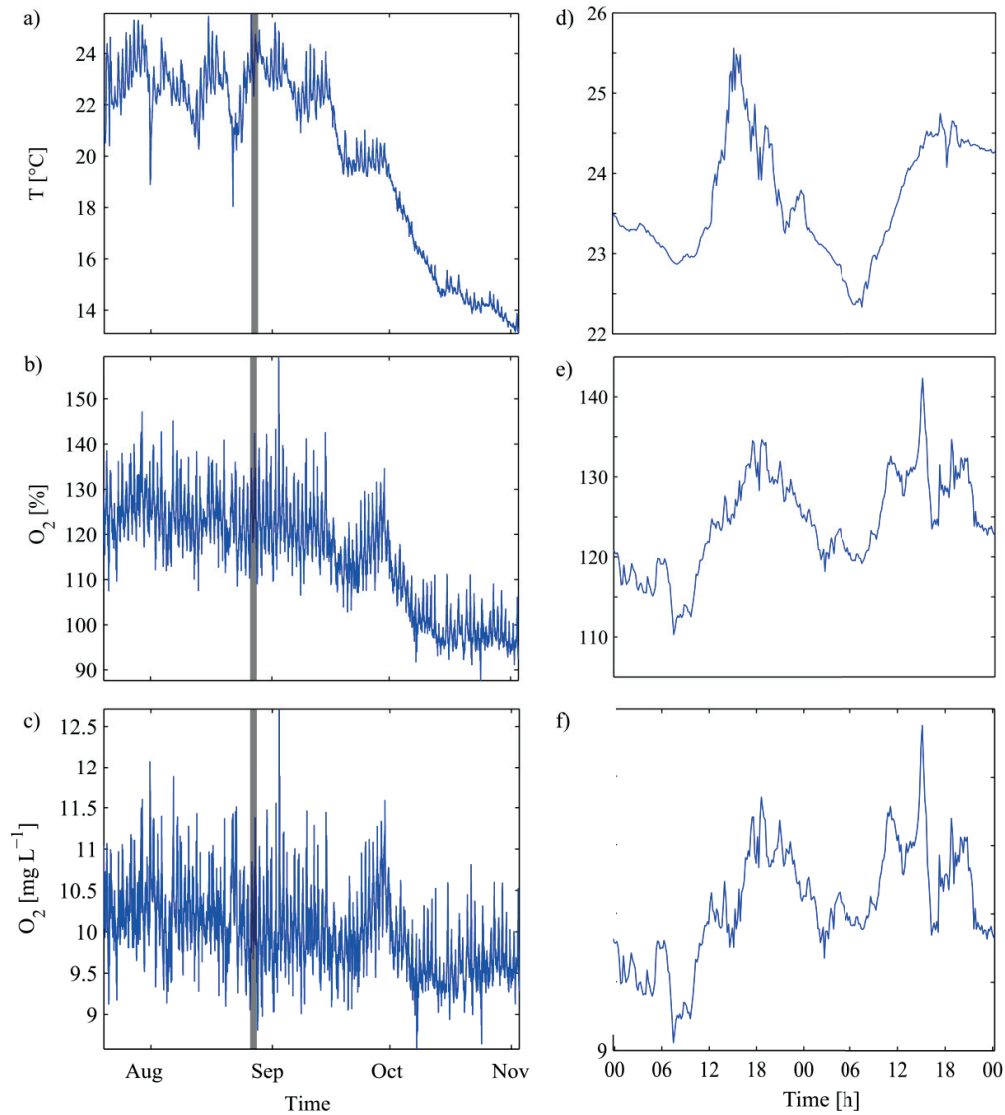


Figure 6.2: Temperature (a,d), oxygen saturation (b,e) and oxygen concentration (c,f) 25 cm below the surface of Lake Geneva at the meteorological station close to Buchillon (Schwefel et al., unpublished data). a,b,c: whole measurement period between July and November 2016. d,e,f: 26/27 of August 2016 (grey area in a,b,c). Strong sub-daily fluctuations are visible driven by atmospheric exchange and oxygen production during day-time and convection at night.

6.2.3 Modelling oxygen depletion

According to Thomas Kuhn, scientific theories are principally underdetermined. The decision between two different theoretical descriptions of a phenomenon cannot be made solely based on experimental results since these results itself rely on the interpretation of the scientist and the underlying scientific society. Hence, additional criteria – called scientific values – are necessary to estimate the quality of a theory. These values include, amongst others, simplicity and universality (Kuhn, 1962/1969). Modelling oxygen depletion processes in lakes is a good example for Kuhn's understanding of scientific theories: The coarse spatial and temporal resolution of long-term monitoring programs makes it intrinsically impossible, to validate oxygen models which rely largely on the correct parameterization of small-scale processes. State-of-the-art oxygen depletion or water quality models generally rely on a large amount of free parameters which are difficult to determine experimentally or are based on statistical analysis without a proper emulation of the underlying biological and physical processes. Better understanding of the relevant processes for oxygen depletion would enable to use oxygen models with reduced empirical calibration efforts and hence increase their universality. Quantifying the relative importance of single processes allows increasing model simplicity by neglecting irrelevant processes. This also reduces the risk of achieving a correct result for the wrong reasons (overestimating one parameter which corrects for the underestimation of another) which simplifies empirical validation. A good model has to take all the relevant processes into account without introducing a too high complexity.

While the oxygen model proposed in chapter 5 is able to reproduce the general patterns of oxygen depletion quite well, it still relies on experimentally determined oxygen depletion rates. A better connection between the primary production in the productive zone and the mineralization rates in the hypolimnion would improve the conceptual strength of the model and enable to assess directly the impact of changing primary production on the oxygen budget. While the long-term averaged biomass production and net sedimentation is quite close to the measured oxygen depletion rate (chapters 3 and 5), the annual values show no significant correlation between these two quantities. A more detailed investigation of the connection between primary production and oxygen depletion is necessary to explain this unexpected discrepancy and would help to establish

a more process-based simulation of oxygen depletion processes which is less dependent on purely statistically derived depletion rates.

Coupling the SOU to the hydrodynamic conditions at the BBL is not directly possible in a one-dimensional model since the currents are horizontally averaged and the values for energy dissipation reflect mean values for the whole layer which are difficult to translate directly into BBL conditions. A three-dimensional approach would be more realistic for this problem but requires significantly higher computational costs. Only a σ -layer model with high resolution close to the sediment would be able to simulate the relevant processes in reasonable accuracy to reproduce the turbulence at the BBL which is highly relevant for the oxygen flux into the sediment. The three-dimensional model GETM was already successfully run for Lake Geneva, combining the output with the relationships between BBL turbulence and oxygen uptake presented in chapter 3 would provide valuable insight of the temporal and spatial variability of SOU in a large lake.

The models used in *Schwefel et al.* 2016 and in chapter 5 of this thesis are using an inductive modelling approach which tries to understand and reproduce the relevant processes for the oxygen budget with a minimum of purely statistically derived relationships and only few tunable parameters. Another approach is the prediction of variables based on deductive relationships derived from statistical analysis of measured data from the past. Even if the responsible processes for these relationships might be unknown, these model often perform better in the reconstruction of measured datasets than inductive models. Starting with *Vollenweider* (1968), a wealth of empirical models to predict variables such as chlorophyll concentration (*Dillon and Rigler* 1974), fish concentration (*Hanson and Legget* 1984), transparency (*Vollenweider and Kerekes* 1980) or oxygen depletion (*Lazenby* 1975, *Cornett and Rigler* 1979) were developed. Already in the 1980s, a discussion of the role of prediction in limnology arose. Due to the success of descriptive limnology and the high predictive power of these models, the criticized lack of insight and understanding of deductive models was accepted (*Peters* 1986). However, descriptive models rely on the choice of correct independent variables and results from the past. Hence, unexpected new phenomena such as the weak correlation between the reduction of phosphorus input in lakes and the oxygen depletion in the hypolimnion observed in the last decades can hardly be predicted based on statistical model only. An important improvement would be a better combination of descriptive and inductive modelling, e.g. the use of descriptive modelling to fill gaps in relevant

data or to describe processes which are too complex for adequate modelling. On the other hand, inductive models can help to explain the outputs of purely data-driven models conceptually. A comparison of the oxygen model presented in this thesis with a purely data driven model is planned and might help to improve the predictive power of oxygen modelling by an identification and exact quantification of the parameters driving the observed variability (*Bouffard et al.*, in prep.).

References

- Beutel, M., I. Hannoun, J. Pasek, and K. B. Kavanagh. 2007. Evaluation of hypolimnetic oxygen demand in a large eutrophic raw water reservoir, San Vicente Reservoir, Calif. *J. Environ. Eng.* **133**: 130–138. doi:10.1061/(ASCE)0733-9372(2007)133:2(130)
- Bouffard, D., J. D. Ackerman, and L. Boegman. 2013. Factors affecting the development and dynamics of hypoxia in a large shallow stratified lake: Hourly to seasonal patterns. *Water Resour. Res.* **49**: 2380–2394. doi:10.1002/wrcr.20241
- Bouffard, D., R. Schwefel, G. Sugihara, H. Ye, V. Frossard. Towards an integration of inductive and deductive model for ecosystem management: The case of deep oxygen in Lakes. In preparation for PNAS.
- Bryant, L. D., C. Lorrai, D. McGinnis, A. Brand, A. Wüest, and J. C. Little. 2010. Variable sediment oxygen uptake in response to dynamic forcing. *Limnol. Oceanogr.* **55**: 950–964. doi:10.4319/lo.2009.55.2.0950
- Brand, A., D. F. McGinnis, B. Wehrli, and A. Wüest. 2008. Intermittent oxygen flux from the interior into the bottom boundary of lakes as observed by eddy correlation. *Limnol. Oceanogr.* **53**: 1997. doi:10.4319/lo.2008.53.5.1997
- Cornett, R. J., and F. H. Rigler. 1979. Hypolimnetic oxygen deficits: Their prediction and interpretation. *Science* **205**: 580–581. doi:10.1126/science.205.4406.580

- Dillon, P. J., and F. H. Rigler. 1974. The phosphorus-chlorophyll relationship in lakes. *Limnol. Oceanogr.* **19**: 767–773. doi:10.4319/lo.1974.19.5.0767
- Dugan, H., R. I. Woolway, A. Santoso, and others. 2016. Consequences of gas flux model choice on the interpretation of metabolic balance across 15 lakes. *Inland Waters* **6**: 581–592. doi:10.5268/IW-6.4.836
- Hanson, J. M., and W. C. Leggett. 1982. Empirical prediction of fish biomass and yield. *Can. J. Fish. Aquat. Sci.* **39**: 257–263. doi:10.1139/f82-036
- Kuhn, T. 1962/69. The structure of scientific revolutions, with a postscript from 1969. The University of Chicago Press, third edition. Chicago 1996.
- Lasenby, D. C. 1975. Development of oxygen deficits in 14 southern Ontario lakes. *Limnol. Oceanogr.* **20**: 993–999. doi:10.4319/lo.1975.20.6.0993
- Livingstone, D. M., and D. M. Imboden. 1996. The prediction of hypolimnetic oxygen profiles: a plea for a deductive approach. *Can. J. Fish. Aquat. Sci.* **53**: 924–932. doi:10.1139/f95-230
- McGinnis, D. F., P. Berg, A. Brand, C. Lorrai, T. J. Edmonds, and A. Wüest. 2008. Measurements of eddy correlation oxygen fluxes in shallow freshwaters: Towards routine applications and analysis. *Geophys. Res. Lett.* **35**: L04403. doi:10.1029/2007GL032747
- MacIntyre, S., A. Jonsson, M. Jansson, J. Aberg, D. E. Turney, and S. D. Miller. 2010. Buoyancy flux, turbulence, and the gas transfer coefficient in a stratified lake. *Geophysical Research Letters* **37**: L24604. doi:10.1029/2010GL044164
- Müller, B., L. D. Bryant, A. Matzinger, and A. Wüest. 2012. Hypolimnetic oxygen depletion in eutrophic lakes. *Environ. Sci. Technol.* **46**: 9964–9971. doi:10.1021/es301422r
- Peters, R. H. 1986. The role of prediction in limnology. *Limnol. Oceanogr.* **31**: 1143–1159. doi:10.4319/lo.1986.31.5.1143

- Schwefel, R., A. Gaudard, A. Wüest, and D. Bouffard (2016a). Effects of climate change on deepwater oxygen and winter mixing in a deep lake (Lake Geneva): Comparing observational findings and modeling. *Water Resources Research* **52**(12). doi: 10.1002/2016WR019194.
- Schwefel, R., M. Hondzo, A. Wüest, and D. Bouffard (2016b): Scaling oxygen microprofiles at the sediment interface of deep stratified waters, submitted to GRL.
- Thorez, S (2016): River intrusions: implications for lake water quality. Eindhoven University of Technology / École Polytechnique Fédérale de Lausanne. Internship Report.
- Vollenweider, R. A. 1968. Water management research. OECD, Paris. 183 p.
- Vollenweider, R. A., and J. Kerekes. 1980. OECD cooperative programme on monitoring of inland waters (eutrophication control). Synthesis Rep.
- Wang, J., L. Zhao, R. Fan, and H. Wei. 2016. Scaling relationships for diffusive boundary layer thickness and diffusive flux based on in situ measurements in coastal seas. *Progress in Oceanography* **144**: 1–14. doi:10.1016/j.pocean.2016.03.001

Curriculum Vitae

Robert Schwefel

Date of birth: 23. January 1987 in Heidelberg (Germany)

Current Address: Sur Villard 6

1026 Denges

Switzerland

Phone: ++41 78 7284084

E-Mail: robert.schwefel@epfl.ch

Work Experience and Education:

1/2013 – 12/2016: Doctorate studies in Environmental Engineering

Physics of Aquatic Systems Laboratory, ENAC, EPF Lausanne

Topic of the PhD-thesis: Oxygen depletion in Lake Geneva.

3/2012 – 9/2012: Scientific assistant at the Institute for Environmental Physics (University of Heidelberg).

10/2006 – 3/2012: Diploma in Physics

Ruprecht-Karls Universität Heidelberg

Topic of the diploma thesis: Methoden zur Probenaufbereitung von Eis- und Grundwasserproben zur ^{39}Ar -Datierung mittels „Atom Trap Trace Analysis“ (*Methods for Sample Preparation of Groundwater and Ice Samples for ^{39}Ar -Dating with „Atom Trap Trace Analysis“*).

2006

Abitur

Kurfürst-Friedrich Gymnasium Heidelberg

Articles

Schwefel, R., A. Gaudard, A. Wüest, D. Bouffard (2016): *Effects of climate change on deep-water oxygen and winter mixing in a deep lake (Lake Geneva) – Comparing observational findings and modeling*. Water Resour. Res. **52**(11) : 8811–8826. doi:10.1002/2016WR019194

Schwefel, R., M. Hondzo, A. Wüest, D. Bouffard: *Scaling oxygen microprofiles at the sediment interface of deep stratified waters*. Geophys. Res. Lett. **44**. doi:10.1002/2016GL072079

Articles submitted and in preparation

Bouffard, D., R. Schwefel, G. Sugihara, H. Ye, V. Frossard: *Towards an integration of inductive and deductive model for ecosystem management: The case of deep oxygen in Lakes*. In preparation.

Gaudard, A., R. Schwefel, L. Raman-Vinnå, D. Bouffard, A. Wüest: *Optimizing the parameterization of deep mixing and internal seiches in one-dimensional hydrodynamic models*. Submitted to Geosci. Model Dev.

Schwefel, R., T. Steinsberger, D. Bouffard, L. Bryant, B. Müller, A. Wüest: *Oxygen depletion in deep lakes: Using small-scale measurements to understand spatial variability of oxygen depletion in a large perialpine lake*. Submitted to Limnol. Oceanogr.

Steinsberger, T., M. Schmid, A. Wüest, R. Schwefel, B. Wehrli, B. Müller: *Organic carbon mass accumulation rate regulates the flux of reduced substances from the sediments of deep lakes*. Submitted to Biogeosciences

Conference Contributions

Wüest, A., R. Schwefel, L. Bryant, A. Matzinger, B. Müller (2016): *Oxygen depletion in stratified lakes – why shallow and deep lakes react differently?* Lake2016: Conference on Conservation and Sustainable Management of Ecologically Sensitive Regions in Western Ghats. Mangalore, India. Oral Presentation.

Schwefel, R., D. Bouffard, A. Wüest (2016): *Effects of climate change on deep-water oxygen and winter mixing in a deep lake (Lake Geneva)*. EGU General Assembly 2016. Vienna, Austria. Oral Presentation.

Schwefel, R., D. Bouffard, A. Wüest (2015): *Impact of deepwater mixing on hypoxia in Lake Geneva*. Aquatic Sciences Meeting. Granada, Spain. Oral Presentation.

Bouffard, D., R. Schwefel, A. Wüest, P. Holtermann and L. Umlauf. (2014): *Process based modelling of Lake Geneva*. Aquatic Sciences Meeting. Honolulu, USA. Oral Presentation.

Bouffard, D., R. Schwefel, A. Gaudard, U. Lemmin, A. Wüest (2014): *Process-based modelling of Lake Geneva*. 17th International Workshop on Physical Processes in Natural Waters. Trento, Italy. Oral Presentation.

Schwefel, R., D. Bouffard, L. Bryant, A. Wüest (2014): *Sediment Oxygen Uptake in Lake Geneva*. 46th International Liege colloquium, Low oxygen environments in marine, estuarine and fresh waters. Liège, Belgium. Poster Presentation.

Schwefel, R., T. Reichel, W. Aeschbach-Hertig, D. Wagenbach (2012): *Preparation of water and ice samples for ³⁹Ar dating by atom trap trace analysis (ATTA)*. EGU General Assembly 2012. Vienna, Austria. Poster Presentation.

Reichel, T., R. Schwefel, A. Kollefrath, W. Aeschbach-Hertig, J. Welte, F. Ritterbusch, M. Oberthaler (2011): *Setup for water degassing and argon separation from air*. IAEA Symposium 2011, Monaco. Poster Presentation.